

Acoustic Backscatter in Arteries

Measurements and Modelling of Arterial Wall and Blood

ISBN 90-9006182

The investigations published in this thesis were supported by The Netherlands Organization for Applied Scientific Research (TNO) and by the Interuniversity Cardiology Institute of the Netherlands (ICIN).

Financial support by the Netherlands Heart Foundation for the publication of this thesis is gratefully acknowledged.

Printed by: Universiteitsdrukkerij Erasmus, Rotterdam.

Acoustic backscatter in arteries

Measurements and modelling of arterial wall and blood

*Verstrooiing van ultrageluid in bloedvaten.
Meten en modelleren.*

proefschrift

ter verkrijging van de graad van doctor aan de
Erasmus Universiteit Rotterdam
op gezag van de rector magnificus
prof.dr. C.J. Rijnvos
en volgens besluit van het college van dekanen.

De openbare verdediging zal plaatsvinden op

Dinsdag 22 juni 1993 om 15.30 uur.

door

Machteld de Kroon
geboren te 's-Gravenhage

PROMOTIECOMMISSIE:

Promotores: Prof.Dr.Ir. N. Bom

Prof.Dr.Ir. A.J. Berkhout

Overige leden: Prof.Dr. C. Borst

Prof.Dr. P.W. Serruys

*Voor mijn ouders,
voor Arie.*

Table of contents

Summary	1
I INTRODUCTION	5
I.1 Anatomy of the arterial wall and atherosclerosis	6
I.2 Composition of blood	8
II ANGULAR DEPENDENCE OF BACKSCATTER FROM ARTERIAL TISSUE	11
II.1 Introduction	12
II.2 Materials and Methods	13
II.3 Results	18
II.4 Discussion	29
II.5 Conclusion	32
III BACKSCATTER BEHAVIOUR OF HUMAN BLOOD: CHANGES IN ECHOGENICITY DURING THE CARDIAC CYCLE	35
III.1 Introduction	35
III.2 Behaviour of blood under various flow conditions	37
III.3 Measurements of blood echogenicity in-vivo: case study	39
III.4 Evaluation	45
IV ULTRASONIC BACKSCATTER BEHAVIOUR OF HUMAN BLOOD IN-VITRO: MANIPULATED BLOOD SAMPLES AND SHEAR RATE DEPENDENCE	53
IV.1 Introduction	54
IV.2 Materials and methods	54
IV.3 Results	59
IV.4 Discussion	65
IV.5 Conclusion	68
V MODELLING OF THE ACOUSTICAL BEHAVIOUR OF ARTERIAL TISSUE AND BLOOD	73
V.1 Introduction	73
V.2 Geometry of angle dependent backscatter measurements	75
V.3 Backscatter pressure from a scattering volume - general mathematical formulation	75
V.4 Scattering by cylinders	78

V.5	Transducer characterization	88
V.6	Results of simulations	91
V.7	Discussion	108
V.8	Conclusion	110
Appendix A	Shear rate between coaxial cylinders	113
Appendix B	Mathematical expression for backscatter pressure from scattering volume	115
Appendix C	Fraunhofer condition in focal region	123
Appendix D	Scattering from inhomogenities	127
Appendix E	Integration of the delta function	131
Appendix F	Some standard integral solutions	133
Appendix G	Least squares estimates	134
Samenvatting	135
Nawoord	140
Publications by the Author	142
Curriculum Vitae	144

Summary

The aim of this thesis was to investigate the feasibility of quantitative arterial tissue characterization from ultrasonic puls-echo measurements, acquired with an intravascular ultrasonic catheter (30 MHz). Two major complications, that arise in an attempt to perform quantitative tissue characterization were investigated. These complications were the angle dependence of the backscatter intensity and the effect of the presence of blood in-vivo on the image quality.

The study consisted of three parts. The first part (Chapter II) deals with the quantitative effect on the backscatter power of the angle of incidence of the ultrasonic beam with respect to the arterial wall. In the second part of the study (Chapters III and IV) the acoustical behaviour of blood was investigated. Finally in the third part (Chapter V) the backscatter behaviour of both arterial tissues and blood was simulated on the basis of general acoustic theory. Before these subjects are reported, a short survey on the morphology of the arterial wall and the properties of blood is given in the introduction (Chapter I).

In Chapter II it is shown that variation in the angle of incidence causes grey-level variations in the B-mode picture of the arterial wall, which are not directly related to the underlying morphology. Angle variations are likely to occur during in-vivo application of the intravascular ultrasonic imaging catheter, e.g. if the catheter is excentrically positioned in the artery, if the cross-section of the artery has a non-circular shape or if the artery is curved. The angle dependent backscatter from the arterial wall complicates visual interpretation of the B-mode image. Moreover, it has great effect on quantitative characterisation methods, such as backscatter power analysis.

The quantitative effect of the angle of incidence on the backscatter power was investigated in-vitro. In this study a distinction was made between the angle variation in the plane perpendicular to the long axis of the artery (so-called tangential plane), and the angle variation in the plane through the long axis of the artery (axial plane). In-vitro measurements on 13 specimens of the iliac artery showed that each tissue type of the arterial wall has its own specific angle dependent behaviour.

Both the elastic and the muscular media showed anisotropy in their angle dependent scattering: the change of backscatter power with the angle of incidence was stronger in the tangential plane than in the axial plane. A change in the tangential plane in the angle of incidence of 10 degrees (with respect to perpendicular incidence), caused approximately a 2 dB decrease in backscatter power from the muscular media, and approximately 7 dB in backscatter power from the elastic media. For a 10 degrees change in the axial plane, the respective decreases were 0 dB and 3 dB approximately. The anisotropic behaviour of the muscular media can be explained by the orientation of the smooth muscle cells

observed in histologic sections of the muscular media. An explanation for the anisotropic nature of the elastic media based on the histologically observed structure of the tissue is not available.

Both loose and dense collagen lesions in the intima did not display anisotropy in their angle dependent backscatter behaviour. In both directions a decrease in backscatter power of approximately 3 dB was observed. This anisotropic behaviour agrees with the observed histology of collagen lesions, which showed randomly oriented collagen fibers.

Also the angle dependent backscatter power of the adventitia and the external elastic lamina was measured. The spread in the measurements on these tissues was relatively large. For the adventitia this can be explained by its inhomogeneous structure.

From each backscatter power versus angle curve tissue parameters were estimated. One of these is the so-called directivity parameter, which is a measure of the rate of angle dependence of the backscatter power. The second parameter is the maximum backscatter power, which represents the backscatter power at perpendicular incidence on the tissue layer. Because the directivity parameter is sensitive to the direction of the angle variation (tangential or axial plane), from the measurements two directivity parameters were deduced: the tangential and the axial directivity parameter. The measurement results strongly suggest that quantitative arterial tissue characterization is possible using the three parameters: tangential directivity, axial directivity and maximum power.

In Chapter III the effect of the high echogenicity of blood on the visualization of the luminal border using a 30 MHz intravascular ultrasonic imaging device is demonstrated. Also a survey from literature of the acoustic properties of blood is given. Hematocrit, red blood cell aggregation, deformation and orientation of red blood cells, are known to have influence on the backscatter properties of blood in the frequency range of 1-15 MHz. The relatively high echogenicity of blood with respect to the echogenicity of tissue observed at 30 MHz, is not reported at these lower frequencies. Furthermore, it is known that in the low frequency range (1-15 MHz) blood echogenicity is influenced by the local shear rate: a decreasing shear rate results in an increased echogenicity. Because red blood cells aggregate at decreasing shear rate and the aggregates disperse when the shear rate increases, it is assumed that the shear rate dependent state of aggregation causes the observed changes in echogenicity.

The echogenicity of blood, imaged with an intravascular ultrasonic imaging device (30 MHz), was measured during the cardiac cycle in three patients. Cyclic changes of the blood echogenicity synchronous with the changes in blood pressure were observed. The results suggest that these variations were related to changes in the state of red blood cell

aggregation, which are induced by the varying shear rate during the cardiac cycle.

In **Chapter IV** a study on the acoustic properties of blood at high frequencies (20-40 MHz) for varying aggregation conditions is reported. Several blood samples were prepared either to enhance aggregation (Rouleaux enlarged blood samples) or to suppress aggregation (Rouleaux suppressed blood samples) of red blood cells. On these samples a series of experiments was conducted at varying shear rate. Shear rate was varied using a specially developed measurement device based on a Couette Viscometer. In this device the shear rate is approximately constant within the acoustic measurement volume, which is not the case in the conventional tube flow measurements performed by others.

Obtained quantitative acoustical parameters were the integrated backscatter power and the spectral spectral slope of the backscatter power in the frequency range of 20 to 40 MHz. A decrease of approximately 13 dB in the integrated backscatter power of whole blood was observed when the shear rate was increased from 0.7 s^{-1} to 200 s^{-1} . The spectral slope increased from 1 to 3, when the shear rate was increased from 0.3 s^{-1} to 10 s^{-1} . For the rouleaux enlarged blood samples approximately the same change in integrated backscatter power and slope was observed, though higher shear rates appeared to be necessary to effectuate these changes. The integrated backscatter power and spectral slope of rouleaux suppressed blood were not affected by changes in the shear rate.

The results of this study show that the shear rate, which is known to influence the state of aggregation, has significant influence on the backscatter properties of blood at 30 MHz. The changes with shear rate of the integrated backscatter power and the spectral slope of whole blood and rouleaux enlarged blood suggest that at small shear rates ($< 0.3 \text{ s}^{-1}$) aggregates are fully developed. Then between 0.3 s^{-1} and 200 s^{-1} aggregates are broken and only single red blood cells are present at shear rates higher than 200 s^{-1} .

The measured spectral slope indicates that a further increase of the acoustical frequency will enhance blood echogenicity and thus probably aggravate the problem of discriminating arterial wall and lumen.

In **Chapter V** a mathematical model describing the acoustical backscatter behaviour of arterial tissue and blood at high frequency (30 MHz) is introduced. Both arterial tissue and aggregated blood were considered to consist of a distribution of cylindrical scatterers in 3D space. The properties of this distribution of scatterers are described by several parameters, i.e. the average distance and the spread in the distance between the scatterers, the average size and the spread in the size of the cylinders, and finally the average orientation and the spread in the orientation of the cylinders. Also the properties of a focussed transducer were incorporated in the model. From the angle dependent measurement of the reflection against a plane reflector, the parameters describing the transducer properties were obtained.

First the influence of the model parameters on the simulated backscatter pressure was studied by repeated calculations for varying parameter values. It is shown that the angle dependent backscatter pressure of a distribution of irregularly spaced scatterers was hardly affected by the spacing of the scatterers but was mainly determined by the size and orientation of the scatterers.

Next, simulation results of the angle dependence of backscatter pressure from tissue mimicking scattering media are reported. The muscular media was thought of as an irregular distribution of cylindrical scatterers aligned in the same direction. The dimensions and the spacing of the cylinders were set equal to the dimensions and spacing of the smooth muscle cells observed in histological sections of the muscular media. The simulated angle dependence of the backscatter pressure from this tissue mimicking distribution of cylindrical scatterers corresponded well to the experimental results of Chapter II. Dense and loose collagen lesions were assumed to be a distribution of irregularly spaced thin cylinders (fibers) with random orientation in a plane parallel to the arterial wall. The rate of angle dependence of the backscatter pressure was mainly determined by the length of the cylinders. For an average cylinder length of 120 μm the results of the simulations are in good concordance with the experimental results. Finally, the backscatter measurements on blood were simulated. Aggregated red blood cells in blood were represented by a distribution of irregularly spaced cylinders oriented perpendicular to the incident pressure beam. Aggregation of blood cells was simulated by an increase of the average cylinder length with a proportional decrease of the number of cylinders. The simulated aggregation had the same effect on the calculated backscatter power as the decrease of shear rate on the measured backscatter power in the experiments reported in Chapter IV.

I INTRODUCTION

With the rapid progress in interventional radiology and cardiology and in particular, the introduction of therapeutic techniques such as mechanical atherectomy and laser angioplasty, there is an increased demand for methods that enable visualisation of the morphology of the arterial wall. Damage to the arterial wall must be avoided and this requires knowledge of the location, geometry, and composition of an obstruction.

Initial reports on high-frequency intravascular ultrasonic catheters have demonstrated that the location and geometry of lesions can be determined by these techniques [1]. It was suggested [7] that the proximity of the region of interest (arterial wall and possible lesions), the fluid filled acoustic path between transducer and region of interest and the applied high frequency allow greater opportunities for tissue characterization than in traditional trans-thoracic echocardiography. The aim of the study of this thesis was to assess the feasibility of quantitative arterial tissue characterization. Two major complicating features were encountered in an attempt to perform quantitative arterial tissue characterization. The first of the encountered difficulties is the effect of the angle of incidence of the ultrasonic beam on the tissue. The second difficulty is the presence of blood, which shows high backscatter intensity at the applied high frequency (30 MHz) and thus limits the visualization of the arterial wall.

This thesis describes studies on these complicating features. In Chapter II an in-vitro study on the angle dependent behaviour of backscatter from arterial tissues is reported. Chapter III gives a survey of literature on the acoustic properties of blood and in-vivo observations of cyclic changes during the cardiac cycle of the backscatter intensity from blood are reported. In Chapter IV an in-vitro study on the backscatter behaviour of blood under various flow conditions is described. Finally, in Chapter V the acoustic wave theory is applied in order to get better insight in the acoustic behaviour of arterial tissue and blood and to understand more precisely the results of the experimental studies.

Before going into detailed description and discussion of experiments and modelling, some useful back-ground information on the morphology of the arterial wall, the atherosclerotic process and on the properties of blood are given in the following paragraphs of this Chapter.

I.1 Anatomy of the arterial wall and atherosclerosis

I.1.1 The arterial wall

Histologic studies [3][4][6][8] have shown that the arterial vessel wall consists of three layers: tunica intima (innermost layer), tunica media (middle layer), tunica adventitia (outermost layer). Basically two types of arteries are differentiated in the human vasculature: muscular and elastic arteries, with the main difference found in the composition of the media.

Intima

The intima is composed of a single layer of endothelial cells, a thin (about 80 nm thick) basal lamina and a subendothelial layer. The polygonal endothelial cells are only 0.2-0.5 μm thick and tend to be elongated in the direction of the blood flow. The subendothelial layer is composed of collagenous bundles, elastic fibrils, a few longitudinally oriented smooth muscle cells and perhaps some fibroblasts. The thickness of the subendothelial layer increases with age (see paragraph I.1.2).

Media of the muscular artery

In the muscular artery the media predominantly consists of circularly and concentrically arranged smooth muscle cells, which are 25-80 μm long and 1-8 μm in diameter. Only a few elastin fibers as well as some connective tissue may be present [6]. In the smallest vessels the media is only 3 to 4 cell layers thick, while in the larger vessels the thickness is up to 40 cell layers.

Media of the elastic artery

The elastic media may be up to 500 μm thick and is formed of numerous and distinct concentric elastic lamellae (up to 2.5 μm thick), which are spaced 6 to 18 μm apart. The lamellae are extensively fenestrated and interconnected by branches so that they form a three-dimensional network. The main component of the elastic lamellae is the protein elastin. The elastic lamellae have spirally arranged smooth muscle cells with surrounding collagen sandwiched in between. The pitch of these spirally arranged cells may be different for each concentric layer. The volume concentration of smooth muscle cells is less in the elastic media than in the media of the muscular artery and their shape is more irregular with multiple cellular extensions.

I.1 Anatomy of arterial wall and atherosclerosis

Adventitia

The thickness of the adventitia varies considerably depending on the type and location of the blood vessel. Generally, for elastic arteries it constitutes only 10 % of the vascular wall, while in muscular arteries this might be up to 50 %. The adventitia contains of dense fibroelastic tissue. Arterioles, venules, blood capillaries and lymphatic vessels, collectively referred to as "vasa vasorum", and also nerves are found in the adventitia.

Elastic laminae

The intima is separated from the underlying layer (media) by the internal elastic lamina, and the media is separated from the adventitia by the external elastic lamina. In the muscular arteries the internal and external elastic lamina are present as solitary features, while in elastic arteries they are the first and last of the concentrically arranged elastic lamellae in the elastic media.

I.1.2 Atherosclerosis

With age, diffuse concentric thickening of the intimal layer occurs. This development is induced by the migration of smooth muscle cells from the media through the natural occurring orifices in the internal elastic lamina into the subendothelial spaces. Diffuse intimal thickening involves the arteries of all humans and is considered a normal development, which is not related to the development of atherosclerotic lesions [6]. Clinically important are advanced lesions (also called atherosclerotic lesions), which project eccentrically and considerably above the intimal surface. An atherosclerotic lesion is either a fibrous collagen-rich lesion or presents as a lesion including an atheroma surrounded by a collagen-rich fibrous cap [6]. The atheroma contains cell debris, fatty materials, cholesterol esters and possibly calcium. Although this description suggests that an atherosclerotic lesion has a characteristic morphologic appearance, the contrary is true. A large variety in morphology exists: from atherosclerotic lesions consisting of more than one atheroma with fibrous tissue in between to lesions mainly consisting of fibrous materials [5].

I.2 Composition of blood [2]

Blood consist of blood plasma, in which blood cells and chymicrons (fluid particles) are suspended.

Blood plasma is a watery solution with inorganic and organic constituents and proteins solved in it. One of these proteins, i.e. fibrinogen, is involved in the coagulation process.

Chymicrons are relatively small fluid particles (0.2-0.5 μm), which are responsible for the transport of fat.

Three different kind of *blood cells* are present in blood: blood platelets or Trombocytes, white blood cells or Leucocytes and red blood cells or Erythrocytes (Table I.1).

The *red blood cell* (RBC) or *Erythrocyte* has the shape of a biconcave disk, of which the diameter is approximately 8 μm , and its thickness varies from 1 to 3 μm . The RBC consists of a thin membrane filled with a saturised haemoglobin solution in water (34 gram/ml). Haemoglobin is responsible for the oxygen transport.

The *white blood cell* or *Leucocyte* is roughly spherically shaped and has a diameter of 7 to 22 μm . They are important in prohibiting infections.

Blood platelets or *Trombocytes* are rounded or oval cells of 2 to 4 μm . They are important for the ending of haemorhage.

In whole blood the blood cell concentrations are: $0.2-0.5 \cdot 10^{15} \text{ m}^{-3}$ Trombocytes, $5-10 \cdot 10^{12} \text{ m}^{-3}$ Leucocytes and $4-5 \cdot 10^{15} \text{ m}^{-3}$ Erythrocytes. The commonly used measure of red blood cell concentration is the Hematocrit, which is the volume percentage of red

Table I.1 Concentration, shape and size of blood cells [2].

cell type	concentration (l^{-3})	shape/size
Erythrocytes or red blood cells (RBC)	$4-5 \cdot 10^{12}$	biconcave, diameter = 7-8 μm , thickness= 1-3 μm
Leucocytes or white blood cells	$5-10 \cdot 10^9$	roughly spherical, 7-22 μm
Trombocytes or platelets	$0.2-0.5 \cdot 10^{12}$	rounded or oval, 2-4 μm

1.2 Composition of blood

blood cells in the suspension. In healthy patients the Hematocrit varies between 35% and 45%.

Because of their low concentration, it is assumed that leucocytes do not contribute to the acoustic scattering of blood. Although, platelet concentration is very high, their influence on acoustic scattering is also neglected because they have smaller dimensions than erythrocytes. As a consequence, only erythrocytes are assumed to be responsible for the acoustic scattering properties of blood.

References

- [1] Bom N., Roelandt J.: *Intravascular ultrasound, techniques, developments, clinical perspectives*. Kluwer Academic Publishers, 1989.
- [2] Caro C.G., Pedley T.J., Schroter R.C., Seed W.A.: *The mechanics of the circulation*. Oxford, University Press, 1978.
- [3] Dingemans K.P., Jansen N., Becker A.E.: *Ultrastructure of the normal human aortic media*. *Virgoffs Archiv A* 392: 199-216, 1981.
- [4] Ghadially F.N., Walley V.M.: *Ultrastructure and architecture of arteries and veins*. In: *Cardiovascular pathology*, Ed.: Silver M.D., Churchill Livingstone, New York: 103-129.
- [5] Gotto A.M., Robertson A.L., Epstein S.E., DeBakey M.E., McCollum C.H.: *Atherosclerosis*. Scope publication.
- [6] Haust M.D.: *Atherosclerosis - Lesions and sequelae*. In: Silver M.D. ed, *Cardiovascular pathology*, Vol II. New York: Churchill Livingstone: 191-315, 1983.
- [7] Linker D.T., Yock P.G., Grønningsæther A., Johansen E., Angelsen B.A.J.: *Analysis of backscattered ultrasound from normal and diseased arterial wall*. *Int J Cardiac Imaging* 4: 177-185, 1989.
- [8] Rhodin J.A.G.: *Architecture of the vessel wall*. In: Bohr D.F., ed. *Handbook of Physiology*, sec.2 (The Cardiovascular System). American Physiological Society: 1-31, 1980.



II ANGULAR DEPENDENCE OF BACKSCATTER FROM ARTERIAL TISSUE

As partly been published in:

De Kroon M.G.M., Van der Wal L.F., Gussenhoven W.J., Bom N.: Angle dependent backscatter from the arterial wall. *Ultrasound Med Biol* 17: 121-126, 1991.

De Kroon M.G.M., Van der Wal L.F., Gussenhoven W.J., Rijsterborgh H., Bom N.: Backscatter directivity and integrated backscatter power of arterial tissue. *Int J Cardiac Imaging* 6: 265-275, 1991.

Abstract

The quantitative effect of the angle of incidence on the backscatter power was investigated in-vitro. In this study a distinction was made between the angle variation in the plane perpendicular to the long axis of the artery (so-called tangential plane), and the angle variation in the plane through the long axis of the artery (axial plane). In-vitro measurements on 13 specimens of the iliac artery showed that each tissue type of the arterial wall has its own specific angle dependent behaviour.

Both the elastic and the muscular media showed anisotropy in their angle dependent scattering: the change of backscatter power with the angle of incidence was stronger in the tangential plane than in the axial plane. The anisotropic behaviour of the muscular media can be explained by the orientation of the smooth muscle cells observed in histologic sections of the muscular media. An explanation for the anisotropic nature of the elastic media based on the histologically observed structure of the tissue is not available.

Both loose and dense collagen lesions in the intima did not display anisotropy in their angle dependent backscatter behaviour. This isotropic behaviour agrees with the observed histology of collagen lesions, which showed randomly oriented collagen fibers.

Also the angle dependent backscatter power of the adventitia and the external elastic lamina was measured. The spread in the measurements on these tissues was relatively large. For the adventitia this can be explained by its inhomogeneous structure.

From each backscatter power versus angle curve tissue parameters were estimated. One of these is the so-called directivity parameter, which is a measure of the rate of angle dependence of the backscatter power. The second parameter is the maximum backscatter power, which represents the backscatter power at perpendicular incidence on the tissue layer. Because the directivity parameter is sensitive to the direction of the angle variation (tangential or axial plane), from the measurements two directivity parameters were deduced: the tangential and the axial directivity parameter. The measurement results strongly suggest that quantitative arterial tissue characterization is possible using the three parameters: tangential directivity, axial directivity and maximum power.

II.1 Introduction

Initial reports on high-frequency intravascular ultrasonic imaging devices have clearly demonstrated that the location and geometry of lesions can be determined by these techniques [2][16]. Furthermore, it appeared to be possible to discriminate between muscular and elastic arteries as well as to assess the composition of the atherosclerotic lesion by qualitative evaluation of the B-mode echo images [7][8][9][20]. Studies on quantitative arterial tissue characterization have been reported [17][18], although the significance of the findings has not generally been appreciated in the context of intra-arterial echographic imaging.

To illustrate this point, an intravascular ultrasonic imaging device (30 MHz, [2]) was used to scan two arterial tissue specimens (muscular and elastic) in-vitro, at two different radial positions of the catheter. The images, shown in Figure II.1, show striking contrasts: besides the expected increase in echogenicity as the transducer approaches the wall, some regions within the wall exhibit bands of excess or deficient echogenicity depending on the angle of incidence.

A likely explanation to this phenomenon is the presence of reflective structures in the arterial wall resulting in a variable echogenicity dependent on the angle of incidence.

For an excentric position of the catheter, for a non-circular shape of the arterial cross-section or in a bended or widened artery, the incident beam is likely to be not perpendicular to the surfaces of the tissue layers in the arterial wall (Figure II.2). Variation in the angle of incidence causes grey-level variations in the B-mode picture, which are not directly related to the underlying morphology. This phenomenon complicates visual evaluation of the B-mode image. Moreover, the angle dependence greatly affects quantitative characterisation methods, such as backscatter power analysis [11][17][19].

Picano et al. [18] investigated the influence of the angle of incidence on the backscatter properties of human arterial specimens with various degrees of atherosclerotic involvement in the frequency range of 2-10 MHz. His study was limited to the variation in the backscatter coefficient in relation to one-dimensional changes in the angle of incidence, and so anisotropy of the arterial tissue was not investigated. Since histological studies have shown that most tissue types have anisotropic morphology, also an anisotropic angle dependent scattering is likely to occur.

The aim of the present study is to examine in-vitro the extent to which the backscatter power from different tissue types is affected by the angle of incidence in two dimensions

II.1 Introduction

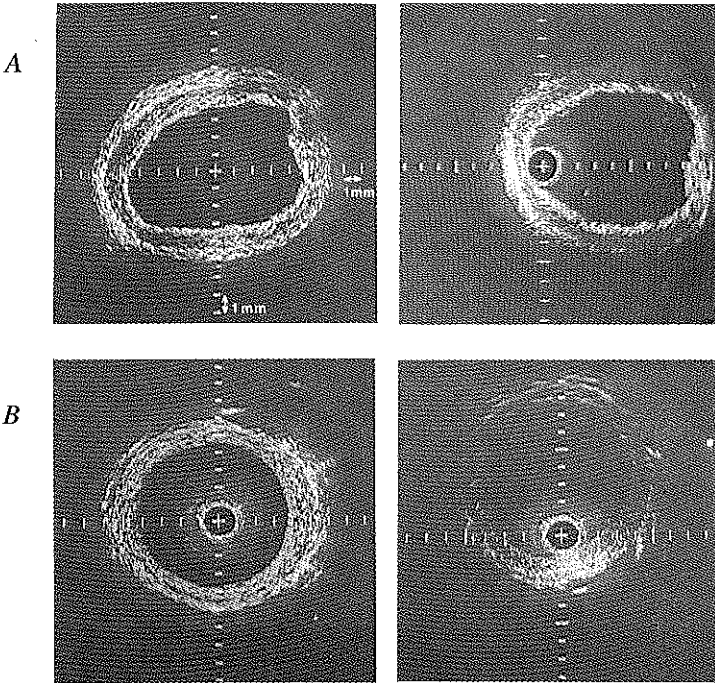


Figure II.1 B-mode images of in-vitro experiments on a muscular (A) and an elastic (B) artery. The right panels give the results on the same tissue sample as the left panels, albeit with the catheter moved out of the center of the artery.

and to investigate reproducibility of this phenomenon. The results have a bearing not only on quantitative tissue identification, but also on the optimal design of the intra-arterial ultrasonic catheter.

II.2 Materials and Methods

Arterial specimens

Thirteen specimens (coming from 13 persons) of the iliac artery (length approximately 10 cm) were removed at autopsy, isolated from redundant surrounding tissues, and stored at -20°C . No significant effect of freezing on the echographic response was found by

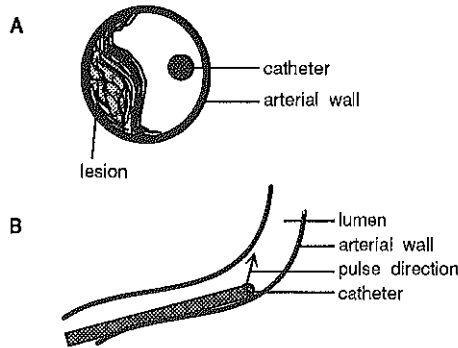


Figure II.2 Geometries for which the incident beam is not always perpendicular to the tissue layers in the arterial wall; A) artery with atherosclerotic lesion, B) bended artery.

Gussenhoven et al. [9]. At the time of examination the specimens were thawed, longitudinally cut, opened and mounted on a sample holder. The experiments were performed at room temperature with the specimens placed in saline solution (0.9%).

Scanning

Line scans both parallel (axial scan) and perpendicular (tangential scan) to the long axis of the artery were performed on the arterial specimens using an ultrasonic microscope [22]. The distance between subsequent recordings during a line scan was 50 μm . The ultrasonic microscope was equipped with a revolving transducer holder, allowing systematic variation in the angle of incidence. Only the angle in the scanning plane, defined by the propagation direction of the emitted pulse and the scanning direction, was varied. Thus, in subsequent axial (a) scans the angle θ_a was varied, whereas the angle θ_t was varied during tangential (t) scanning (Figure II.3). The region of interest in the tissue is positioned at the center of rotation of the revolving transducer holder. With this experimental set-up, the location of the examined region in the tissue and the distance between transducer and region of interest are independent of the actual angle of incidence. Initially a B-mode picture of the whole tissue specimen at perpendicular incidence is produced, which enables to select a region of interest for measuring at varying angle of incidence.

Transducer

A broadband focussed PVDF transducer (Fulmer 27 MHz; focal length 6 mm; diameter 3 mm), mounted on the ultrasonic microscope, was used. The focal point of the transducer

II.2 Materials and methods

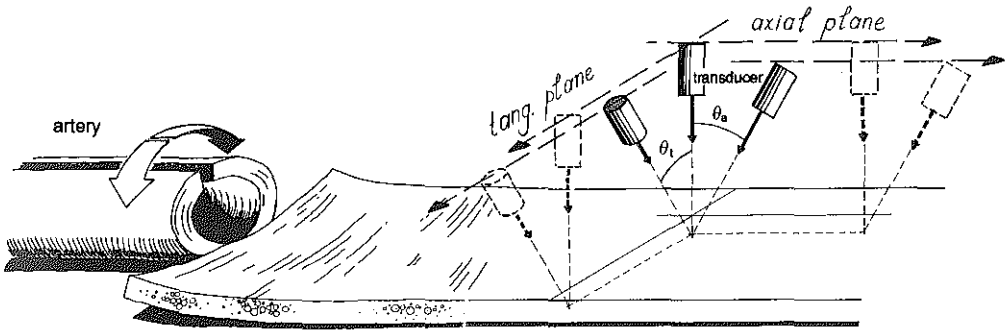


Figure II.3 Experimental set-up. The artery is longitudinally cut and opened flat. Line scans with varying angle of incidence (θ) were performed in axial and tangential direction.

was positioned at the center of rotation and at the region of interest. The transducer was excited with a single sided negative going spike produced by a high frequency pulse generator (Avtech Electrosystems, AVG-2-C).

Microscopic examination

Following ultrasonic examination, pieces of the arteries containing the examined regions were excised, fixed in 10% buffered formalin for 12 hours and subsequently processed for routine paraffin embedding. From the embedded samples several transverse sections (5 μm thick) were cut, ensuring that they were perpendicular to the long axis of the artery. Of two arteries (one muscular, one elastic) also several sections parallel to the long axis were cut in order to visualize the anisotropic nature of the various layers. The histological sections were stained by the haematoxylin azophloxine technique and with Verhoeff's elastin Van Gieson.

Data acquisition

The full rf-signals were digitized with a sampling frequency of 400 MHz, using a high-speed A/D-converter (LeCroy 9450). Scanning was controlled over RS232 interface with a Burleigh inchworm 3-axis positioning system. A dc-motor with gear head and rotation table provided rotation of the transducer holder. The dc-motor was controlled by an IBM compatible 286 computer. The host computer (UNIX system) coordinated linear scan

motion, rotation and data-acquisition. Acquired data were transferred to the hard disk of the host computer.

Signal Processing

Backscatter power from several regions of the artery was obtained according to the method described by Lizzi et al. [12]. In short this method is as follows.

In the B-mode image of a line scan a region of interest of approximately 100 time samples (i.e. 0,25 μ s.) and 50 subsequent traces, i.e. 2.5 mm, in the focal zone was selected. The power spectra of the subsequent traces in this region of interest were calculated, averaged and normalized with respect to a reference spectrum, i.e. the power spectrum of the reflection from a flat metal surface in the focus of the transducer. The average normalized power spectrum was integrated within the relevant frequency interval, which is restricted by the bandwidth of the emitted pulse (1-70 MHz, -20 dB level of reference spectrum).

The integrated backscatter power was calculated in corresponding regions of subsequent measurements at various angles of incidence. Of each tissue specimen 1-4 different regions of interest were selected in each available tissue type. The resulting backscatter power versus angle curves visualize the directivity of the backscatter power of the specific tissue type. Because of the Gaussian appearance of these curves, a Gaussian function was fitted to the experimental data:

$$P(\theta^*) = P_0 e^{-a_s(\theta^* - \theta_0)^2} \quad (\text{II.1})$$

In this equation θ_0 is the angle between the normal on the scan direction and the normal on the tissue specimen and θ^* is the angle position of the transducer with respect to the normal on the scan direction (Figure II.4). P_0 is the power at normal incidence, at which $\theta^* = \theta_0$. The parameters P_0 , a_s and θ_0 were estimated using the least squares method applied to the logarithmic transform of equation (II.1) (Appendix G). The parameter a_s is a measure of the directivity of the backscatter power and, as such, is a characteristic property of each tissue type. Theoretically the directivity parameter ranges from zero to infinity when going from omnidirectional to maximally directive. In practice the upper limit of the directivity parameter depends on the transducer characteristics (aperture angle) and can be determined by measuring the angle dependent reflection from a flat plate in focus. The directivity parameter a_s will be expressed in units dB/degree².

For convenient comparison of the angle dependent power curves, the power data were

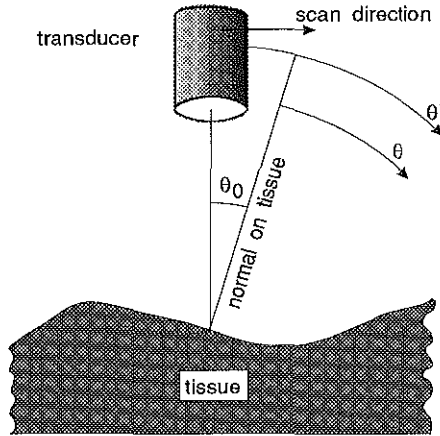


Figure II.4 Definition of angles θ^* , θ_0 and θ .

normalized with respect to the power at normal incidence P_0 , and the angles were calculated with respect to the normal on the tissue:

$$\begin{aligned} P^{norm}(\theta) &= P(\theta)/P_0 \\ \theta &= \theta^* - \theta_0 \end{aligned} \quad (II.2)$$

where P^{norm} is the normalized power and θ is the angle between the direction of the incident beam and the normal on the tissue (Figure II.4.).

Statistical analysis

Of each tissue specimen a number of paired data series (θ_i, P_i) were obtained. To each of these series the Gaussian relation of equation (II.1) was fitted. Including stochastic errors, the following relationship between P_i and θ_i was assumed:

$$\log(P_i) = \log(f(\theta_i)) + \delta_{i(p)} + \underline{\varepsilon} \quad (II.3)$$

In this equation the function f represents the Gaussian relation of equation (II.1), $\delta_{i(p)}$ is the stochastic effect of the specimen and $\underline{\varepsilon}$ represents the experimental error. It is to be realised that the experimental error contains two independent components, $\underline{\varepsilon}_1$ and $\underline{\varepsilon}_2$ ($\underline{\varepsilon} = \underline{\varepsilon}_1 + \underline{\varepsilon}_2$): the variation $\underline{\varepsilon}_1$ due to fluctuations caused by electronic and acoustic noise in

the experimental devices (pulser, transducer, pre-amplifier and receiver) and by measurement errors, and the variation ($\underline{\epsilon}_0$) generated by the 'small scale' inhomogeneities of the tissue¹⁾.

From repeated measurements on one tissue specimen after repositioning the tissue specimen the variance of $\underline{\epsilon}$ was estimated. From repeated measurements at a fixed position on one tissue specimen the variance of $\underline{\epsilon}_1$ was estimated.

In order to investigate the validity of the model, the deviations of the observed data from the Gaussian model were compared to the experimental error applying a F-test. Also a F-test was applied to investigate whether the noise level of the measurement devices was small compared to the total experimental error ($\underline{\epsilon}_1$ compared to $\underline{\epsilon}$).

If it turns out that the model provides a good approximation of the data (good in comparison with the experimental error) further statistical analysis may be carried out on the four parameters: $a_{s,tang}$ (tangential directivity), $a_{s,axial}$ (axial directivity), $P_{0,tang}$ (tangential maximum power) $P_{0,axial}$ (axial maximum power). In order to investigate whether there exist differences between different tissue types with respect to each of these four parameters, inorthogonal²⁾ variance analyses were carried out on the basis of observations from 13 tissue specimens (from 13 different persons) of which 6 different tissue types were examined.

II.3 Results

II.3.1 Qualitative evaluation

Histological examination showed that 4 of the 13 specimens were elastic arteries, and 9 were muscular arteries. The 4 elastic arteries had no atherosclerotic lesion. Of the 9 muscular arteries 3 showed an advanced atherosclerotic lesion, which precluded to perform measurements in layers below the lesion. Because of the inhomogeneous composition of

¹⁾ When a measurement at a specific position on one tissue specimen is repeated after removing and repositioning the same tissue specimen, there will be a deviation in the exact position of the region of interest with respect to the first measurement. This position inaccuracy causes deviations in the measurements due to the 'small scale' inhomogeneities in tissue.

²⁾ Inorthogonality is due to the fact that the number of particular examined tissue types and the number of measurements per tissue type was not the same for each tissue specimen.

II.3 Results

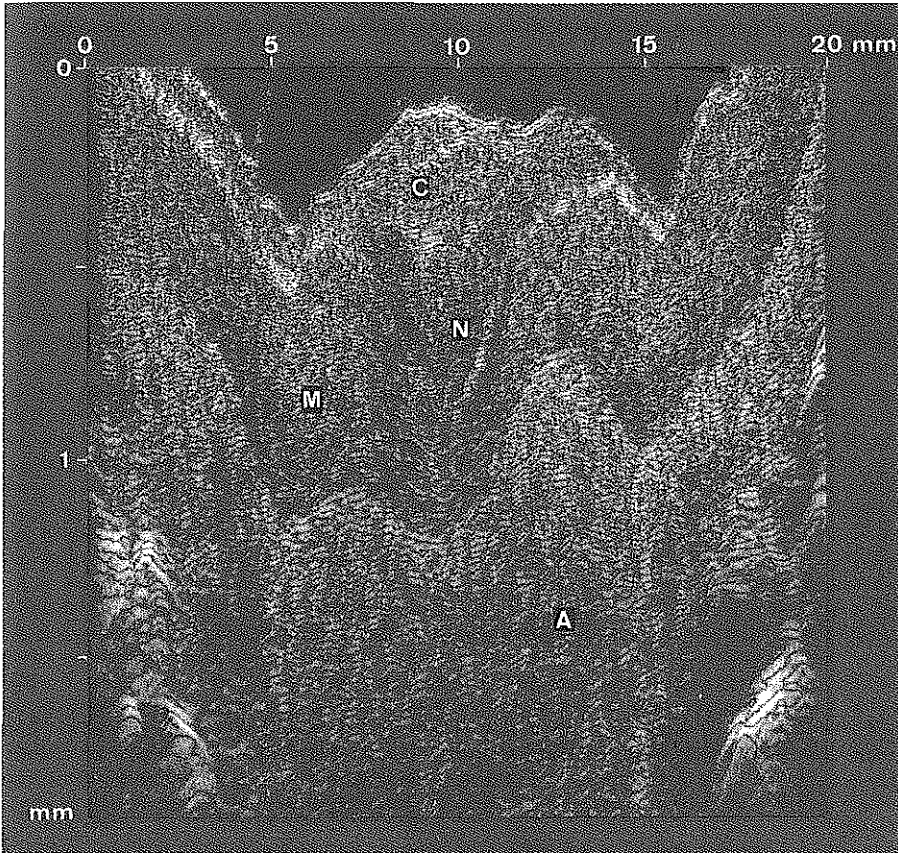


Figure II.5 B-mode image from a tangential scan of the muscular arterial wall. *M* = muscular media, *A* = adventitia, *C* = collagen cap, *N* = 'necrotic' atheroma.³⁾

the atheroma of the advanced lesions, quantitative analysis of the acoustic behaviour of³⁾ this tissue type proved very difficult. A major problem was to define criteria for selection of regions of interest. As a consequence measurements were restricted to the following tissue types: muscular and elastic media, adventitia, the elastic lamina and collagen lesions. In the histologic sections loose and dense collagen lesions were distinguished.

³⁾ Note that the picture is not displayed isometrically, which strongly exaggerates the irregularity of the surface.

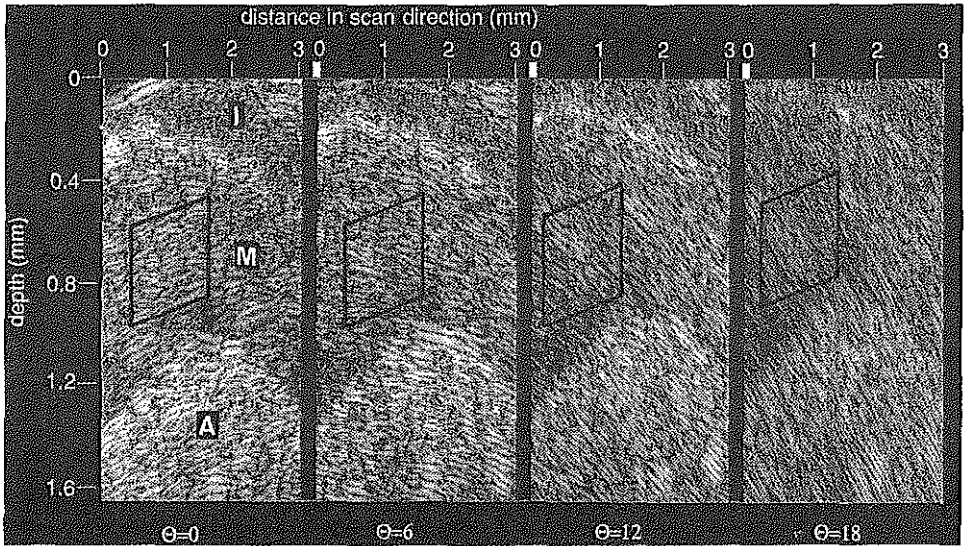


Figure II.6 Subregion of the image of Figure II.5 scanned at four different angles of incidence in the tangential plane. A region of interest in the media is indicated. *M* = muscular media, *A* = adventitia, *I* = intima.

An example of a B-mode picture of a muscular artery scanned in tangential direction is shown in Figure II.5. A subregion of the tissue specimen was scanned at various angles of incidence. The B-mode pictures resulting from scans at four different angles of incidence (0, 6, 12 and 18 degrees) are shown in Figure II.6. A decrease in grey-level in the media with increasing angle in tangential direction is observed. Results of measurements with angle variations in the axial plane on the same arterial specimen are shown in Figure II.7. Although the appearance of the B-mode picture changes with the axial angle of incidence, the average grey-level of the media seems to remain constant. The corresponding histologic sections, cut respectively perpendicular and parallel to the long axis of the artery, are shown in Figure II.8. In the tangential histologic section the long smooth muscle cells in the media can be seen. In the axial histologic section these cells are cut perpendicular to their long axis and small circular cross-sections of the cells are apparent.

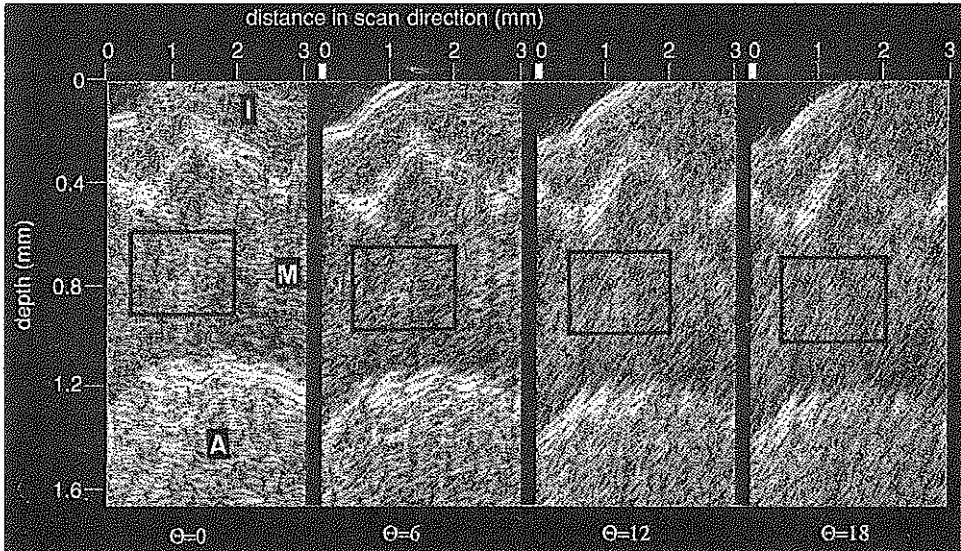


Figure II.7 The same tissue specimen as in Figure II.6, however scanned at four different angles of incidence in the axial plane. A region of interest in the media is indicated. *M* = muscular media, *A* = adventitia, *I* = intima.

II.3.2 Quantitative results

To illustrate the effect of the angle of incidence on the measured backscatter power, backscatter power versus angle curves of one measurement on a muscular media, an elastic media and a dense collagen lesion will be shown. Of the other tissue types (loose collagen lesion, external elastic lamina and adventitia) only the parameters a_s and P_0 estimated according to equation (II.1) will be given.

Muscular media

The normalized power versus angle curves in tangential and axial direction of one specimen of the muscular media are shown in Figure II.9. A change in the angle of incidence from 0 to 10 degrees in the tangential direction resulted in an almost 2 dB reduction in backscatter power from the muscular media, whereas in the axial direction no change in

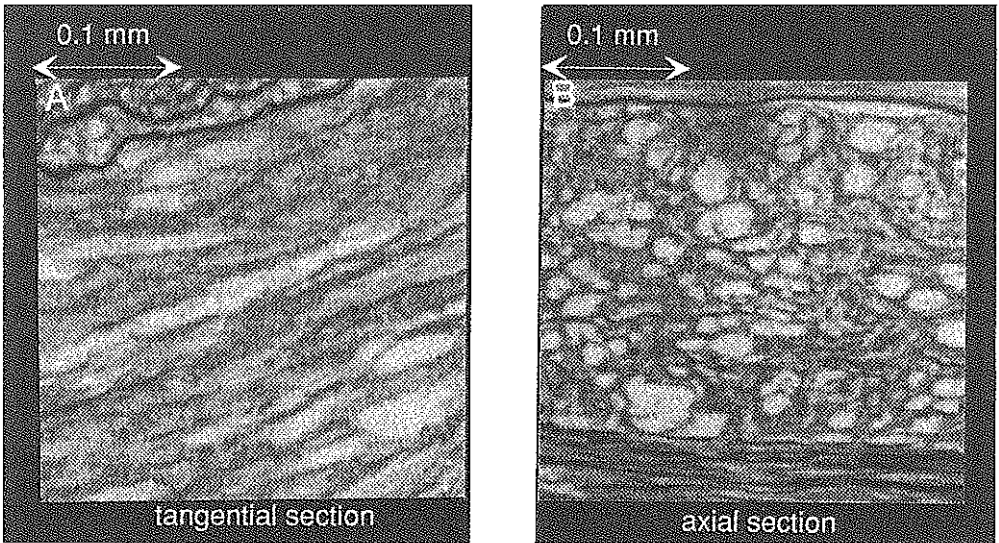


Figure II.8 Histologic sections of the ultrasonically examined muscular media of Figure II.6 and Figure II.7. A) tangential section (perpendicular to long axis of artery), B) axial section (along long axis).

backscatter power was observed. The Gaussian curve fitted to the experimental data according to equation (II.1) is also shown in Figure II.9. The assumed Gaussian curve appears to give an adequate description of the angle dependence.

Elastic media

Figure II.10 shows the same results for measurements on the media of an elastic artery. It can be seen that the backscatter of this artery had higher directivity in both scan planes than the backscatter of the muscular artery. A 5 dB decrease in backscatter power was observed at an angle of incidence of 10 degrees in tangential direction. In the axial direction a change of 10 degrees resulted in a reduction of 3 dB in backscatter power. Again the angle dependence was anisotropic: in the axial direction the decrease in backscatter was less than in the tangential direction.

Collagen lesion

Finally, the power versus angle curves of one specimen of an intimal lesion are shown in Figure II.11. The histologic sections of this specimen indicated that the lesion mainly consisted of dense collagen fibers, randomly oriented. This tissue type behaved moderately

II.3 Results

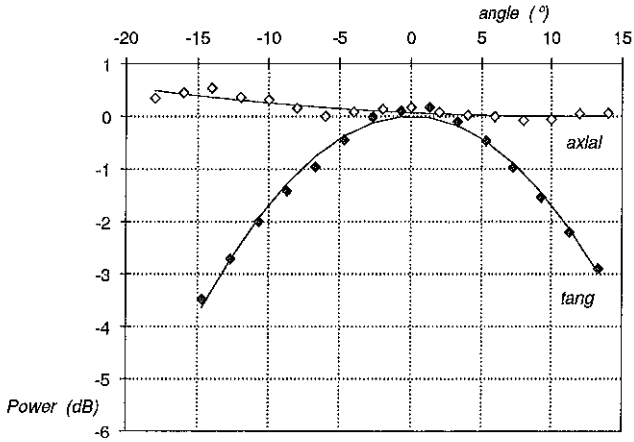


Figure II.9 Normalised power versus angle curves of one specimen of the muscular media scanned in the tangential and in the axial plane.

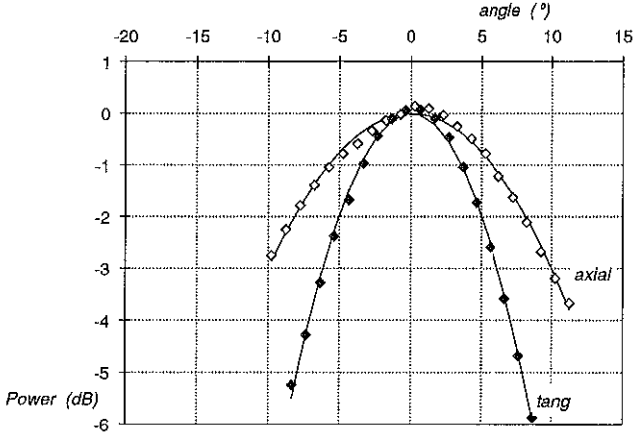


Figure II.10 Normalised power versus angle curves of one specimen of the elastic media scanned in the tangential and in the axial plane.

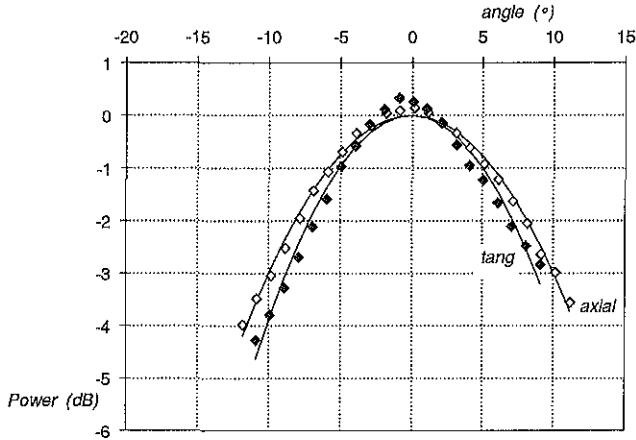


Figure II.11 Normalised power versus angle curves of a dense collagen lesion of one specimen from a tangential and an axial scan.

directive, i.e. the decrease in power was almost 3 dB for an angle variation of 10 degrees in both tangential and axial directions. No anisotropy was observed.

These observations were confirmed by measurements on other tissue specimens of the same tissue types.

Directivity and maximum power

For each measurement series of each tissue type in each tissue specimen a least squares fit to the Gaussian curve (equation (II.1)) was calculated. The calculated directivity parameter a_s and maximum power P_0 of all measurements on various tissue types are presented in Figure II.12 and Figure II.13 respectively. In these plots the calculated parameter in the tangential direction is on the horizontal axis and the corresponding axial parameter on the vertical axis. Besides the results of measurements on the muscular media, elastic media and dense collagen lesions, also results of loose collagen lesions, of the external elastic lamina and of the adventitia are shown. Note that all measurements are shown in these figures, including repeated measurements on one tissue type within one tissue specimen.

II.3 Results

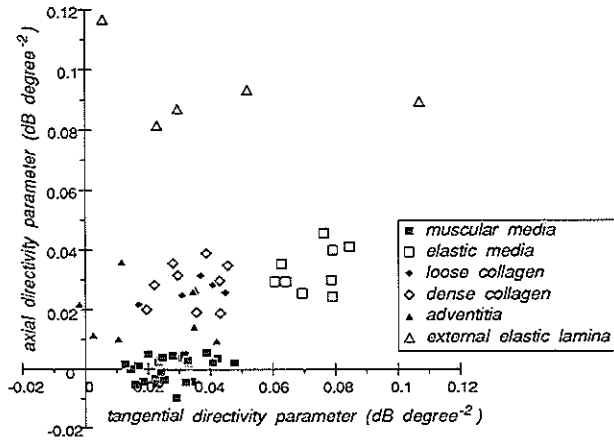


Figure II.12 Directivity parameter in tangential and axial direction of all measurements on various tissue types in thirteen tissue specimens.

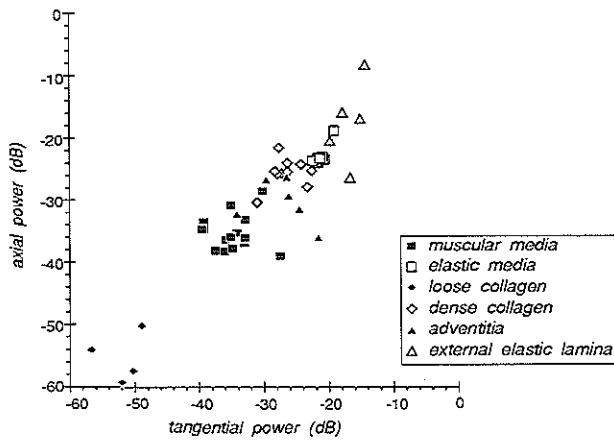


Figure II.13 Maximum power in tangential and axial direction of all measurements on various tissue types of thirteen tissue specimens.

Angle dependence of the reflection from a flat plate in the focus of the transducer was also measured. The flat plate had a directivity parameter of approximately 0.14 dB/degree², which is much larger than the directivity parameter of any arterial tissue.

From Figure II.12 it follows that the muscular media, elastic media and intima had distinct angular behaviour. No difference in the angle dependence between the dense and loose collagen lesions was observed. The angular behaviour of the adventitia and external elastic lamina could barely be discriminated from the angular behaviour of the intima. A large spread in results from the adventitia and the external elastic lamina is apparent.

It is found that the maximum power of the tissues was hardly influenced by the scan direction (Figure II.13). This is to be expected, as maximum power is the power at normal incidence and normal incidence in tangential and axial directions is, by definition, the same. The maximum power of the loose collagen lesion was the lowest, followed by the muscular media, adventitia, dense collagen lesion, elastic media, and the external elastic lamina, which had the highest maximum power. Regions of different tissue types overlap one another except for the loose collagen lesion, which had a distinctly lower maximum power than all the other tissue types.

Statistical analysis

Applying the method of analysis of variance (ANOVA) showed that the variation of $\underline{\epsilon}_1$, due to noise and measurement error is small compared to the total variation of the experimental error $\underline{\epsilon}$ ($P < 0.001$). This implies that the measurement accuracy is good enough for the purpose of this study.

Moreover it appeared that the differences between the measured values of $\log(P)$ and the estimated values based on the model were of the same order of magnitude as the variation due to the experimental error $\underline{\epsilon}$ ($P > 0.5$). This implies that the model gives an adequate description of the relation between $\log(P)$ and the angle θ . This result justifies to apply further statistical analysis to the four parameters of the model: $a_{s,tang}$ (tangential directivity), $a_{s,axial}$ (axial directivity), $P_{0,tang}$ (tangential maximum power) $P_{0,axial}$ (axial maximum power). From the repeated measurements at a fixed position on a tissue specimen it was calculated that the standard deviation due to noise and measurement error and due to the curve fitting procedure equals $2.5 \cdot 10^{-4}$ dB/degree² for the estimated directivity parameter and 0.023 dB for the estimated maximum power. The results of the ANOVA on these parameters were as follows (see also Table II.1).

II.3 Results

Table II.1 Effect of tissue specimen, tissue type and the interaction between specimen and tissue on the parameters of the model.

effect of ↓	on →	directivity parameters (a_s)	maximum powers (P_0)
tissue specimen		large ($P < 0.01$)	large ($P < 0.01$)
tissue type		very large ($P < 0.0001$)	very large ($P < 0.0001$)
interaction		not significant	large ($P < 0.01$)

For the directivity parameters $a_{s,tang}$ and $a_{s,axial}$ it was found that:

- The effect of specimen was large with respect to the experimental error ($P < 0.01$).
- There was no statistical evidence for the existence of interaction between tissue type and tissue specimen.
- The effect of tissue type was very large with respect to the experimental error ($P < 0.0001$).

For the maximum powers $P_{0,tang}$ and $P_{0,axial}$ it was found that:

- The effect of specimen was large with respect to the experimental error ($P < 0.01$).
- Interaction between tissue type and tissue specimen was significant ($P < 0.01$).
- The effect of tissue type was very large with respect to the experimental error ($P < 0.0001$).

These results indicate that the four model parameters constitute a basis for characterization of tissue types. Although there existed effects of tissue specimen (person), these were small compared to the differences between tissue types⁴.

To illustrate the spread in the data between measurements on different specimens, the mean values of the parameters were calculated from multiple measurements on each specimen per tissue type. Because the maximum power in tangential direction is, by definition, equal to the maximum power in axial direction, which is strongly supported by the observations (Figure II.13), the mean value of the maximum power is calculated from both the measured tangential and axial maximum powers. Figure II.14 gives the mean values of each specimen of the tangential and axial directivity and the maximum power per tissue type.

⁴ Separate one-way analysis for each tissue type showed that the effect of specimen is different for different tissue types.

II Angular dependence of backscatter from arterial tissue

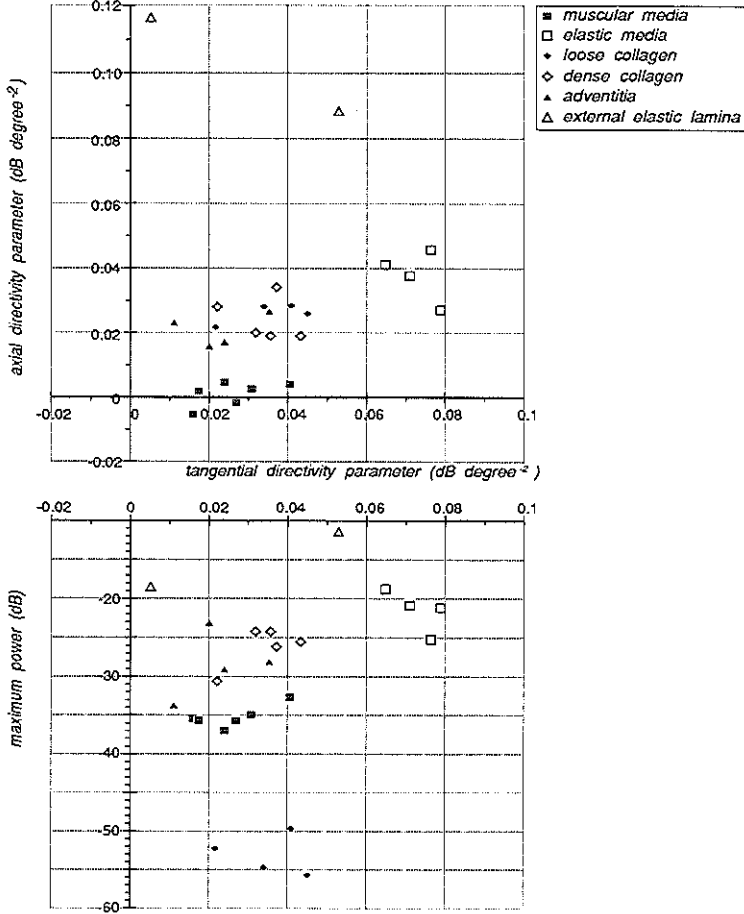


Figure II.14 Mean values per specimen of tangential and axial directivity and maximum power.

II.4 Discussion

Angle dependent behaviour of backscatter has also been reported in studies on myocardial tissue characterisation [13][15]. Picano et al. [18] specifically measured the angle dependence of the backscatter coefficient of human arterial samples with various degrees of atherosclerotic involvement at 2-10 MHz. This study however does not provide a complete picture of the influence of the angle of incidence because it was limited to the variation in the backscatter coefficient in relation to one-dimensional changes in the angle of incidence. In contrast, the experimental set-up used in the present study does provide the possibility to systematically study anisotropic materials at a variety of angles and orientations.

The data shown in Figure II.12 and Figure II.13 illustrate that each tissue type has its own characteristic angle dependent behaviour. In most cases the directivity parameter is larger than zero, which means that in the frequency range of interest (1-70 MHz) the arterial tissue does not behave like a Rayleigh scattering medium. As the directivity parameter of a flat plate is much larger, the tissue cannot be seen as a plane reflector. Probably the size of the scattering structures is in the order of magnitude of one wavelength, being 50 μm at the main frequency (30 MHz). As the axial directivity parameter of the muscular media is about zero, this tissue is likely to consist of structures of which the axial dimensions are much smaller than the wavelength.

Both the elastic and the muscular media have an anisotropic scattering nature. The anisotropic behaviour of the muscular media can be explained by the orientation of the smooth muscle cells in these layers. According to histologic studies, smooth muscle cells in the media are circularly oriented [10][21] (Figure II.8). This histologic information is in agreement with the observed anisotropy of the angle dependent backscatter.

Gussenhoven et al. [9] have reported that the echogenicity of an elastic media is higher than that of a muscular media. They hypothesized that elastic lamellae⁵⁾, which are only present in an elastic media and not in muscular media, are responsible for this increase in echogenicity. Uptill now, an anisotropic arrangement of these lamellae in the elastic media has not been observed during histologic studies. In the elastic media the muscle cells

⁵⁾ Elastic lamellae are sheetlike structures, that are parallel to the vessel wall. In the elastic media lamellae are present alternating with sheets of muscle cells. The lamellae are extensively fenestrated and interconnected by branches.

packed between the elastic lamellae have circular orientation. Maybe the explanation for the angle dependent backscatter of the elastic media and its anisotropic nature has to be found in the combination of the complex structure of the elastic lamellae with the circularly arranged muscle cells.

The collagen lesions in the intima do not display scattering anisotropy. It is assumed that thickening of the intima is a rather chaotic process, which does not lead to a dominant orientation of structures. This agrees with the observed histology of collagen lesions.

In contrast with the directivity parameter, the maximum power discriminates between loose and dense collagen lesions. A possible explanation is the difference in density of the collagen fibers, which might affect the maximum power but not the directivity.

The large spread in measured directivity and maximum power of the adventitia is probably due to its predominantly inhomogenous morphology (see Chapter I.1). The large spread in the measurements from the external elastic lamina is possibly due to its complex fenestrated structure [6]. Another explanation may be the difficulties encountered in the selection of a representative region of interest. Finally, the large shape irregularities might have caused the large spread. These shape irregularities in this originally rather plane structure arise after excision out of the body. More measurements on the external elastic lamina are necessary to achieve a satisfactory picture of the acoustic behaviour of this tissue type.

The region of interest has a certain depth with respect to the surface of the tissue. The presence of intervening tissue might influence the results, for instance if attenuation of the intervening tissue is angle dependent. This effect is expected to be relatively small for measurements on intima and media, because in these cases the intervening tissue is of minimal thickness. For the measurements on the external elastic lamina and adventitia this effect remains to be investigated. Possibly this effect causes the large spread in the measurements on these tissue types.

Variation of the angle of incidence with 10 degrees results in a decrease in backscatter power of 0 to almost 9 dB, depending on the tissue type. Superimposing this variation in backscatter power on the backscatter power at perpendicular incidence (Figure II.13) indicates that discrimination of different tissue types is not possible by considering backscatter power alone, when angle variations of this size actually occur in clinical situations.

Although the angle dependent behaviour of the backscattered signal complicates the subject of tissue characterisation, it also may open new perspectives as a means to differentiate tissue types in the arterial wall. The results of Figure II.14 suggest that discrimination between tissue types is possible, using both the directivity parameters and the maximum power. The elastic media and muscular media can be discriminated from each other and from other tissue types using the directivity parameters alone. Any overlap between adventitia and the muscular media is compensated for by the discrimination supplied by the maximum power. Loose and dense collagen lesions can be discriminated from one another using the maximum power. Obviously it seems impossible to distinguish between dense collagen lesion and adventitia. Generally, however, these structures can easily be recognized given their anatomic location. These results are that promising that it seems worthwhile to perform additional measurements, especially on the intima, external elastic lamina and adventitia, to confirm these findings.

It should be kept in mind that the present conclusions are based on in-vitro measurements. It is not necessary that similar conclusions apply to in-vivo measurements. Detailed histological investigations of the structure of the arterial wall in-vivo have established that the orientation of the smooth muscle cells in the media depends on the functional state of the vessel [6][21]. The principal orientation is perpendicular to the long axis, but a spiral structure with a 45 degrees pitch may also be present. Thus, in-vivo observations might detect another angle dependent behaviour.

For in-vivo application of the proposed discrimination procedure, the in-vivo measurement equipment has to be adapted. One can think of several changes in the measurement equipment that enable acquisition of angle dependent data. One possibility is to add two acoustic elements to the present one in the tip of the catheter, which are tilted with a fixed angle with respect to the original element. One of these elements has to be tilted in the tangential plane, the other in the axial plane. Another possibility is to perform a 2D Fourier transformation on the data in the region of interest. Yaremko [24] has shown that the 2D Fourier transformed data of a B-mode image can give information on the directivity of scattering. However, this method demands a wide aperture angle of the applied acoustic element [1][14] and averaging of at least 10 statistically independent data sets is necessary. Both mentioned techniques to obtain angle information in-vivo need further research to assess their feasibility.

II.5 Conclusion

From the results presented above it is concluded that the response of the arterial wall to ultrasound is highly angle dependent. These results reflect the morphology of the tissues. Although the angle dependent behaviour of backscattered signal complicates quantitative tissue characterisation, it may also offer new means to differentiate tissues in the arterial wall.

The directivity parameter and maximum power seem to be appropriate differentiating parameters for various tissue types in the arterial wall.

References

- [1] Berkhout A.J.: Applied seismic wave theory. Amsterdam, Elsevier 1987
- [2] Bom N., Roelandt J.: Intravascular ultrasound, techniques, developments, clinical perspectives. Kluwer Academic Publishers, 1989.
- [3] Borst C.: Percutaneous recanalization of arteries: status and prospects of laser angioplasty with modified fibre tips. *Lasers Med Sci* 2: 137-151, 1987.
- [4] Choy D.S., Stertz S., Rotterdam H.Z., Sharrock N., Kaminow I.P.: Trans-luminal laser catheter angioplasty. *Am J Cardiol* 50: 1206-1208, 1982.
- [5] De Kroon M.G.M., van der Wal L.F., Gussenhoven W.J., Bom N.: Angle dependent backscatter from the arterial wall. *Ultrasound Med Biol* 17: 121-126, 1991.
- [6] Dingemans K.P., Jansen N., Becker A.E.: Ultrastructure of the normal human aortic media. *Virchows Archiv A* 392: 199-216, 1981.
- [7] Gussenhoven W.J., Essed C.E., Fricman P., Mastik F., Lancee C., Slager C., Serruys P.: Intravascular echographic assessment of vessel wall characteristics: a correlation with histology. *Int J Card Imaging* 4: 105-116, 1989.
- [8] Gussenhoven W.J., Essed C.E., Fricman P., van Egmond F., Lancee C.T., van Kappellen W.H., Roelandt J., Serruys P.W., Gerritsen G.P., van Urk H., Bom N.: Intravascular ultrasonic imaging. Histologic and Echographic correlation. *Eur J Vasc Surg* 3: 571-576, 1989.
- [9] Gussenhoven W.J., Essed C.E., Lancee C.T., Mastik F., Fricman P., van Egmond F.C., Reiber H., Bosch H., van Urk H., van Roelandt J., Bom N.: Arterial wall characteristics determined by intravascular ultrasound imaging: an in vitro study. *J Am Coll Card* 14 (4): 947-952, 1989.

References

- [10] Haust M.D.: Atherosclerosis - Lesions and sequelae. In: Silver M.D. ed, Cardiovascular pathology, Vol II, New York: Churchill Livingstone: 191-315, 1983.
- [11] Landini L., Sarnelli R., Picano R., Salvadori M.: Evaluation of frequency dependence of backscatter coefficient in normal and atherosclerotic aortic walls. *Ultrasound in Med & Biol.* 12 (5): 397-401, 1986.
- [12] Lizzi F.L., Greenebaum M., Feleppa E.J., Elbaum M., Coleman D.J.: Theoretical framework for spectrum analysis in ultrasonic tissue characterization. *J Acoust Soc Am* 73: 1366-1373, 1983.
- [13] Madaras E.I., Perez J., Mottley J.G., Miller J.G.: Anisotropy of the ultrasonic backscatter of myocardial tissue: II. Measurements in vivo. *J Acoust Soc Am* 83(2): 762-769, 1988.
- [14] Mesdag P.R.: Estimation of medium parameters by acoustic echo measurements. Thesis, Technical University Delft, The Netherlands, Gebotekst, 1985.
- [15] Mottley J.G., Miller J.G.: Anisotropy of ultrasonic backscatter of myocardial tissue: I. Theory and measurements in vitro. *J Acoust Soc Am* 83(2): 755-761, 1988.
- [16] Pandian N.G., Kreis A., Brockway B., Inzer J.M., Sacharoff A., Boleza E., Caro R., Muller D.: Ultrasound angioplasty: realtime, two dimensional, intraluminal ultrasound imaging of blood vessels. *AM J Cardiol* 62: 493-5, 1988.
- [17] Picano E., Landini L., Distante A., Sarnelli R., Bernassi A., L'Abbate A.: Different degrees of atherosclerosis detected by backscattered ultrasound: An in vitro study on fixed human aortic walls. *J Clin Ultrasound* VII: 375-379, 1983.
- [18] Picano E., Landini L., Distante A., Salvadori M., Lattanzi F., Masini M., L'Abbate A.: Angle dependence of ultrasonic backscatter in arterial tissues: a study in vitro. *Circulation* 72(3): 572-576, 1985.
- [19] Picano E., Landini L., Lattanzi A., Salvadori M., Benassi A., L'Abbate A.: Time domain echo pattern evaluations from normal and atherosclerotic arterial walls: a study in vitro. *Circulation* 77(3): 654-659, 1988.
- [20] Potkin B.N., Bartorelli A.L., Gessert J.M., Neville R.F., Almagor Y., Roberts W.C., Leon M.B.: Coronary artery imaging with intravascular high-frequency ultrasound. *Circulation* 81: 1575-1585, 1990.
- [21] Rhodin J.A.G.: Architecture of the vessel wall. In: Bohr D.F., ed. *Handbook of Physiology*, sec.2 (The Cardiovascular System). American Physiological Society: 1-31, 1980.
- [22] Stelwagen U., Ramackers P.P.J., van't Veen P.P., van der Wal L.F.: Non-destructive evaluation of ceramics by scanning acoustic microscopy. *Non-destructive Testing Proc. 12th World Conference.* ed. J. Boogaard, G.M. van Dijk: Elsevier Scientific Publ., 1989.

- [23] Waller B.F.: 'Crackers, breakers, stretchers, drillers, scrapers, shavers, burners, welders and melters' - the future treatment of atherosclerotic coronary artery disease? A clinical-morphologic assessment. *J Am Coll Cardiol* 13: 969-987, 1989.
- [24] Yaremko M., Lizzi F.L., Fecleppa E.J., Coleman D.J., King D.L.: Two-dimensional power spectrum analysis for ultrasonic tissue characterization. *IEEE Ultrasonics Symposium*: 933-936, 1986.

III BACKSCATTER BEHAVIOUR OF HUMAN BLOOD: CHANGES IN ECHOGENICITY DURING THE CARDIAC CYCLE

As partly been published in:

De Kroon M.G.M., Slager C.J., Gussenhoven W.J., Serruys P.W., Roelandt J.R.T.C., Bom N.: Cyclic changes of blood echogenicity in high-frequency ultrasound. *Ultrasound Med Biol* 17: 723-728, 1991.

Abstract

The effect of the high echogenicity of blood on the visualization of the luminal border using a 30 MHz intravascular ultrasonic imaging device is demonstrated. Also a survey from literature of the acoustic properties of blood is given. Hematocrit, red blood cell aggregation, deformation and orientation of red blood cells, are known to have influence on the backscatter properties of blood in the frequency range of 1-15 MHz. The relatively high echogenicity of blood with respect to the echogenicity of tissue observed at 30 MHz, is not reported at these lower frequencies. Furthermore, it is known that in the low frequency range (1-15 MHz) blood echogenicity is influenced by the local shear rate: a decreasing shear rate results in an increased echogenicity. Because red blood cells aggregate at decreasing shear rate and the aggregates disperse when the shear rate increases, it is assumed that the shear rate dependent state of aggregation causes the observed changes in echogenicity.

The echogenicity of blood, imaged with an intravascular ultrasonic imaging device (30 MHz), was measured during the cardiac cycle in three patients. Cyclic changes of the blood echogenicity synchronous with the changes in blood pressure were observed. The results suggest that these variations were related to changes in the state of red blood cell aggregation, which are induced by the varying shear rate during the cardiac cycle.

III.1 Introduction

The resolution of intravascular ultrasound imaging devices has recently been improved by the increase of the frequency from 20 MHz to 30 MHz [5]. However with the increase of the frequency the echogenicity of blood increased with respect to the tissue echogenicity [5] and thus the visualization of the luminal border is limited [17][18]. This is illustrated in Figure III.1, which shows two cross-sectional images of a human superficial femoral

artery obtained in-vivo with a 30 MHz intravascular imaging device (DUMED, Rotterdam, The Netherlands). In Figure III.1A the lumen is filled with blood, while the image in Figure III.1B was taken after saline was injected in the artery. The intima, which can clearly be observed in the saline-filled artery, cannot be discriminated from the blood in the blood-filled artery. To enhance discrimination between lumen and arterial wall in the images of the 30 MHz ultrasound imaging device, investigation of the backscatter properties of human blood at high frequency might be useful.

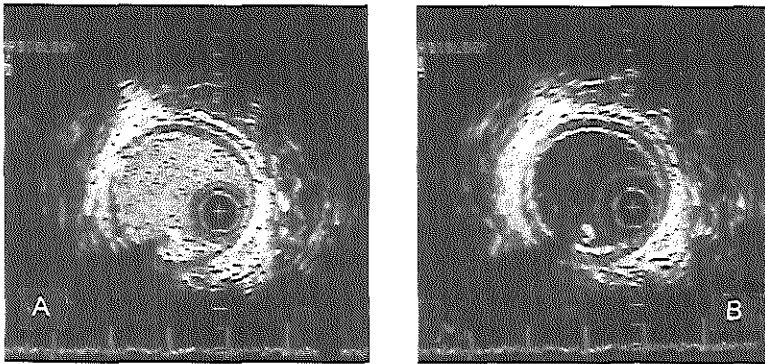


Figure III.1 Cross-sectional images of human superficial femoral artery in-vivo obtained with a 30 MHz intravascular imaging device. A) lumen filled with blood, B) lumen filled with saline solution. Bright spot with shadow is caused by guidewire.

Since it is commonly assumed that red blood cells (RBCs) are responsible for the acoustic scatter properties of blood, it is desirable to study the behaviour of RBCs under various flow conditions. In the past several measurement techniques have been used to assess the behaviour of RBCs under various flow conditions. Among these, the most important measurement techniques are viscosity measurement [8][11][30][33], optical measurement techniques (light reflection measurements [6][9][20][45], light transmission measurements [31][32], viewing and filming the motions of the individual RBCs using a microscope [14][24][28][30][32][35] and laser-doppler technique [1][2]) and finally acoustic backscatter measurements [3][36][38][39][41][43][47][48][49]. The relevant results on blood properties obtained with these techniques will be summarized in paragraph III.2.

III.1 Introduction

Studies so far only deal with the acoustic properties of blood under stationary flow conditions. In-vivo, blood flow is pulsatile and backscatter behaviour of blood may change during the cardiac cycle. The study reported in paragraph III.3 demonstrates the changes during the cardiac cycle in acoustic behaviour of flowing blood in-vivo at high frequency (20 - 40 MHz). In the last paragraph a simplified mathematical description of sound scattering is given, which may explain the observed increased echogenicity of blood with respect to tissue for increased frequency.

III.2 Behaviour of blood under various flow conditions

Red blood cell aggregation

Aggregation of RBCs is a process, where red blood cells stick to each other due to the presence of certain macromolecules in plasma [7][25][34]. These macromolecules (fibrinogen and γ -globulin) adhere to the surface of the RBCs, thus acting as bridging molecules. In static blood (shear rate is zero), the aggregation is maximal, so large, branching networks are formed [29]. Applying shear stress causes these complex aggregates to disperse into smaller unbranched aggregates, called rouleaux. An equilibrium between the adhering forces between RBCs and shear forces results in an average rouleau size. At high shear rates only single RBCs are present. According to Goldsmith [13] rouleaux and also single RBCs tend to align to the applied shear stress.

It has been shown [20][48] that, besides shear rate and fibrinogen concentration, also temperature, acid number, osmotic pressure and Hematocrit influence the state of aggregation. Increasing temperature or increasing Hematocrit enhances aggregation. Also the aggregate size increases with increasing acid number. And if osmotic pressure is too low, no aggregation takes place.

Transit times between different states of aggregation are characterized by the half-time of aggregation. Jansonius et al. [20] determined the half-time of aggregation by measuring the light reflection of blood (syllectometry). According to his measurements, the half-time of aggregation is approximately 10 seconds in whole blood (HTC of 40%). Schmid-Schonbein et al. [31][32] used a light transmission technique to determine the half-time of aggregation. They reported an aggregation half-time of 3.5 seconds of blood of normal patients. However, frequently they observed two different half-time constants: a short one in the range of 0.5-1.5 seconds and the conventional one of 3.5 seconds. It was also noted

that the half-time of aggregation increases strongly with decreasing RBC concentration.

Blood viscosity

Caro et al. [8] deduced the behaviour of RBCs under various flow conditions from the results of viscosity measurements. Although blood plasma behaves like a Newtonian fluid⁹, i.e. the viscosity does not depend on the applied shear stress, they found that the presence of RBCs causes the viscosity of blood to change with the applied shear stress. Only for high shear stresses ($> 1000 \text{ s}^{-1}$), when the RBCs are deformed into ellipsoids, blood behaves Newtonian. With decreasing shear stress an increase of the viscosity was observed (shear thinning). It was assumed that shear thinning in blood is mainly caused by aggregation of RBCs.

Also the viscosity of blood in an oscillating (sinusoidal) flow was investigated [11]. It appeared that at an oscillating frequency of 1 Hz and lower, the viscosity is influenced by the state of aggregation of RBCs. For higher frequencies no effect of aggregation on viscosity was observed.

Tube flow

Since shear rate is found to have influence on the state of aggregation, it is interesting to evaluate the velocity profile in arteries (tube flow), from which the shear rate can be deduced.

For a Newtonian fluid, the velocity profile of a stationary non-turbulent flow in a tube is a parabola (Poiseuille flow). Because in blood the viscosity increases with decreasing shear stress, the velocity profile is flattened, resulting in what is usually called a *plug-flow* [4][16]. This flattening is even enhanced by the fact that RBC concentration is lower near the tube wall than in the center of the flow [2][16][26].

Acoustic properties of blood

The echogenicity of flowing blood may depend on several factors: concentration of RBCs [38][40][48], which may vary across the arterial lumen [1][2][15], deformation and alignment of RBCs and their shear rate dependent state of aggregation [3][21][41][42][43], and the ultrasound frequency [36][49].

⁹ For a Newtonian fluid the shear force per unit area (= shear stress) is linearly proportional to the negative of the velocity gradient.

III.2 Behaviour of blood under various flow conditions

Shung et al. [36][38][39][40] and Yuan et al. [48][49] measured the backscatter intensity of RBCs in a Ringer's solution at varying Hematocrit values and varying ultrasound frequencies (5-15 MHz). Their results show that the prepared RBC-solution followed Rayleigh's scattering theory for small particles, i.e. the backscatter intensity increased with the fourth power of the ultrasound frequency. They also reported that the backscatter intensity increased with increasing Hematocrit up to peak values in the Hematocrit range of 17 - 24%. At higher Hematocrit values backscatter intensity decreased.

These measurements however were carried out under conditions that aggregation of RBCs was prevented, due to the Ringer's solution. Sigel et al. [43][42] showed that blood echogenicity at 10 MHz was influenced by the local shear rate and that a decreasing shear rate resulted in an increased echogenicity. Because red blood cells aggregate at decreasing shear rate and the aggregates disperse when the shear rate is increased, he assumed that the shear rate dependent state of aggregation caused the changes in echogenicity. This was confirmed by several other observations showing increased echogenicity at decreasing shear rate [3][22][41][48].

III.3 Measurements of blood echogenicity in-vivo: case study

III.3.1 Materials and methods

Intravascular ultrasound system

By mechanical rotation of a 30 MHz single element transducer (16 rotations per second) mounted in the tip of a 5F catheter, real-time cross-sectional images of the arterial lumen and the vessel wall were obtained [5]. During one rotation 400 pulse-echo measurements were performed. Time-dependent gain was applied on each received signal to compensate for attenuation. The signals were demodulated, logarithmically amplified, and digitized (8 bits). Finally they were transmitted to a digital scan converter and circularly displayed in video format with 256 grey-levels at 50 fields per second and registered on videotape. Both the ECG and the pressure in the catheterized artery were simultaneously recorded and superimposed on the video images. In Figure III.2 a schematic diagram of the imaging device is depicted.

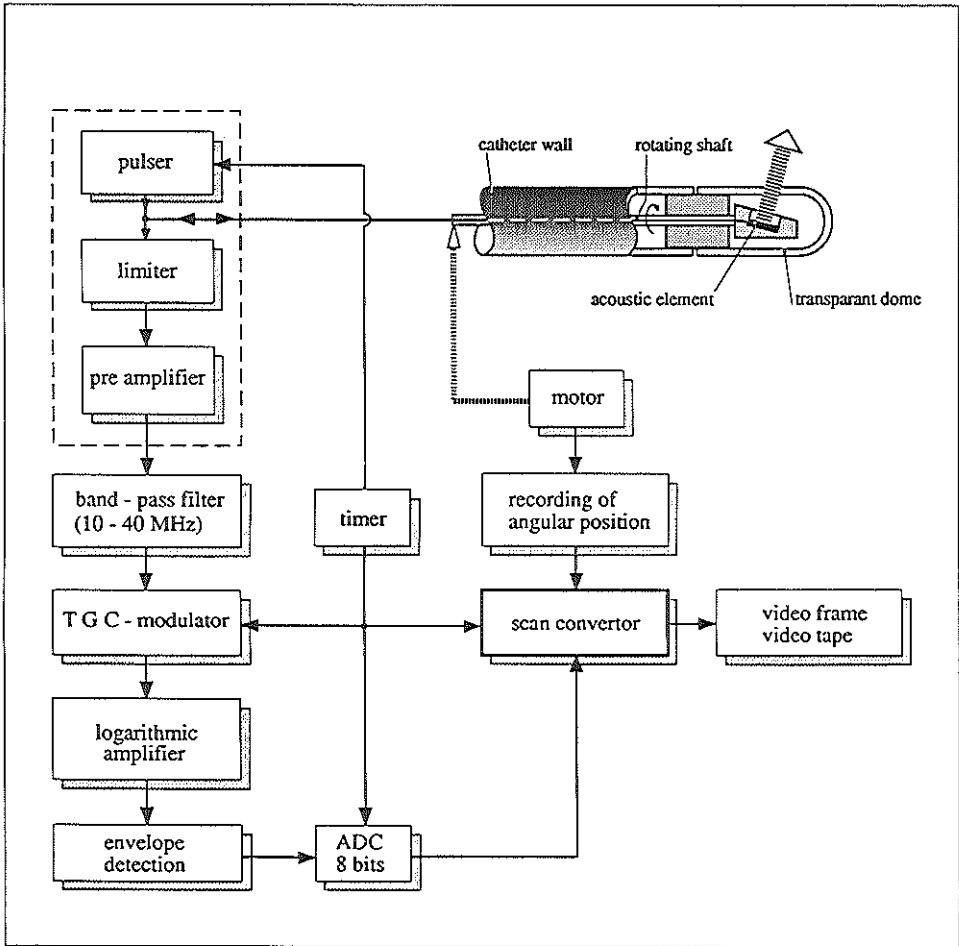


Figure III.2 Experimental set-up and data acquisition and imaging scheme of intravascular ultrasonic imaging device.

Catheterization procedure

Three patients, who underwent diagnostic coronary angiography, were asked to participate with the intravascular ultrasound study. For this purpose the femoral artery was punctured routinely and a 9F-sheath was introduced prior to the routine coronary angiography. The

intravascular catheter was positioned in the iliac artery via the sheath.

The system gain of the imaging device was kept constant during the period in which data were analysed. However, gain setting might be changed between subsequent catheterisations. The Hematocrit values of the blood of the three patients varied between 38 % and 43 %.

Qualitative evaluation

The evaluation of the acoustic behaviour of blood was only performed at locations, where the lumen was not visibly obstructed by intimal thickening. The video images of the three patients were visually evaluated. The added pressure signal on the video images provided a time reference. Slowly running the tape facilitated accurate assessment.

Quantitative evaluation

A video-densitometric [44] system was used to quantify the blood echogenicity. This system digitized the video signal and calculated the echodensity, defined as the average grey level, within a selected region in a video image. The video top-white was defined as 256 and none of the signals exceeded this value.

Three regions of interest were selected in the lumen of the arterial cross section: one region close to the arterial wall (region 1), one in the center (region 2) and one near the catheter (region 3). The echodensity was computed in consecutive frames of a recording at a fixed catheter position. This analysis was applied to the arterial images of each patient during three cardiac cycles. The variable gain setting implied that comparison of the absolute grey levels between the three patients is not meaningful. The computed echodensity only gave information on the relative changes in the acoustic behaviour of blood.

III.3.2 Results

When visually analyzing the video images, a cyclic variation of blood echodensity synchronous with the cardiac cycle was observed. During diastole the echodensity increased and immediately after the rise of the arterial pressure (in early systole) the echodensity decreased. This is illustrated in Figure III.3, in which cross sectional images of an artery at end diastole and end systole of patient #1 are shown.

In Figure III.4A the selected regions of the video-densitometric measurements of patient #1 are indicated. The calculated echodensity in these regions as a function of time and the

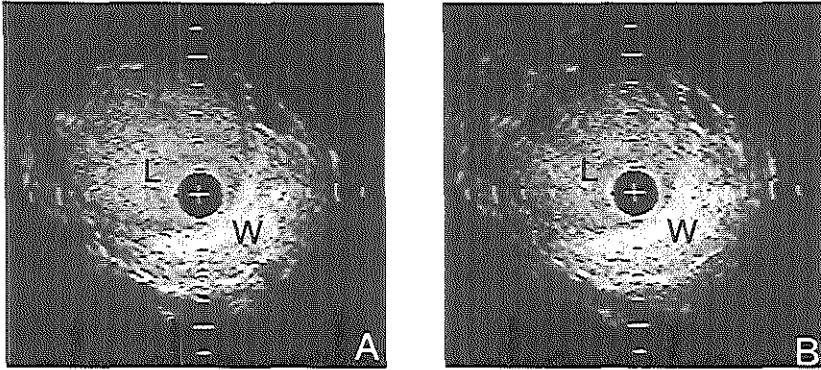


Figure III.3 B-mode picture of the iliac artery at end diastole (A) and end systole (B). L: lumen; W: arterial wall.

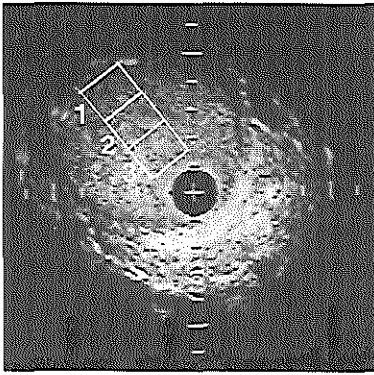
simultaneously recorded intra-arterial pressure are presented in Figure III.4B.

The density-versus-time plot (Figure III.4B) indicates that the variations in the blood echodensity closely followed the pressure changes during the cardiac cycle: echogenicity increased during diastole and decreased rapidly at early systole.

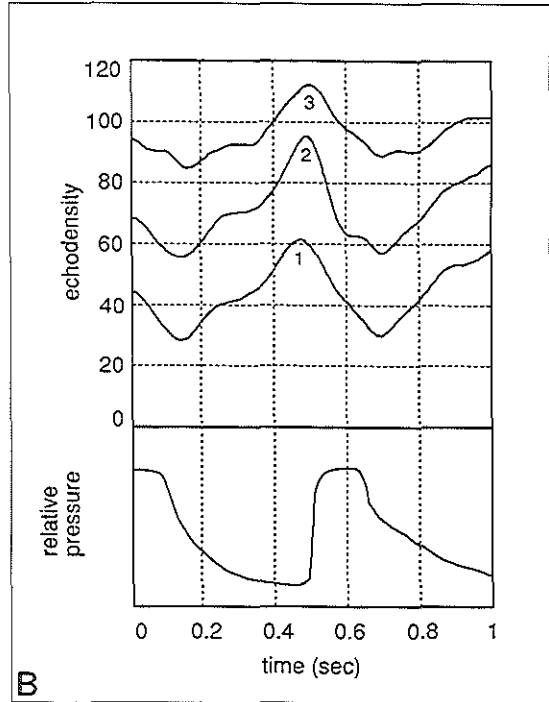
In Figure III.5 the measured echodensity of all three patients at end diastole and at end systole are given. Note that the grey-level is a logarithmically scaled quantity and that absolute variations in grey-level are related to relative changes in intensity.

Care must be taken in mutually comparing the absolute values of the three selected regions, because the echodensity was also affected by the distance to the transducer. Attenuation, geometric spreading of the sound wave and the time dependent gain caused distance dependent echodensity variations.

III.3 Measurements of blood echogenicity in-vivo: case study



A



B

Figure III.4 A) Selected regions in the lumen, in which the echodensity was calculated; B) Measured echodensity in the indicated regions and the relative blood pressure in the catheterized artery as a function of time.

III.3.3 Discussion.

As described in Chapter III.2 the echogenicity of flowing blood may depend on several factors, among which the concentration of RBCs, the deformation and alignment of RBCs, the shear rate dependent state of RBC-aggregation and the ultrasound frequency.

Elongation and alignment of RBCs

Although the elongation of RBCs and their alignment to the flow direction might have some influence on the echogenicity of blood, these features alone cannot explain the observed

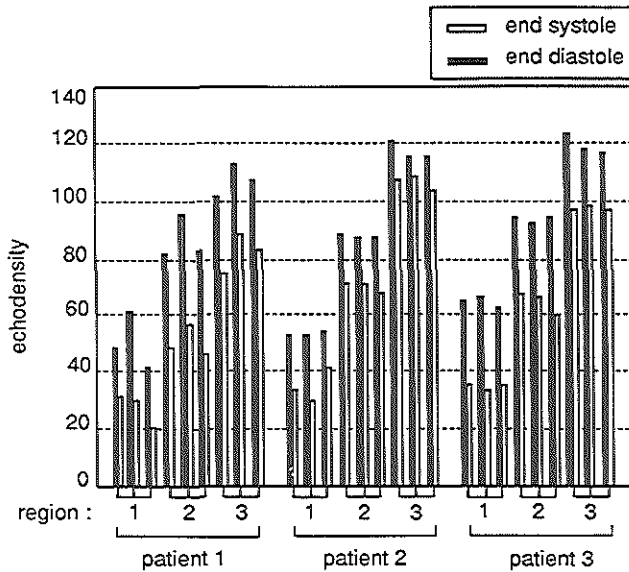


Figure III.5 Measured echodensity averaged over three regions in the lumen of three parts (1-3) in the video recording of three patients. Density is given at end diastole and end systole of the three analyzed cardiac cycles.

cyclic variations of the echodensity [14][46]. Alignment of RBCs would enhance echodensity during systole, which is not in accordance with the results presented here.

RBC aggregation

From the pressure curve, the arterial flow rate curve can be estimated (gradient of the pressure curve). The echodensity seems to follow the inverse of the expected flow rate curve rather than the pressure curve. This might indicate that the cyclic echodensity variation is a flow related phenomenon. It is supposed that the flow related phenomenon that caused the changes in echodensity is the shear rate dependent state of aggregation of RBCs. During diastole the decreasing blood flow velocity resulted in lower shear rates, enabling the formation of new and longer aggregates. This supposedly caused the increase in echodensity during diastole. At early systole, the higher shear rates break down the aggregates, which would explain the decrease in echodensity. So far, observations with

III.3 Measurements of blood echogenicity in-vivo: case study

ultrasound of fast changes in the state of aggregation have not been reported. The measured half-time of aggregation [31][32] suggests that one second may be sufficient to detect changes in the state of aggregation. Moreover, applying higher frequency (30 MHz) than in conventional ultrasonography (2.5-5 MHz) allows the observation of smaller aggregates. Because the development of aggregates depends on casual collision of RBCs, small aggregates are probably formed faster than larger ones.

Also the shape and orientation of the aggregates may influence echogenicity. Under shear only unbranched aggregates, called "rouleaux", are present [10]. According to Goldsmith [13], these rouleaux align to the direction of the flow. The specific shape of rouleaux and their alignment may play an important additional role in explaining the echogenicity of flowing blood. Higher echogenicity will be observed when the direction of the sound wave is perpendicular to the alignment of the rouleaux. In the present study the direction of the sound wave is almost perpendicular to the rouleaux alignment, which is a good condition to measure the supposed effect of aggregation on echogenicity of blood.

Conclusion

The findings of this study support the hypothesis that cyclic variations in RBC aggregation, as a result of the changing shear rates during the cardiac cycle, influence the blood echogenicity. However, control experiments are necessary to rule out other explanations.

III.4 Evaluation

As mentioned in the introduction, the previous study was performed in persuance of the relatively high echogenicity of blood, which was observed in-vivo at 30 MHz. In the previous paragraphs several features influencing blood echogenicity were discussed. However these features do not give a direct explanation why at 30 MHz blood has the same level of echogenicity as tissue, while at lower frequencies (< 10 MHz) tissue echogenicity is considerably higher. The simplified mathematical model for the scattering process described below might help to understand this phenomenon.

Morse and Ingard [27] gave an expression for the total power Π_s scattered by a sphere in a plane incident wave field:

$$\Pi_s \approx \begin{cases} \frac{256 \pi^5 a^6 f^4}{9 c^4} I_0 & \text{for } a < \lambda/2\pi \\ 2 \pi a^2 I_0 & \text{for } a > \lambda/2\pi \end{cases} \quad (\text{III.1})$$

in which a is the sphere radius, f is the acoustical frequency, I_0 is the intensity of the incident pressure field, c is the sound propagation velocity and λ is the wavelength. Although this expression cannot be applied to a sphere with a diameter in the order of magnitude of the wavelength, it gives a rough indication of the frequency and size dependence of scattered power.

Figure III.6 shows the frequency dependence of the scattered power according to equation (III.1) for various sphere radii. In the frequency range where the sphere diameter has the order of magnitude of the wavelength, i.e. around the point $a = \lambda/2\pi$, these curves only give

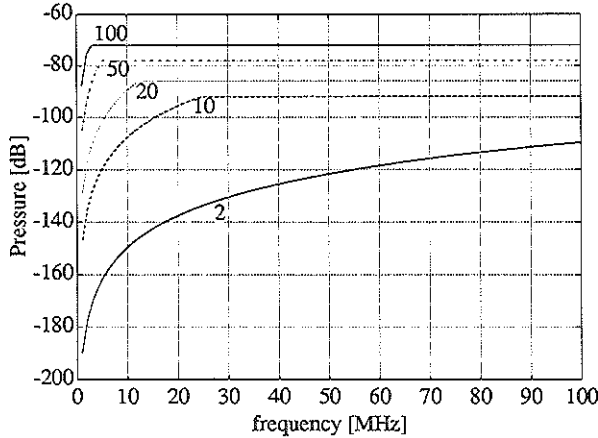


Figure III.6 Total power scattered by a sphere as a function of the frequency, for various radii (2, 10, 20, 50, 100 μm), according to equation (III.1).

III.4 Evaluation

a rough indication of the power scattered by a sphere. Both the scattering by tissue and by blood can roughly be described by one of these curves. However, the relative change with frequency of the blood echogenicity with respect to the tissue echogenicity, observed in-vivo, cannot be explained with these curves, regardless whether RBCs aggregate or not. In the following several hypothetical situations are considered, for which this relative change can be understood.

As a starting-point it is assumed that the blood scatterers are smaller than the tissue scatterers, and so the curves of Figure III.7A might apply. Though these curves show a

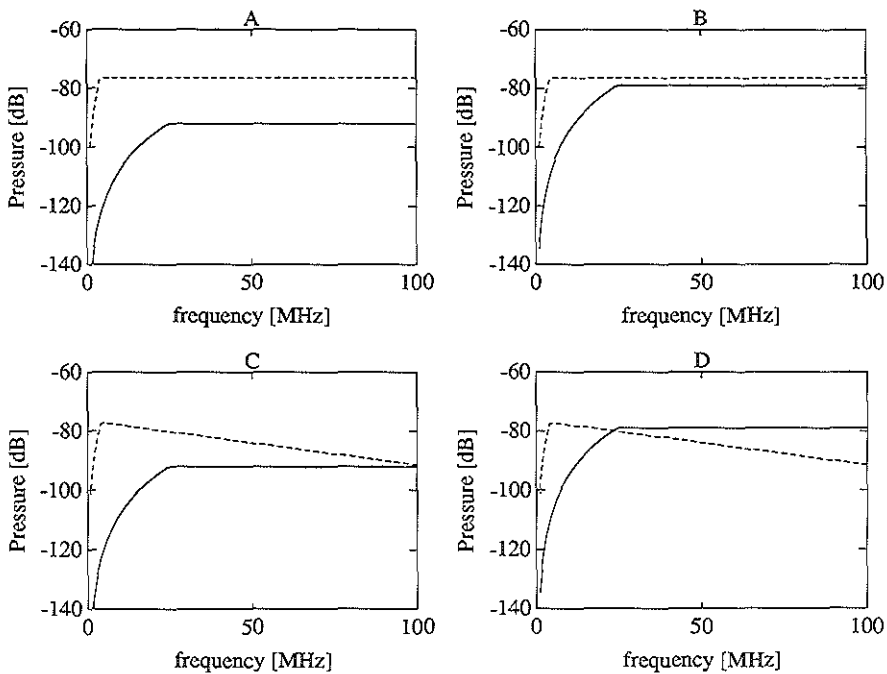


Figure III.7 Total power scattered by tissue (dashed line) and blood (solid line) (simplified model); A) blood and tissue have same reflectivity; B) increased reflectivity of blood scatterers; C) tissue pressure is attenuated; D) B and C combined.

decrease in the difference in echogenicity between tissue and blood for increasing frequency, obviously the tissue echogenicity remains substantially higher than the echogenicity of blood. For these curves the same reflectivity of blood and tissue scatterers is assumed, which is probably not realistic. If the reflectivity of red blood cells in plasma is higher than the reflectivity of the scattering tissue cells in their surrounding medium, the blood curve will be lifted with respect to the tissue curve. The blood curve also has to be lifted if the volume concentration of scatterers in blood is higher than in tissue. The echogenicity curves of Figure III.7B, give an indication of the possible result. It is obvious that for this situation the echogenicity of blood with respect to tissue is relatively small at low frequency, while it has the same order of magnitude at higher frequencies. Another phenomenon, which might change the relative echogenicity with frequency, is frequency dependent attenuation [19]. For this moment it is assumed that in the clinical application the propagation path of the ultrasound scattered by tissue is longer than the propagation path of sound scattered by blood. Applying higher attenuation to the backscatter pressure from tissue than from blood on the original echogenicity curves of Figure III.7A, one might obtain the curves as indicated in Figure III.7C. It follows that, thanks to the difference in attenuation, the blood and tissue curves can cross each other, and so the echogenicity of blood with respect to the tissue echogenicity increases with frequency. Combining the effect of reflectivity (Figure III.7B) and the effect of attenuation (Figure III.7C), which results in the echogenicity curves of Figure III.7D, gives an even stronger relative echogenicity change with frequency.

Of course, a more extensive quantitative analysis and corresponding experiments are required to validate the rather qualitative explanation given here. This analysis should also take into account the aggregation of red blood cells and their influence on the frequency dependent backscatter from blood.

References

- [1] Aarts P.A.M.M.: The role of hemodynamic factors in the interaction of blood platelets with the vessel wall. Thesis, University of Utrecht, The Netherlands, 1985.

References

- [2] Aarts P.A.M.M., van den Broek S.A.T., Prins G.W., Kuiken G.D.C., Sixma J.J., Heethaar R.M.: Blood platelets are concentrated near the wall and red blood cells in the center of flowing blood. *Arteriosclerosis* 8(6): 819-824, 1988.
- [3] Beitler J.C., Sigel B., Machi J., Justin J.R.: The effect of temperature on blood flow echogenicity in vitro. *J Ultrasound Med* 2: 529-533, 1983.
- [4] Bird R.B., Stewart W.E., Lightfoot E.N.: *Transport phenomena*. John Wiley & Sons, 1960.
- [5] Bom N., ten Hoff H., Lancée C.T., Gussenhoven W.J., Bosch J.C.: Early and recent intraluminal ultrasound devices. *Intravascular Ultrasound, techniques, developments, clinical perspectives*. Ed.: N. Bom, J. Roelandt. Kluwer Academic Publishers: 78-88, 1989.
- [6] Brinkman R., Zijlstra W.G., Jansonius N.J.: Quantitative evaluation of the rate of rouleaux formation of erythrocytes by measuring light reflection ("syllectometry"). *Medicine*: 234-248, January 1963.
- [7] Brooks D.E., Greig R.G., Janzen J.: *Mechanisms of erythrocyte aggregation, Erythrocyte mechanics and blood flow*. Edited by Cokelet G.R., Meiselman H.J., Brooks D.E. New York, Alan R Liss Inc: 119-140, 1980.
- [8] Caro C.G., Pedley T.J., Schroter R.C., Seed W.A.: *The mechanics of the circulation*. Oxford, University Press. 1978.
- [9] Chabanel A., Samama M.: Evaluation of a method to assess red blood cell aggregation. *Biorheology* 26: 785-797, 1989.
- [10] Charm S.E., Kurland G.S.: *Blood flow and Microcirculation*. Wiley New York: Chapter 2 (Blood viscosity): 23-63, 1974.
- [11] Chien C.: *Blood rheology. From: Quantitative cardiovascular studies*, Ed.: Hwang N.H.C., Gross D.R., Patel D.J., Baltimore, University Park Press: 241-287, 1979.
- [12] De Kroon M.G.M., Slager C.J., Gussenhoven W.J., Serruys P.W., Roelandt J.R.T.C., Bom N.: Cyclic changes of blood echogenicity in high-frequency ultrasound. *Ultrasound in Med Biorheology* 17 (7): 723-728, 1991.
- [13] Goldsmith H.L., Mason S.G.: The flow of suspensions Through Tubes I. Single spheres, rods and discs. *J Colloid Sci* 17: 448-476, 1962.
- [14] Goldsmith H.L.: Deformation of human red cells in blood flow. *Biorheology* 7: 235-242, 1971.

- [15] Goldsmith H.L.: The flow of model particles and blood cells and its relation to thrombogenesis. In spaet T.H. (ed.). *Progress in hemostasis and thrombosis 1*: 97-139, Grunc and Stratton New York, 1972.
- [16] Goldsmith H.L., Karino T.: Physical and mathematical models of blood flow: experimental studies. From: *Erythrocyte dynamics and blood flow*. Ed.: Cokelet G.R., Meiselman H.J., Brooks D.E., New York, Alan R Liss Inc: 165-194, 1980.
- [17] Gussenhoven W.J., Essed C.E., Frietman P., Egmond van F., Lancée C.T., Kapellen van W.H., Roelandt J., Serruys P.W., Gerritsen G.P., Urk van H., Bom N.: Intravascular Ultrasound imaging: Histologic and echographic correlation. *Eur J Vasc Surg* 3: 571-576, 1989.
- [18] Gussenhoven W.J., Essed C.E., Lancée C.T., Mastik F., Frietman P., Egmond van F.C., Reiber J., Bosch H., Urk van H., Roelandt J., Bom N.: Arterial wall characteristics determined by intravascular ultrasound imaging: An in-vitro study. *J Am Col Card* 14(4): 947-952, 1989.
- [19] Hill C.R., Bamber J.C., ter Haar G.T., Dickinson R.J., Fish P.J., Miller E.B.: *Physical principles of medical ultrasonics*. Chichester, Ellis Horwood, 1986.
- [20] Jansonius N.J. , Zijlstra W.G.: Various factors influencing rouleaux formation of erythrocytes studied with the aid of syllectometry. *Proc Kon Ned Akad Wet (Zeries C)* 68: 121-127, 1965.
- [21] Jeffery G.B.: The motion of ellipsoidal particles in a viscous fluid. *Proc Roy Soc London* 102: 161-179, 1922.
- [22] Kallio T., Alanen A.: A new ultrasonic technique for quantifying blood echogenicity. *Investigative Radiology* 23: 832-835, 1988.
- [23] Machi J., Sigel B., Beitler J.C., Coelho J.C.U., Justin J.R.: Relation of in vivo blood flow to ultrasound echogenicity. *J Clin Ultrasound* 11: 3-10, 1983.
- [24] McMillan D.E., Utterback N.G., Lee M.M.: Red cell slide as they form doublets and deform in rouleaux. *Biorheology* 26: 899-906, 1989.
- [25] Meiselman H.J.: Measures of blood rheology and erythrocyte mechanics, Erythrocyte mechanics and blood flow. Ed.: Cokelet G.R., Meiselman H.J., Brooks D.E., New York, Alan R Liss Inc: 75-117, 1980.
- [26] Mellema J., Blom C.: Rheology, its basic concepts. *NVKC* 15(3): 78-83, 1990.
- [27] Morse P.M., Ingard K.U.: *Theoretical acoustics*. Princeton University Press, Princeton, 1968.

References

- [28] Neumann F.J., Schmid-Schönbein H., Ohlenbusch H.: Temperature dependence of red cell aggregation. *Pflügers Arch* 408: 524-530, 1987.
- [29] Samsel R.W., Perelson A.S.: Kinetics of rouleau formation: I A mass action approach with geometric features. *Biophys J* 37: 473-514, 1982.
- [30] Schmid-Schonbein H., Gachtgens P., Hirsch H.: On the shear rate dependence of red cell aggregation in-vitro. *J Clin Inv* 47: 1447-1454, 1968.
- [31] Schmid-Schonbein H., Kline K.A., Heinrich L., Volger E., Fischer T.: Microrheology and light transmission of blood. III: The velocity of red blood cell aggregation. *Pflügers Arch* 354: 299-317, 1975.
- [32] Schmid-Schonbein H., Gallasch G., v.Gosen J., Volger E., Klose H.J.: Red cell aggregation in blood flow. I: New methods of quantification. *Klin Wschr* 54: 149-157, 1976.
- [33] Schmid-Schonbein H., Volger E., Kieseewetter H., Dauer U., Heilmann L.: New hemorheological techniques for routine laboratory. *Clinical Hemorhology* 2: 99-105, 1982.
- [34] Schmid-Schonbein H., Malotta H., Striesow F.: Erythrocyte aggregation: causes, consequences and methods of assesment. *NVVC* 15(3): 88-97, 1990.
- [35] Shiga T., Imaizumi K., Harada N., Sekiya M.: Kinetics of rouleaux formation using TV image analyzer. I. Human crythrocytes. *Am J Physiol* 245: 252-258, 1983.
- [36] Shung K.K., Sigelmann R.A., Reid J.M.: Scattering of ultrasound by blood. *IEEE Trans Biomed Eng* 23(6): 460-467, 1976.
- [37] Shung K.K., Reid J.M.: Ultrasonic instrumentation for hematology. *Ultrasonic Imaging* 1: 280-294, 1979.
- [38] Shung K.K.: On the ultrasound scattering from blood as a function of hematocrit. *IEEE Trans Son Ultrason* 29(6): 327-331, 1982.
- [39] Shung K.K., Yuan Y.W., Fei D.Y.: Effect of flow disturbance on ultrasonic backscatter from blood. *J Acous Soc Am* 75(4): 1265-1272, 1984.
- [40] Shung, K.K., Lim, C.: The effect of Hematocrit on Doppler Spectrum. *J Ultrasound Med* 9, S51: Abstract #1305, 1990.
- [41] Sigel B., Coelho J.C.U., Schade S.G., Justin J., Spigos D.G.: Effect of plasma proteins and temperature on echogenicity of blood. *Investigative Radiology* 17: 29-33 1982.

- [42] Sigel B., Machi J., Beitler J.C., Justin J.R., Coelho J.C.U.: Variable Ultrasound Echogenicity in flowing blood. *Science* 218: 1321-1323, 1982.
- [43] Sigel B., Machi J., Beitler J.C., Justin J.R.: Red cell aggregation as a cause of blood-flow echogenicity. *Radiology* 148: 799-802, 1983.
- [44] Ten Cate F.J., Jong de N., Mittertreiner W., Serruys P.W., Roelandt J.R.T.C.: Myocardial contrast two dimensional echocardiography. *Int J Card Im* 4: 53-56, 1989.
- [45] Usami S., Chien S.: Optical reflectometry of red cell aggregation under shear flow. *Bibl Anat* 11: 91-97, 1973.
- [46] Visser K.R.: Electric properties of flowing blood and impedance cardiology. *Annals of Biomed Eng* 17: 463-473, 1989.
- [47] Wolverson M.K., Nouri S., Joist J.H., Sundaram M., Heiberg E.: The direct visualisation of blood flow by real ultrasound: clinical observations and underlying mechanisms. *Radiology* 140: 443-448, 1981.
- [48] Yuan Y.W., Shung K.K.: Ultrasonic backscatter from flowing whole blood. I: Dependence on shear rate and hematocrit. *J Acoust Soc Am* 84(1): 52-58, 1988.
- [49] Yuan Y.W., Shung K.K.: Ultrasonic backscatter from flowing whole blood. II: Dependence on frequency and fibrinogen concentration. *J Acous Soc Am* 84(4): 1195-1200, 1988.
- [50] Yuan Y.W., Shung K.K.: Echoicity of whole blood. *J Ultrasound Med* 8: 425-434, 1989.

IV ULTRASONIC BACKSCATTER BEHAVIOUR OF HUMAN BLOOD IN-VITRO: MANIPULATED BLOOD SAMPLES AND SHEAR RATE DEPENDENCE

Van der Heiden M.S., De Kroon M.G.M., Bom N., Borst C.: Ultrasound backscatter at 30 MHz from Human blood: manipulated blood samples and shear rate dependence.

Abstract

A study on the acoustic properties of blood at high frequencies (20-40 MHz) for varying aggregation conditions is reported. Several blood samples were prepared either to enhance aggregation (Rouleaux enlarged blood samples) or to suppress aggregation (Rouleaux suppressed blood samples) of red blood cells. On these samples a series of experiments was conducted at varying shear rate. Shear rate was varied using a specially developed measurement device based on a Couette Viscometer. In this device the shear rate is approximately constant within the acoustic measurement volume.

Obtained quantitative acoustical parameters were the integrated backscatter power and the spectral slope of the backscatter power in the frequency range of 20 to 40 MHz. A decrease (approximately 13 dB) in the integrated backscatter power of whole blood was observed when the shear rate was increased from 0.7 s^{-1} to 200 s^{-1} . The spectral slope increased from 1 to 3, when the shear rate was increased from 0.3 s^{-1} to 10 s^{-1} . For the rouleaux enlarged blood samples approximately the same change in integrated backscatter power and slope was observed, though higher shear rates appeared to be necessary to effectuate these changes. The integrated backscatter power and spectral slope of rouleaux suppressed blood were not affected by changes in the shear rate.

The results of this study show that the shear rate, which is known to influence the state of aggregation, has significant influence on the backscatter properties of blood at 30 MHz. The changes with shear rate of the integrated backscatter power and the spectral slope of whole blood and rouleaux enlarged blood suggest that at small shear rates ($< 0.3 \text{ s}^{-1}$) aggregates are fully developed. Then between 0.3 s^{-1} and 200 s^{-1} aggregates are broken and only single red blood cells are present at shear rates higher than 200 s^{-1} .

The measured spectral slope indicates that a further increase of the acoustical frequency will enhance blood echogenicity and thus probably aggravate the problem of discriminating arterial wall and lumen.

IV.1 Introduction

Since it is of great interest to achieve adequate signal transmission through blood at 30 MHz in order to be able to assess the morphology of the arterial wall, and since especially at this high frequency high backscatter power of blood is observed, further investigation of the backscatter of human blood at high frequency is desirable. In paragraph III.3 cyclic changes of echogenicity during the cardiac cycle have been reported and it was suggested that these variations might be related to changes in the state of red blood cell aggregation, which are induced by varying shear rate.

The aim of the study reported in this Chapter was to obtain quantitative information on the effect of RBC aggregation on the backscatter behaviour of blood at high frequencies (20-40 MHz). For this purpose several blood samples were prepared either to enhance aggregation or to suppress aggregation of red blood cells (RBCs). On these samples a series of backscatter measurements was conducted at varying shear rate. Shear rate was varied using a newly developed measurement device, which is based on the Couette Viscometer [2]. In this device the shear rate is approximately constant within the measurement volume, which is not the case in the conventional tube flow measurements performed by others [5][22][23][26].

Obtained quantitative acoustical parameters were the integrated backscatter power and the spectral slope of backscatter in the frequency range of 20 to 40 MHz.

IV.2 Materials and methods

Blood sample preparation

Whole blood (120 ml), freshly drawn from eight healthy volunteers, was anticoagulated with citrate (10% vol). Five sub-samples were taken from each blood sample and prepared as follows.

1. Whole blood (B) without alteration (except for use of anticoagulants) was used.
2. By addition of 4.5 mg/ml Dextran 200, *rouleaux enlarged blood* (R*) was obtained [6].

IV.2 Materials and methods

3. Whole blood was centrifuged and the plasma and buffy coat⁷⁾ were removed. The remaining red blood cells were suspended in 0.9 % saline solution. As a result of this treatment the proteins (fibrinogen and γ -globulin), that are relevant for the aggregation process [7], were no longer present, which resulted in *rouleaux suppressed blood* (R⁻).
4. After removing the plasma and buffy coat the red blood cells were suspended in 0.4 % saline solution. As a result of the low environmental salt concentration osmotic pressure caused the red blood cells to explode. This solution is referred to as *hemolysed blood* (H).
5. The red and white blood cells were removed, leaving platelet rich *blood plasma* (P).

It was taken care of that the blood manipulations did not change the Hematocrit value of the blood sample (except for the P-sample).

As a control measurement, a pure saline solution (S) was also examined. Since a pure saline solution should not contain any acoustic scatterers, it may safely be assumed that the measurements on the saline solution give a good estimation of the acoustic and electronic noise present in the measurement system.

Microscopic images

For comparison purposes, light microscopic images of each blood sample (B, R⁺ and R⁻) were produced under static conditions. The blood samples were illuminated with green light to enhance image contrast. The number of RBCs per aggregate were counted to obtain an aggregate size distribution.

Control of shear rate

The acoustic behaviour of various blood samples was investigated using an experimental device based on a Couette Viscometer (Figure IV.1). The dimensions of the Couette cylinders were adapted to the dimensions of the acoustic element and the acoustic measurement volume. The instrument essentially consists of a stationary inner cylinder, 70 mm in diameter, surrounded by a concentric rotating cylinder of 76 mm diameter. The blood sample (30 ml) is put in the interstice of 3 mm between the two coaxial cylinders.

⁷⁾ The buffy coat contains the white blood cells.

It can be shown that for the applied cylinder diameters the shear rate is approximately constant within the interstice (maximum relative error is 8%, see Appendix A). The driver unit performed fourteen logarithmically equidistant rotation rates in a shear rate range from 0.02 to 1000 s^{-1} . In addition, measurements on static blood were performed, using a fixed non-rotating outer cylinder.

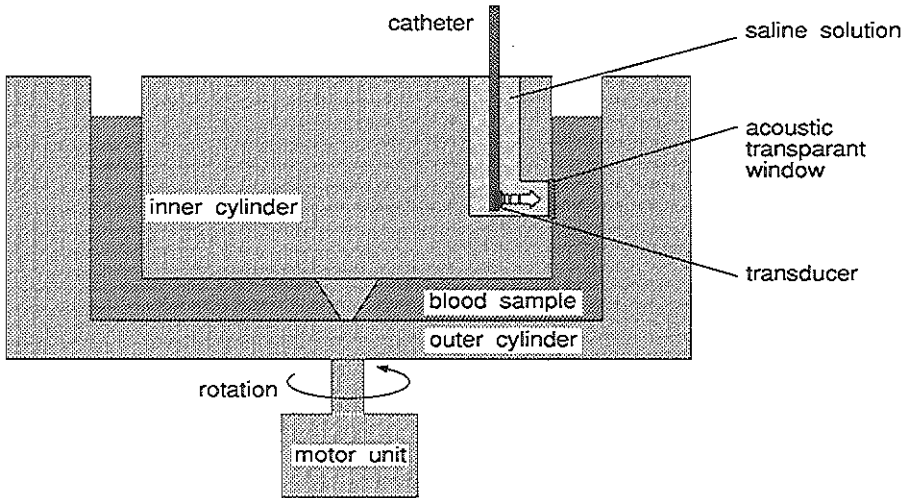


Figure IV.1 Diagram of modified Couette Viscometer to obtain controlled shear rate in blood.

Ultrasound system

For the acoustic backscatter measurements the catheter, pulser and linear preamplifier of a clinical intravascular ultrasonic (IVUS) device were used (DUMED, Rotterdam, The Netherlands, [3]). This device is equipped with a 30 MHz plane circular transducer with diameter of 1 mm. The transducer was mounted in a chamber in the inner cylinder of the modified Couette viscometer (Figure IV.1). This chamber, which was filled with a 0.9% saline solution, was separated from the blood filled interstice by an acoustically transparent window (TPX film). Since the transducer was positioned at a distance of 5 mm in front of the acoustic window, the blood sample behind this window was in the far field of the

transducer.

The received RF-signal was linearly amplified and then digitised at a sampling frequency of 400 MHz, using a digital oscilloscope (LeCroy 9450, with 80 MHz low pass filter). Acquired data were transferred to the hard disk of an IBM compatible personal computer.

Measurement procedure

Prior to each measurement less than two minutes of time were required to reach an equilibrium in the state of aggregation in the sheared blood sample. Then, during 30 seconds, 100 RF backscatter signals of 1500 samples each (duration 3.75 μ m) emanating from the blood sample were recorded. Static blood measurements were performed on all manipulated blood samples of six different individuals. Shear dependent measurements were performed only on whole (B), rouleaux enlarged (R⁺) and rouleaux suppressed (R⁻) blood of six individuals, of which four were the same individuals as the ones of the static blood measurements. All measurements were performed at room temperature (20° C).

Reference measurement

The reflection against a flat agar-agar reflector was measured. The agar-agar reflector was positioned at 6.5 mm distance from the transducer, which equals the distance to the center of the interstice. The power spectrum calculated from the reflected signal (Figure IV.2B) was used as a reference spectrum in the data analysis of the backscatter signals.

Signal processing

Data processing of the recorded RF signals was performed off-line. After applying a Hamming window on the data, the power spectra of the adjacent time traces were calculated and averaged (Figure IV.2A). From the average power spectrum the *integrated backscatter power* from 20 to 42 MHz, which is the -30 dB bandwidth of the reference spectrum, was calculated.

Also the average power spectrum was normalised with the reference power spectrum of the agar-agar reflector, resulting in what is usually called the frequency dependent *backscatter coefficient* $\mu_{bs}(f)$ [18][19][25] (Figure IV.2C).

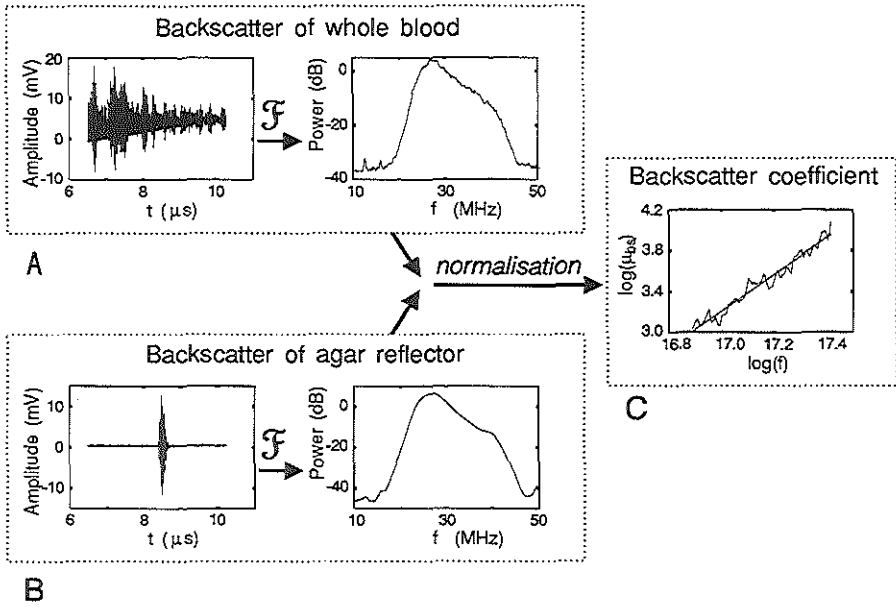


Figure IV.2 A) Time signal and averaged backscatter power spectrum of whole blood. B) Time signal and power spectrum from a flat agar-agar reflector at 6.5 mm distance from the transducer. C) Backscatter coefficient of whole blood.

It is assumed that the backscatter coefficient is linearly proportional to the N^{th} power of the frequency [25]:

$$\mu_{bs}(f) \sim f^N \quad (\text{IV.1})$$

The parameter N , which will be referred to as the *spectral slope of backscatter*, was estimated by simple linear regression of $\log(\mu_{bs})$ as a function of $\log(f)$, where the frequency f ranges from 22 to 37 MHz.

Statistical analysis

In order to investigate the significance of the effect of blood type on the results of the static measurements, a two-way analysis of variance (ANOVA) was carried out on both the measured integrated backscatter power and the spectral slope for a random sample of 6 persons. The two-way ANOVA was carried out considering differences between blood types as fixed effect and the differences between persons as a random effect. The pair-wise differences between blood types were investigated using the method of Scheffé [11].

IV.3 Results

Rouleaux size distribution.

Figure IV.3 shows examples of the light microscopic images of whole blood (B), rouleaux enlarged (R^+) and rouleaux suppressed (R^-) blood. The number of RBCs per rouleaux on the light microscopic images of the blood samples of all eight individuals were counted and divided by the total number of counts. Figure IV.4 shows the resulting cumulative

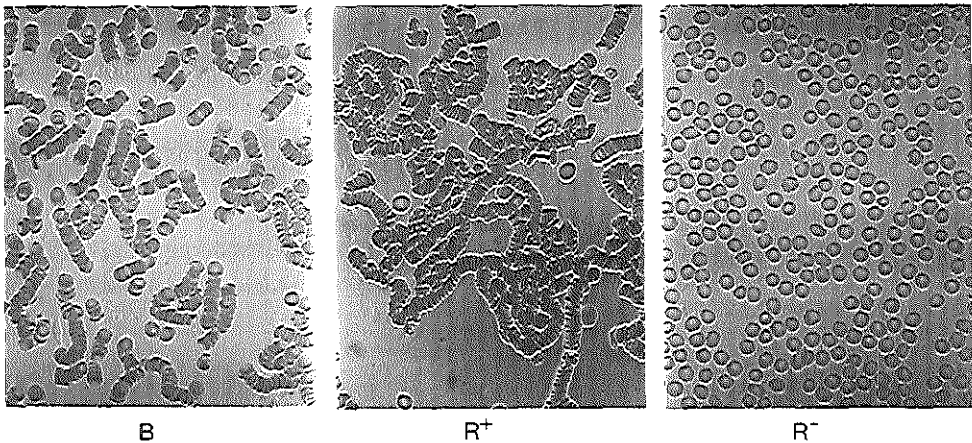


Figure IV.3 Light microscopic images of whole blood (B), rouleaux enlarged (R^+) and rouleaux suppressed (R^-) blood.

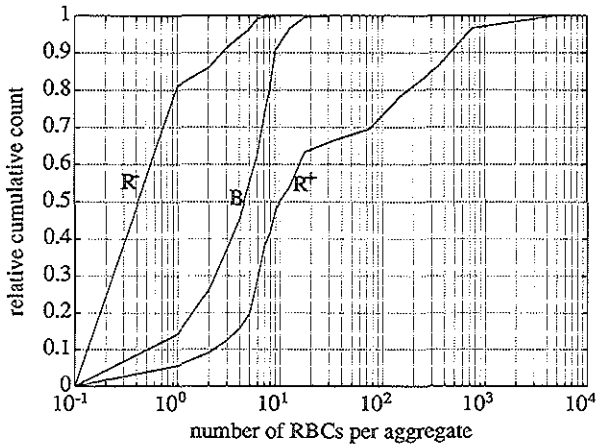


Figure IV.4 The relative cumulative count curves obtained from light microscopic images; B: whole blood, R⁺: rouleaux enlarged blood, R: rouleaux suppressed blood.

count curves, with on the vertical axis the relative number of RBCs present in aggregates of which the length is between zero and the length indicated on the horizontal axis. This figure clearly shows the effect of rouleaux enlargement and rouleaux suppression on the rouleau length distribution. For rouleaux suppressed blood most RBCs were unaggregated and as a consequence the cumulative count curve increases rapidly for rouleau length between zero and one RBC. Whole blood consisted of rouleaux mostly shorter than 10 RBCs, while in rouleaux enlarged blood extremely large rouleaux were present (up to thousands of RBCs per aggregate).

Static blood measurements

The measured integrated backscatter power of all manipulated blood types for a sample of six persons are given in Table IV.1.

The applied ANOVA proved that there exists a prominent effect of blood type (F-test: $P < 10^{-6}$) as is apparent from the estimated mean values shown in Figure IV.5. The standard errors of the mean indicated in this figure were calculated per blood type.

IV.3 Results

Table IV.1 Measured integrated backscatter power of all manipulated blood types of six persons.

person	blood type					
	B	R ⁺	R ⁻	H	P	S
1	23.4092	24.0998	13.2869	3.2026	1.3114	-0.9204
2	23.7911	22.6948	11.1998	2.3032	0.6531	0.256
3	23.1251	24.4068	11.3123	-3.8021	-9.7852	-9.5725
4	24.3277	24.8828	14.866	1.3465	-9.701	-9.1787
5	21.0692	23.4573	9.9157	2.0372	-4.7059	-5.03
6	23.8977	24.2785	14.2993	3.5406	-2.032	-2.547

From the ANOVA it appeared that the differences between persons were not significant ($0.1 < P < 0.25$).⁸⁾

Having concluded that there are differences between blood types in the integrated backscatter power, Scheffé's method was applied to allocate these differences. From these calculations it followed that apart from the pair B and R⁺, the blood types are pair-wise different from each other ($P < 0.001$). Nevertheless the observations (Table IV.1) suggest that there also exists a small systematic difference between B and R⁺.

It is also observed that the integrated backscatter power of blood plasma does not significantly deviate from the integrated backscatter power of saline solution, which represents the noise level. This confirms the assumption that acoustic scattering is caused by the RBCs.

⁸⁾ It should however be kept in mind that the residual variances in the ANOVA may contain an interaction component between persons and blood types. The measurements of Table IV.1 suggest quite strongly that such an interaction component exists and therefore it does not seem justifiable to neglect differences between persons for different blood types.

IV Backscatter behaviour of blood: manipulated blood samples and shear rate dependence

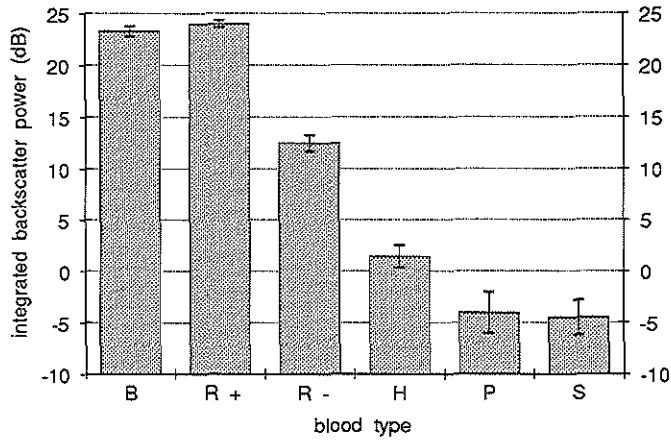


Figure IV.5 Average integrated backscatter power under static conditions; B: whole blood, R⁺: rouleaux enlarged blood, R⁻: rouleaux suppressed blood, H: hemolysed blood, P: blood plasma, S: saline solution.

Table IV.2 Measured spectral slope of four manipulated blood types of six persons.

person	blood type			
	B	R ⁺	R ⁻	H
1	1.0764	1.3241	3.3736	5.0332
2	2.1529	3.7002	3.9949	3.8192
3	1.8054	1.0489	2.134	2.168
4	0.4149	0.0386	2.2211	2.3927
5	1.2068	0.3123	3.8331	4.662
6	1.4206	1.4397	3.2808	1.9439

IV.3 Results

The measured spectral slope of the blood types B, R⁻, R⁺ and H of all six persons are given in Table IV.2. Because the power measured from blood plasma corresponds with the noise level of the measurement system, the spectral slope of this blood type is meaningless and therefore not calculated. According to the applied ANOVA the effect of blood type on the spectral slope is significant again ($P < 0.001$). The estimated mean values and the standard error of the mean per blood type are shown in Figure IV.6. The differences between persons are hardly significant ($0.025 < P < 0.05$). Scheffé's test showed significant pair-wise differences between R⁻ and B, R⁻ and R⁺, H and B, and H and R⁺ ($P < 0.001$), while the pair-wise differences between R⁺ and B, and H and R⁻ are not significant ($P > 0.25$).

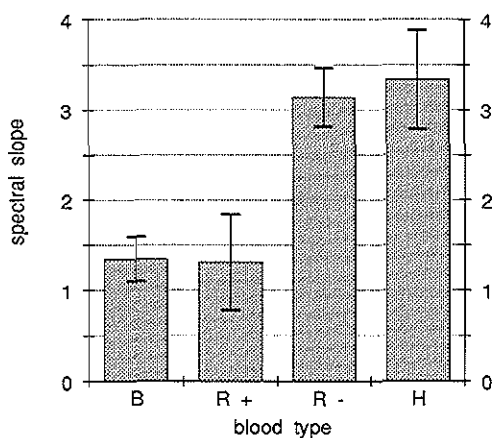


Figure IV.6 Average spectral slope under static conditions; B: whole blood, R⁺: rouleaux enlarged blood, R⁻: rouleaux suppressed blood, H: hemolysed blood.

Shear rate dependent measurements

The measured shear rate dependence of the averaged integrated backscatter power and averaged spectral slope of all three manipulated blood samples (B, R⁺ and R⁻) are shown in Figure IV.7 and Figure IV.8. The results of the whole blood measurements are the average of a sample of six persons, while the rouleaux enlarged and rouleaux suppressed results are the average of only three (out of six) persons.

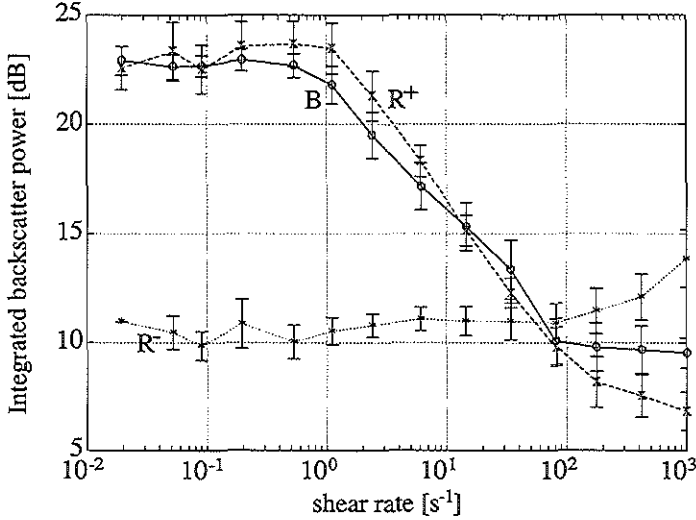


Figure IV.7 Average shear rate dependence of integrated backscatter power of whole blood (—o—), rouleaux enlarged blood (—x—) and rouleaux suppressed blood (…*…).

The curves show that for shear rates below 0.7 s^{-1} both the integrated backscatter power and the spectral slope have approximately the same level as in the static measurements. The curves of rouleaux enlarged blood have the same shape as the whole blood curves, however they appear to be shifted to the right. With shear rate increasing from 0.2 s^{-1} to 11 s^{-1} the backscatter power of whole blood and rouleaux enlarged blood decreases with respectively 13 and 15 dB. The spectral slope increases from approximately 1 to 3 for whole blood and from approximately 0.5 to 3 for rouleaux enlarged blood. Remarkably, for shear rate higher than 11 s^{-1} the slope of rouleaux enlarged blood slightly decreases with increasing shear rate, while for whole blood an additional increase in spectral slope till 3.5 is observed.

Rouleaux suppressed blood exhibits no shear dependent backscatter power nor spectral slope. Only a slight increase of backscatter power is observed at high shear rates ($> 200 \text{ s}^{-1}$). For shear rates smaller than 200 s^{-1} , the backscatter power of rouleaux suppressed blood is almost the same as of whole blood at high shear rate ($> 200 \text{ s}^{-1}$).

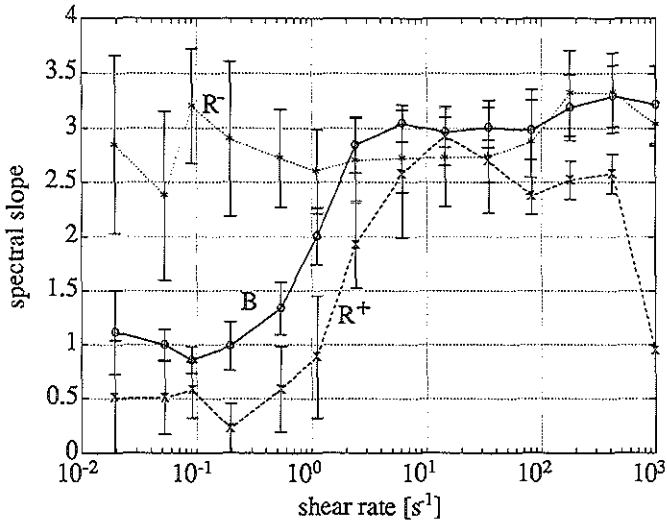


Figure IV.8 Average shear rate dependence of spectral slope of whole blood (—o—), rouleaux enlarged blood (-x-) and rouleaux suppressed blood (...*...).

IV.4 Discussion

Integrated backscatter power

Generally the results of both the static and the shear dependent measurements suggest that the measured integrated backscatter power of blood is related to the size of the RBC aggregates. This corresponds to the theoretical relation between the backscatter intensity of blood and its state of aggregation derived by Hanss and Boynard [14]. They found that at constant Hematocrit the backscatter intensity is linearly proportional to the number of RBCs per aggregate.

For the static measurements a decrease of approximately 11 dB in integrated backscatter power of rouleaux suppressed blood compared to whole blood is observed. According to the theory of Hanss and Boynard, this would indicate that the number of RBCs per aggregate in whole blood is twelve times the number of RBCs per aggregate in rouleaux

suppressed blood. Evaluating the cumulative count curves of Figure IV.4, this seems a realistic estimation.

No prominent effect of rouleaux enlargement on the backscatter power was observed in the static measurements. It has to be noted however that, evaluating the results of Table IV.1, for all persons except one, the integrated backscatter power of rouleaux enlarged blood is higher than of whole blood. These differences are masked by the variations in the backscatter power between persons for both blood types. The effect of person on measured power might be due to several physiological quantities, e.g. Hematocrit or fibrinogen concentration, of which the values in the examined blood samples were not known.

It also has to be considered that the theory of Hanss and Boynard is based on the assumption of Rayleigh scattering, which implies that the scatterers are much smaller than the wavelength. As a consequence this theory cannot probably be applied to the larger aggregates. One can imagine that for large aggregates a kind of saturation of the effect of further aggregation on backscatter power will occur. This might be the case for the backscatter measurements of rouleaux enlarged blood compared to whole blood.

The fact that hemolysed blood has significantly lower backscatter power than the other blood samples (B, R^+, R^-) suggests that not the shell of a red blood cell but the hemoglobin solution inside this shell is mainly responsible for the scattering by blood.

Spectral slope

The results indicate that the measured spectral slope is related to the aggregation conditions of RBCs in blood. Theoretically for scatterers that are much smaller than the acoustical wavelength, a fourth power dependence of the backscatter power on the frequency is to be expected (Rayleigh scattering). When scatterer size increases with respect to the wavelength, the fourth power relationship no longer holds and scatter intensity becomes more linearly proportional to the frequency. At even larger scatterer sizes, the scatter intensity becomes independent of frequency. For such large scatterer sizes the term reflector is more appropriate.

The measured spectral slope of both whole and rouleaux enlarged blood (i.e. 1.3 at rest) is much lower than the spectral slope of rouleaux suppressed blood (i.e. 3.1 at rest). This corresponds to the assumed aggregate size, which is much larger in whole and rouleaux enlarged blood than in rouleaux suppressed blood. No significant difference in spectral slope between the whole and rouleaux enlarged blood samples was observed.

The spectral slope of backscatter from single RBCs (R^-) at rest is somewhat lower (i.e. 3.1)

than the spectral slope for Rayleigh scattering (i.e. 4). Considering the size of a RBC (diameter 7 - 8 μm , thickness 1 - 3 μm) it follows that even a single RBC will not behave like a perfect Rayleigh scatterer. Moreover no correction for the frequency dependent attenuation in the intervening medium between transducer and region of interest is applied to the experimental data. Therefore the spectral slope of backscatter is likely to be underestimated.

Hemolysed blood almost behaves like a Rayleigh scattering medium, as is illustrated by the measured spectral slope (i.e. approximately 3.3). Probably the neglected influence of attenuation on the measured spectral slope is the cause of the deviation of the spectral slope from 4, the value for perfect Rayleigh scattering.

Shear rate dependence

The change with shear rate of the integrated backscatter power and the spectral slope of whole blood indicates that for small shear rates (0.02 - 0.7 s^{-1}) rouleaux were fully developed. Then between 0.7 s^{-1} and 200 s^{-1} rouleaux were broken and only single RBCs were present at shear rates higher than 200 s^{-1} .

The shift to the right of the shear dependent curves of rouleaux enlarged blood with respect to whole blood (Figure IV.7 and Figure IV.8), suggests that higher shear forces are necessary to break aggregates in rouleaux enlarged blood.

Because in rouleaux suppressed blood there were no aggregates, it exhibited no change in backscatter power and spectral slope with changing shear rate, except for a small increase of backscatter power at high shear rates. This increase might be caused by shear induced deformation and orientation of RBCs [10][16].

The effect of shear rate on backscatter power was investigated before, albeit at lower frequencies (1-15 MHz). In these studies the same influence of shear rate on the backscatter power of blood was observed [5][22][23][26]. However, a different experimental set-up was used to obtain this information, i.e. backscatter from blood flowing in a tube was measured with varying flow velocity and possibly varying tube diameter. The main advantage of our experimental set-up is the fact that shear rate is approximately constant within the measurement volume, while in a tube shear rate increases almost linearly with radial distance. Another advantage of our experimental set-up is the small quantity of blood required (30 ml), which makes experimenting more feasible.

Clinical relevance

Although the relevance of the results of this study with regard to clinical diagnostics is speculative at this moment, some potential usefulness should be discussed. For quantitative tissue identification with an intravascular ultrasonic imaging device, also differentiation between vessel wall and blood is relevant. The results of this study give insight in the backscatter properties of blood, which might be helpful in future research in the field of quantitative tissue identification.

Measurement of blood echogenicity may also offer the possibility to assess the state of vascular disease. E.g. Kallio [17] observed that patients with vascular disease have higher blood echogenicity than healthy volunteers. Kallio even made the hypothetical statement that blood echogenicity might be a more specific measure of disease than the conventional ESR (RBC sedimentation rate). Application of the intravascular catheter eventually allows in-vivo local study and quantitative standardization of the aggregation dynamics of RBCs. Finally local shear force conditions may be derived from the echogenicity of the flowing blood. This could open a new field of studies on e.g. the suggested relationship between local shear forces and the rate of development of arterial wall disease [8][9].

IV.5 Conclusion

It is concluded that varying the aggregation conditions results in changes in backscatter properties of blood, i.e. the integrated backscatter power and the spectral slope, in the frequency range from 10 to 40 MHz. Generally, enhancing aggregation results in higher backscatter power and lower spectral slope, while suppression of aggregation gives lower backscatter power and higher spectral slope.

In particular the results of this study show that the shear rate, which is known to have influence on the state of aggregation [20], has significant influence on the backscatter properties of blood. For whole blood and rouleaux enlarged blood the backscatter power decreases with increasing shear rate and the spectral slope increases with increasing shear rate.

The results of this study do not give proof of the occurrence of red blood cell aggregation in-vivo in a pulsatile flow. However it does show that, if RBCs aggregate in-vivo, it will have significant effect on the measured echogenicity.

With the results the observed increased blood echogenicity with the intravascular imaging

IV.5 Conclusion

device (paragraph III.1), when increasing frequency, can be understood. The measured spectral slope, indicates that further increasing the acoustical frequency will enhance blood echogenicity and thus will probably aggravate problems in discriminating arterial wall and lumen. This effect will even be stronger in blood without aggregates than in blood with aggregates.

References

- [1] Beitler J.C., Sigel B., Machi J., Justin J.R.: The effect of temperature on blood flow echogenicity in vitro. *J Ultrasound Med* 2: 529-533, 1983.
- [2] Bird R.B., Stewart W.E., Lightfoot E.N.: Transport phenomena. John Wiley & Sons, 1960.
- [3] Bom N., ten Hoff H., Lanc c C.T., Gussenhoven W.J., Bosch J.C.: Early and recent intraluminal ultrasound devices. *Intravascular Ultrasound, techniques, developments, clinical perspectives*. Ed.: N. Bom, J. Roelandt. Kluwer Academic Publishers, 1989.
- [4] Boynard M., Lelievre J.C., Guillet R.: Aggregation of red blood cells studied by ultrasound backscattering. *Biorheology* 24: 451-461, 1987.
- [5] Boynard M., Lelievre J.C.: An approach of red blood cell aggregation by ultrasonic echography. *Clinical Hemorheology* 9: 771-779, 1989.
- [6] Boynard M., Lelievre J.C.: Size determination of red blood cell aggregates induced by dextran using ultrasound backscatter phenomenon. *Biorheology* 27 (1): 39-46, 1990.
- [7] Brooks D.E., Greig R.G., Janzen J.: Mechanisms of erythrocyte aggregation, Erythrocyte mechanics and blood flow. Edited by Cokelet G.R., Meiselman H.J., Brooks D.E. New York, Alan R Liss Inc: 119-140, 1980.
- [8] Caro C.G., Fitz-Gerald J.M., Schroter R.C.: Arterial wall shear distribution of early atheroma in man. *Nature (London)* 223: 1159-1161, 1969.
- [9] Fry D.L.: Acute vascular endothelial changes associated with increased blood velocity gradients. *Circ Res* 22: 165-197, 1968.
- [10] Goldsmith H.L.: The flow of model particles and blood cells and its relation to thrombogenesis. In *space T.H. (ed.) Progress in hemostasis and thrombosis* 1: 97-139, Grunc and Stratton New York, 1972.

IV Backscatter behaviour of blood: manipulated blood samples and shear rate dependence

- [11] Green J.R., Margerison D.: Physical sciences data 2: Statistical treatment of experimental data. Elsevier Scientific Publ Company, 1978.
- [12] Gussenhoven W.J., Essed C.E., Fricman P., Egmond van F., Lancée C.T., Kapellen van W.H., Roelandt J., Serruys P.W., Gerritsen G.P., Urk van H., Bom N.: Intravascular Ultrasound imaging: Histologic and echographic correlation. *Eur J Vasc Surg* 3: 571-576, 1989.
- [13] Gussenhoven W.J., Essed C.E., Lancée C.T., Mastik F., Fricman P., Egmond van F.C., Reiber J., Bosch H., Urk van H., Roelandt J., Bom N.: Arterial wall characteristics determined by intravascular ultrasound imaging: An in-vitro study. *J Am Col Card* 14(4): 947-952, 1989.
- [14] Hanss M., Boynard M.: Ultrasound backscattering from blood: hematocrit and erythrocyte aggregation dependence. *Ultr Tissue Char II*, M. Linzer (Ed.), National Bureau of Standards, Spec Publ: 525, 1979.
- [15] Herwerden van L.A., Gussenhoven W.J., Roelandt J., Bos E., Ligvoet C.M., Haalcbos M.M., Mochtar B., Leicher F., Witsenburg M.: Intraoperative epicardial two-dimensional echocardiography. *European Heart Journal* 7: 386-395, 1986.
- [16] Jeffery G.B.: The motion of ellipsoidal particles in a viscous fluid. *Proc Roy Soc London* 102: 161-179, 1922.
- [17] Kallio T., Alanen A., Kormanio M.: The in-vitro echogenicity of flowing blood in patients with vascular disease and the effect of naftidrofuryl. *Ultrasound Med Biol* 15(6): 555-559, 1989.
- [18] Lizzi F.L., Greenbaum M., Feleppa E.J., Elbaum M., Coleman D.J.: Theoretical framework for spectrum analysis in ultrasonic tissue characterization. *J Acoust Soc Am* 73 (4): 1366-1373, 1983.
- [19] Romijn L.: *On the Quantitative Analysis of Ultrasound Signals and Application to Intraocular Melanomas*. Thesis Nijmegen, The Netherlands, 1990.
- [20] Schmid-Schonbein H., Gachtgens P., Hirsch H.: On the shear rate dependence of red cell aggregation in-vitro. *J Clin Inv* 47: 1447-1454, 1968.
- [21] Shung K.K., Cloutier G., Lim C.C.: The effects of hematocrit, shear rate, and turbulence on ultrasonic doppler spectrum from blood. *IEEE Trans Biomed Eng* 39 (5): 462-469, 1992.
- [22] Sigel B., Machi J., Beitler J.C., Justin J.R., Coelho J.C.U.: Variable Ultrasound Echogenicity in flowing blood. *Science* 218: 1321-1323 1982.
- [23] Sigel B., Machi J., Beitler J.C., Justin J.R.: Red cell aggregation as a cause of blood-flow echogenicity. *Radiology* 148: 799-802. 1983.

References

- [24] Ten Cate F.J., Jong de N., Mittertreiner W., Serruys P.W., Roelandt J.R.T.C.: Myocardial contrast two dimensional echocardiography. *Int J Card Im* 4: 53-56, 1989.
- [25] Ueda M., Ozawa Y.: Spectral Analysis of Echoes for Backscattering Coefficient Measurement. *J Acoust Soc Am* 77(1): 38-47, 1985.
- [26] Yuan Y.W., Shung K.K.: Ultrasonic backscatter from flowing whole blood. I: Dependence on shear rate and hematocrit. *J Acoust Soc Am* 84(1): 52-58, 1988.
- [27] Yuan Y.W., Shung K.K.: Echoicity of whole blood. *J Ultrasound Med*: V8: 425-434, 1989.

V MODELLING OF THE ACOUSTICAL BEHAVIOUR OF ARTERIAL TISSUE AND BLOOD

Abstract

A mathematical model, describing the acoustical backscatter behaviour of arterial tissue and blood at high frequency (30 MHz) is introduced. Both arterial tissue and aggregated blood were considered to consist of a distribution of cylindrical scatterers in 3D space. The properties of this distribution of scatterers are described by several parameters, i.e. the average distance and the spread in the distance between the scatterers, the average size and the spread in the size of the cylinders, and finally the average orientation and the spread in the orientation of the cylinders. Also the properties of a focussed transducer were incorporated in the model. From the angle dependent measurement of the reflection against a plane reflector, the parameters describing the transducer properties were obtained.

First, the importance of several features in the model were evaluated. It is shown that the angle dependent backscatter pressure of a distribution of irregularly spaced scatterers was hardly affected by the spacing of the scatterers but was mainly determined by the size and orientation of the scatterers.

Next, simulation results of the angle dependence of backscatter pressure from tissue mimicking scattering media are reported. The simulated angle dependence of the backscatter pressure from the tissue mimicking distributions of cylindrical scatterers corresponded well to the experimental results of Chapter II.

Finally, the backscatter measurements on blood were simulated. Aggregated red blood cells in blood were represented by a distribution of irregularly spaced cylinders oriented perpendicular to the incident pressure beam. Aggregation of blood cells was simulated by an increase of the average cylinder length with a proportional decrease of the number of cylinders. The simulated aggregation had the same effect on the calculated backscatter power as the decrease of shear rate on the measured backscatter power in the experiments reported in Chapter IV.

V.1 Introduction

Generally tissue is thought of as a distribution of inhomogenities in space. Most reported mathematical presentations of the acoustical behaviour of tissue are based on the assumption

that these inhomogenities are much smaller than the applied acoustical wavelength and that their concentration is low [5][8][10]. Thus, only Rayleigh scattering (omnidirectional) was described by these mathematical presentations. In Chapter II the results of the angle dependent measurements showed that scattering from the arterial wall at 30 MHz was not omnidirectional. Therefore it was concluded that the size of the inhomogenities in the arterial wall is not small compared to the wavelength at 30 MHz ($\approx 50 \mu\text{m}$). The experimental results also showed the anisotropic nature of the angle dependent backscatter of the muscular and elastic media. This implies that the dimensions of the inhomogenities in these tissues are anisotropic. The measurement results on e.g. the muscular media indicated that one dimension (the tangential direction) of the scattering inhomogenities is not small compared to the wavelength, while the other dimension (the axial direction) is likely to be much smaller than the wavelength. This anisotropy was also observed in histologic sections of arterial tissue.

Based on these observations it is found that the existing mathematical presentations for tissue scattering are deficient for the description of the acoustical behaviour of arterial tissue at 30 MHz.

Based on the results of the backscatter measurements on blood at varying shear rate (Chapter IV), it was concluded that red blood cell aggregation has significant influence on the backscatter power and the backscatter spectral slope in the applied high frequency range (20-40 MHz). While one RBC (red blood cell) is small ($\leq 8 \mu\text{m}$) compared to the wavelength ($50 \mu\text{m}$ at 30 MHz), an RBC-aggregate might become of the order of magnitude of the wavelength, depending on the number of RBCs per aggregate. Because of the size of these inhomogenities, and also because their concentration is not particularly low, the existing mathematical presentations used to describe tissue scattering [5][8][10] cannot be applied to the scattering by aggregated RBCs.

Mathematical models describing the scattering of blood have also been reported before [3][4]. However, these studies, which were performed for other clinical applications (e.g. doppler ultrasound), only deal with low frequency ultrasound (1-15 MHz) and therefore in these studies it was assumed that the inhomogenities were much smaller than the applied wavelength.

In this Chapter fundamental scattering theory is applied to alternative particle distributions, that are more likely to represent arterial tissues and blood. The assumed scatter models

V.1 Introduction

are based on histologic sections of the tissues and microscopic images of blood, and on the results of the laboratory ultrasonic measurements (Chapter II and IV). Tissue and blood are supposed to consist of a random distribution of cylinders, which are more or less oriented in one direction. The dimensions, orientation, concentration and spatial distribution of these cylinders are variable.

V.2 Geometry of angle dependent backscatter measurements

The mathematical model derived hereafter gives the acoustic backscatter pressure from scatterers within a small volume representing a tissue or blood sample, which is positioned in the focal region of a focussed transducer.

The geometry of the set-up is given in Figure V.1. In this figure symbols for the transducer radius (a_t), the focal distance (z_f), and the scattering volume V_s with length l in z -direction, are introduced. Also a Cartesian coordinate system is defined, in which the focal point is the origin. In the mathematical model the angle of incidence is varied by rotating the scatter volume in the xz -plane with the y -axis being the rotation axis.

Cylindrical inhomogeneities with arbitrary orientation are defined in the scatter volume. By choosing the orientation of the cylindrical inhomogeneities either parallel to the x -axis or parallel to the y -axis both the axial and tangential scan, as defined in the experimental study (Chapter II), can be simulated.

V.3 Backscatter pressure from a scattering volume - general mathematical formulation

In Appendix B an expression for the backscatter pressure P^{bsc} from a scattering volume, filled with density and velocity inhomogeneities, positioned in the focal region of a weakly focussed transducer is deduced. For this deduction the following conditions have to be satisfied.

1. A weakly focussed transducer is applied.
2. The inhomogeneities in the tissue are characterized as small spatial fluctuations in density, $\Delta\rho$, and propagation velocity, Δc , about their mean values, ρ_0 and c_0 respectively. It is assumed that the density and velocity perturbations are small compared to the average density and velocity ($\Delta\rho \ll \rho_0$, $\Delta c \ll c_0$).

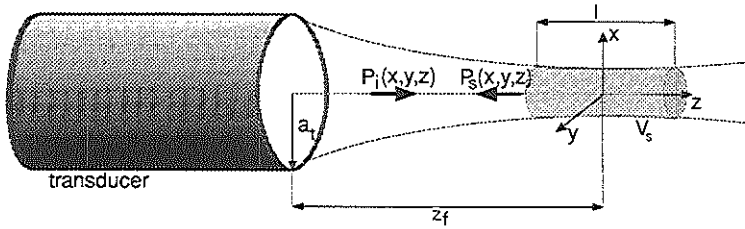


Figure V.1 Configuration of simulated backscatter measurement.

3. Multiple scattering is neglected (Born approximation),
4. Focussing occurs well within the Fresnel region of the transducer ($z_f \ll a_i^2/\lambda$),
5. The radius (a) of the transducer is much larger than the wavelength ($a \gg \lambda$),
6. The transducer surface vibrates normally to the aperture of the transducer with velocity V^n . The velocity is assumed to be uniform in phase and amplitude over the transducer aperture: $V^n(\mathbf{r}, \omega) = V^n(\omega)$
7. The detection sensitivity $T(\mathbf{r}, \omega)$ of the transducer is assumed to be uniform in phase and amplitude over the transducer aperture: $T(\mathbf{r}, \omega) = T(\omega)$.
8. The length of the scattering volume l is small compared to the focal length: $l \ll z_f$.

Then the backscatter pressure is given by:

$$P^{bsc}(\mathbf{r}_0, \omega) = 2jk \rho_0 c_0 T(\omega) V^n(\omega) \int_{V_s} G_i(\mathbf{r}_0, \mathbf{r}_s, \omega) \left[k^2 \frac{2\Delta c(\mathbf{r}_s)}{c_0} + \frac{1}{\rho_0} \nabla_s(\Delta \rho(\mathbf{r}_s)) \cdot \nabla_s \right] [G_i(\mathbf{r}_0, \mathbf{r}_s, \omega)] d^3 \mathbf{r}_s \quad (V.1)$$

in which the so-called transducer Greens function G_i satisfies:

V.3 Backscatter pressure from a scattering volume

$$G_t(r_0, r, \omega) = A e^{-\frac{k^2(x^2+y^2)}{32f_N^2}} \frac{e^{-jk(z+z_f)}}{4\pi z} \quad (\text{V.2})$$

In this equation k is the wavenumber in the homogeneous background medium ($k=\omega/c_0$) and f_N is the f-number of the transducer, which is defined as:

$$f_N := \frac{z_f}{2a_t} \quad (\text{V.3})$$

If $f_N > 1/(2\sqrt{\pi})$ and if the average position of the randomly distributed inhomogeneities is the focal point, then the second term in the integrand can be approximated by (Appendix D.1):

$$G_t \nabla_s(\Delta\rho) \cdot \nabla_s G_t = -jk \frac{\partial(\Delta\rho)}{\partial z} G_t^2 \quad (\text{V.4})$$

It is shown in Appendix D.2 that the integrand in z of the velocity term can be replaced by:

$$\int_{z_-}^{z_+} 2jk \frac{\Delta c(x,y,z)}{c_0} e^{-2jk(z+z_f)} dz = \int_{z_-}^{z_+} \frac{1}{c_0} \frac{\partial}{\partial z} (\Delta c(x,y,z)) e^{-2jk(z+z_f)} dz \quad (\text{V.5})$$

Then, with the definition of the inhomogeneity function χ

$$\chi(x,y,z) := \frac{1}{Z} \frac{\partial Z(x,y,z)}{\partial z} = \frac{1}{\rho_0 c_0} \frac{\partial}{\partial z} [\rho(x,y,z) c(x,y,z)] \quad (\text{V.6})$$

(Z is the local acoustic impedance), the backscatter pressure measured by the transducer positioned at r_0 can be approximated by:

$$p^{bsc}(r_0, \omega) = \frac{-2 \rho_0 c_0}{A} T(\omega) V^n(\omega) \int_{V_s} G_t^2(r_0, r_s, \omega) \chi(r_s) d^3 r_s \quad (\text{V.7})$$

In equation (V.7) the propagation from transducer to the scattering tissue and back is represented by the function G_t^2 . The function χ represents the scatter properties of the tissue or of blood.

V.4 Scattering by cylinders

As mentioned in the introduction of this Chapter, cylindrically shaped inhomogeneities in tissue are assumed to be responsible for the anisotropic angle dependence of the backscatter pressure. For this reason an expression for the backscatter pressure from a cylindrically shaped object as a function of the angle of incidence is calculated. This is done by deducing an equation for the inhomogeneity function χ (equation (V.6)) for the case of a cylindrical object.

V.4.1 Angle dependent backscatter from one cylinder of infinite length

An infinitely long cylinder is centered at the origin and oriented parallel to the the xz -plane. The angle θ between the cylinder-axis and the x -axis is varied in the xz -plane. A new Cartesian coordinate system (x', y', z') is defined, which rotates equally with the rotation of the cylinder (Figure V.2):

$$\begin{cases} x' = x \cos \theta + z \sin \theta \\ y' = y \\ z' = z \cos \theta - x \sin \theta \end{cases} \quad (\text{V.8})$$

Because of the cylindrical symmetry, it is useful to introduce cylindrical coordinates. The cylindrical coordinates (r', ψ', x') are defined with respect to the rotating Cartesian coordinate system:

$$\begin{cases} x' = x' \\ y' = r' \sin \psi' \\ z' = r' \cos \psi' \end{cases} \quad (\text{V.9})$$

In Figure V.2 the geometry of the cylinder and the various coordinates are indicated. For a cylindrical object with radius a_c and length l_c , the acoustic impedance Z is given by:

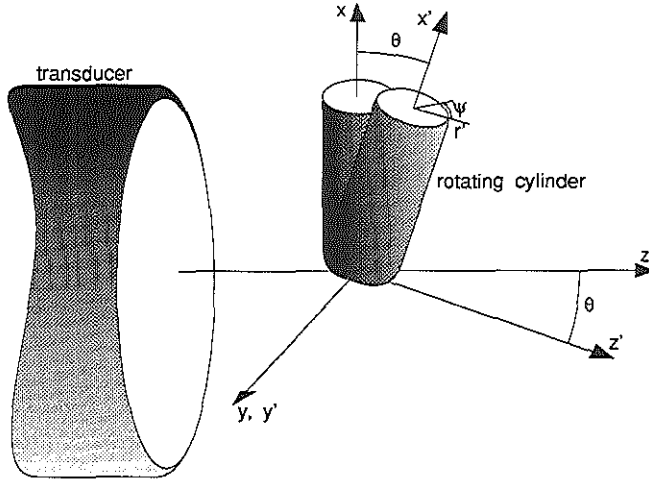


Figure V.2 Geometry of rotating cylinder, rotating Cartesian and cylindrical coordinates.

$$\begin{aligned}
 Z(z', r', \psi') &= \rho(z', r', \psi') c(z', r', \psi') \\
 &= \begin{cases} (\rho_0 + \Delta\rho) (c_0 + \Delta c) & \text{for } r' < a_s \wedge -l_s/2 < z' < l_s/2 \wedge 0 < \psi' < 2\pi \\ \rho_0 c_0 & \text{elsewhere} \end{cases}
 \end{aligned}
 \tag{V.10}$$

The inhomogeneity function can then be calculated according to:

$$\begin{aligned}
 \chi(x, y, z) &= \frac{1}{\rho_0 c_0} \frac{\partial(\rho c)}{\partial z} = \frac{1}{\rho_0 c_0} \frac{\partial(\rho c)}{\partial r'} \frac{\partial r'}{\partial z'} \frac{\partial z'}{\partial z} \\
 &= \cos\theta \cos\psi' R\delta(r' - a_s)
 \end{aligned}
 \tag{V.11}$$

where R is the relative impedance step at the cylinder boundary:

$$R = \frac{\Delta \rho \Delta c}{\rho_0 c_0} \quad (\text{V.12})$$

Rewriting equation (V.7) into the new coordinates (r', ψ', x') , and applying equation (V.11) for the inhomogeneity function, an analytical solution of equation (V.7) can be obtained, if the radius of the cylinder is much smaller than the wavelength, and if the length of the cylinder is much larger than the beamwidth⁹⁾ w_0 (using the standard integral solutions of Appendix F):

$$P^{bsc}(\theta, \omega) = \frac{j\sqrt{\pi}(k a_s)^2 R}{8 f_N} \rho_0 c_0 V^n(\omega) T(\omega) \cos\theta (1 - \tan^2\theta) e^{-2jkz_f} e^{-16f_N^2 \tan^2\theta} \quad (\text{V.13})$$

$$\text{for } l_s > w_0 \wedge a_s < \lambda$$

As was to be expected for a cylinder of infinite length, the change of the backscatter pressure with the angle of incidence only depends on the transducer properties, represented by the f-number (f_N). This equation also shows that the backscatter pressure does not depend on the absolute value of the cylinder radius, but on the cylinder radius with respect to the wavelength (ka_s).

If the radius of the cylinder is not much smaller than the wavelength, no analytical solution of equation (V.7) can be obtained. In this situation it appears to be convenient to calculate the backscatter pressure from the cylinder by superposition of the backscatter pressures from a number of circularly arranged knife edges (Figure V.3). As will be shown in the next paragraph, the backscatter pressure from one single knife edge of infinite length can be solved analytically. The superposition formula to be applied is given in paragraph V.4.3.

⁹⁾ The beamwidth indicates the e^{-1} decrease from the maximum at a specific depth. For a focussed transducer the beamwidth in focus is given by: $w_0 = 2\sqrt{2} f_N/k$.

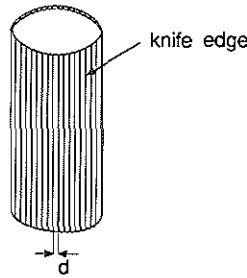


Figure V.3 A cylinder is composed of a number of circularly arranged knife edges; d : width of knife edges.

V.4.2 Scattering from a thin knife edge

A knife edge at arbitrary position and with arbitrary orientation can be described by the following line equation:

$$l: \begin{cases} z = n_z x + q_z \\ y = n_y x + q_y \end{cases} \quad (\text{V.14})$$

In this equation the direction of the knife edge is determined by the parameters $n_y = 1/\tan\alpha_y$ and $n_z = 1/\tan\alpha_z$, where α_y and α_z are the angles between the x-axis and the projection of the knife edge on the xy-plane and the xz-plane respectively (Figure V.4). The position of the knife edge is determined by the parameters q_y and q_z .

Then, for the general problem of scattering from a knife edge of width d , of finite length and with arbitrary orientation, the applicable expression for the inhomogeneity function is¹⁰⁾:

¹⁰⁾ Note that this equation is not applicable for knife edges parallel to the yz-plane ($\alpha_x = \alpha_y = 0$). However the analysis for a knife edge parallel to the yz-plane, is analogous to the analysis presented here.

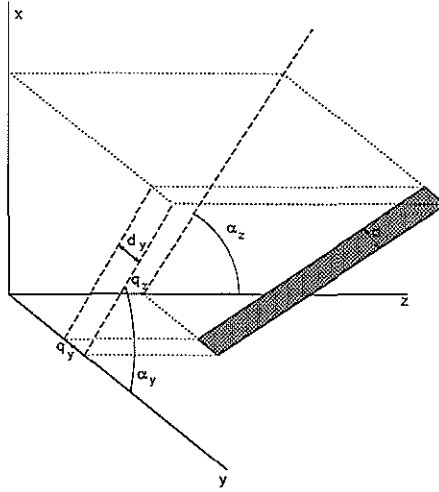


Figure V.4 Knife edge configuration with arbitrary orientation.

$$\chi = \begin{cases} R \delta(z - n_z x - q_z) & \text{for } y \in [n_y x + q_y - d_y/2, n_y x + q_y + d_y/2] \\ & \wedge x \in [x_-, x_+] \\ 0 & \text{elsewhere} \end{cases} \quad (\text{V.15})$$

in which $d_y = d \sqrt{1 + n_y^2}$

In this equation x_- and x_+ indicate the x-coordinates of the end points of the knife edge, d_y is the knife thickness in y-direction (see Figure V.4) and R is the relative impedance step (equation (V.12)). The y- and z-coordinates of the end points of the knife edge can be calculated from x_{\pm} , using equation (V.14).

Equation (V.15) is substituted in equation (V.7), and it is assumed that the knife thickness is much smaller than the wavelength ($d \ll \lambda$). After performing some algebraic manipulations (using results from Appendix E and Appendix F) the result is:

$$p^{bsc}(\omega) = \frac{\rho_0 c_0 V^n(\omega) T(\omega) kdR}{16\pi f_N} \sqrt{1+n_z^2} \exp[-2jk(z_f+q_z)] \quad (V.16a)$$

$$\exp\left[\frac{-(kq_y)^2}{16f_N^2(1+n_y^2)}\right] \exp\left[\frac{2jn_y n_z(kq_y)}{1+n_y^2}\right] \int_{s_-}^{s_+} \exp\left[-s^2 - \frac{8jn_z f_N}{\sqrt{1+n_y^2}} s\right] ds$$

in which:

$$s_{\pm} = \frac{\sqrt{1+n_y^2}}{4f_N} (kx_{\pm}) + \frac{n_y(kq_y)}{4f_N\sqrt{1+n_y^2}} \quad (V.16b)$$

If the knife edge has infinite length ($x_{\pm} \rightarrow \pm\infty$) the integral in equation (V.16) can be solved analytically (using Appendix F):

$$p^{bsc}(\omega) = \frac{\rho_0 c_0 V^n(\omega) T(\omega) kdR}{16\sqrt{\pi}f_N} \sqrt{1+n_z^2} \exp[-2jk(z_f+q_z)] \quad (V.17)$$

$$\exp\left[\frac{-(kq_y)^2}{16f_N^2(1+n_y^2)}\right] \exp\left[\frac{2jn_y n_z(kq_y)}{1+n_y^2}\right] \exp\left[\frac{-16f_N^2 n_z^2}{1+n_y^2}\right]$$

The various expressions in this equation can be explained as follows:

$\exp[-2jk(z_f+q_z)]$ (V.18a) gives the phase shift caused by the two-way wave propagation between transducer and scattering object,

$\exp\left[\frac{2jn_z n_y(kq_y)}{1+n_y^2}\right]$ (V.18b) is the phase resulting from an off-axis position and non-perpendicular incidence,

$$\exp\left[\frac{-(kq_y)^2}{16f_N^2(1+n_y^2)}\right] \quad (\text{V.18c})$$

is an amplitude decrease caused by an off-axis position of the knife edge,

$$\exp\left[\frac{-16f_N^2 n_z^2}{1+n_y^2}\right] \quad (\text{V.18d})$$

gives the amplitude decrease for non-perpendicular incidence,

$$\sqrt{1+n_z^2} \quad (\text{V.18e})$$

gives the amplitude increase, because the tilting of the cylinder causes the cylinder to move to a more sensitive part of the beam (on an average over the cylinder length).

It can be shown that the amplitude decrease, caused by non-perpendicular incidence (equation (V.18d)) dominates the small amplitude increase of equation (V.18e). This corresponds to the general idea that the amplitude must decrease with increasing angle of incidence, where the angle of incidence is defined with respect to the normal on the knife edge.

V.4.3 Superposition of knife edges to calculate cylinder response

In paragraph V.4.1 it has already been mentioned that the backscatter pressure from an arbitrary cylinder can be calculated by superposition of a number of circularly arranged knife edges. The outer surface of the cylinder is covered with a number (N) of equally spaced knife edges. To avoid spatial aliasing, the spacing between the knife edges is smaller than half the wavelength.

The response of one single knife edge can be calculated using equation (V.16), given the position and orientation of the knife edge. The orientation of the knife edges, represented by the parameters n_y and n_z , equals the orientation of the cylinder. The position vectors of the knife edges on the cylinder surface are calculated from the position vector

$x_0=(x_0,y_0,z_0)$ and the radius a_s of the cylinder as follows below.

The angle ψ_i is the angular position of the knife edge defined in a plane perpendicular to the main axis of the cylinder (Figure V.2), and the vector $r=(r_x,r_y,r_z)$ is the direction vector of the cylinder (and thus of the knife edges). A new Cartesian coordinate system is defined, of which one axis equals the cylinder main axis and the two other axes are defined in a plane perpendicular to the cylinder axis. The transform from the original coordinates to this new coordinate system is given by the following matrix:

$$A = \begin{pmatrix} r_x & r_y & r_z \\ \sqrt{1-r_x^2} & \frac{-r_x r_y}{\sqrt{1-r_x^2}} & \frac{-r_x r_z}{\sqrt{1-r_x^2}} \\ 0 & \frac{-r_z}{\sqrt{1-r_x^2}} & \frac{r_y}{\sqrt{1-r_x^2}} \end{pmatrix} \quad (\text{V.19})$$

Then the expression for the position vector x_i of the i^{th} knife edge on the cylinder surface is:

$$x_i = A^{-1}b_i + x_0$$

$$\text{with } b_i = \begin{pmatrix} 0 \\ a_s \cos(\psi_i) \\ a_s \sin(\psi_i) \end{pmatrix} \quad (\text{V.20})$$

In this equation the vector b_i is a vector pointing from the cylinder main axis to the i^{th} knife edge.

From the position vector of a knife edge the position parameters q_y and q_z can easily be calculated using equation (V.14).

The relative impedance step R_i of each knife edge has to be corrected for the orientation of the cylinder surface with respect to the incident beam, as is incorporated in the definition of the inhomogeneity function (equation (V.6)). Thus, the size of the relative impedance step R_i to be applied for the i^{th} knife edge depends on the angle ψ_i , corresponding to the particular knife edge, and on the orientation of the cylinder:

$$\mathcal{R}_i = \left[\sin\psi_i \left(\frac{-r_y}{\sqrt{1-r_x^2}} \right) + \cos\psi_i \left(\frac{r_x r_z}{\sqrt{1-r_x^2}} \right) \right] \mathcal{R} \quad (\text{V.21})$$

where \mathcal{R} is the relative impedance step at the cylinder boundary as given in equation (V.12).

V.4.4 Rotation of the transducer

The rotation of the transducer in the angle dependent experiments (Chapter II), is equivalent with a rotation of the scatter volume. The scatter volume will always be rotated in the xz -plane with the y -axis being the rotation axis. The knife edge parameters used in equation (V.15), $(n_z, n_y, q_z, q_y, x_-, x_+)$ depend on the rotation angle θ . If $(x_{\pm}, y_{\pm}, z_{\pm})$ are the coordinates of the begin and end points of the knife edge for $\theta=0$, then after rotation over an angle θ the begin end end points are given by:

$$\begin{pmatrix} x'_{\pm} \\ y'_{\pm} \\ z'_{\pm} \end{pmatrix} = \mathbf{R}_{\theta} \begin{pmatrix} x_{\pm} \\ y_{\pm} \\ z_{\pm} \end{pmatrix} = \begin{pmatrix} x_{\pm} \cos\theta + z_{\pm} \sin\theta \\ y_{\pm} \\ z_{\pm} \cos\theta - x_{\pm} \sin\theta \end{pmatrix} \quad (\text{V.22})$$

In this equation \mathbf{R}_{θ} represents the rotation over the angle θ , with the y -axis being the rotation axis, and the rotated coordinates are indicated by a prime: '.

If the initial direction and position of the knife edge at $\theta=0$ are described by the parameters n_z, n_y, q_z, q_y (equation V.4.2), then after rotation over an angle θ the knife edge parameters are given by:

$$\begin{aligned}
 n_y' &= \frac{n_y}{\cos\theta + n_z \sin\theta} \\
 n_z' &= \frac{n_z \cos\theta - \sin\theta}{\cos\theta + n_z \sin\theta} \\
 q_z' &= q_y \cos\theta - \frac{q_z \sin\theta (n_z \cos\theta - \sin\theta)}{\cos\theta + n_z \sin\theta} \\
 q_y' &= q_y + \frac{n_y q_z \sin\theta}{\cos\theta + n_z \sin\theta}
 \end{aligned}
 \tag{V.23}$$

The rotation can be introduced in equations (V.15), by substitution of the parameters n_x , n_y , q_x and q_y by the angle dependent parameters n_x' , n_y' , q_x' and q_y' of equation (V.23). This results in an analytical expression for the angle dependent backscatter of a knife edge with arbitrary initial orientation and position. By superposition of the response of an appropriate set of knife edges the response of any cylinder can thus be simulated.

V.4.5 Random scatterer distribution

A distribution of scatterers has to be defined in the scatter volume V_s . Basically a regular 3D grid is defined. In each grid-point a cylinder with fixed size and orientation is defined. To each coordinate of each grid-point a random deviation according to a uniform distribution is added. The length and radius of each cylinder are also a sample out of a uniform distribution, while a normal distribution is applied to the orientation of the cylinder.

V.5 Transducer characterization

In the previous paragraphs it appeared that besides the properties of the tissue, also the transducer properties have influence on the measured backscatter pressure from tissue. In this paragraph the transducer properties ($V^n(\omega)$ $T(\omega)$ and f_N) are estimated from the angle dependent reflection measurements on a flat plate.

V.5.1 Mathematical model

Equation (V.7) can also be used to calculate the angle dependent reflection from a flat plate positioned in focus. The angle dependent inhomogeneity function of a flat plate, which has a reflection coefficient R and which is oriented parallel to the xy -plane at $\theta=0$, is:

$$\chi = R \delta(z - x \tan\theta) \quad (\text{V.24})$$

Substituting equation (V.24) into the 3D-integral of equation (V.7) and applying the integral solutions given in Appendices E and F results in:

$$P^{refl}(\omega) = \frac{1}{2} \rho_0 c_0 V^n(\omega) T(\omega) R e^{-2jkz_f} \sqrt{1 + \tan^2\theta} e^{(-16f_N^2 \tan^2\theta)} \quad (\text{V.25})$$

From equation (V.25) it follows that the rate of angle dependence of the reflected pressure only depends on the f -number of the transducer. The spectral behaviour of the reflected pressure depends on the vibration and detection properties of the transducer and the receive and transmit electronic devices.

V.5.2 Measurements

A flat plate is positioned in focus of a focussed transducer. A revolving transducer holder is used to vary the angle of incidence. The angle indicated by the transducer holder is represented by the symbol θ^* . At $\theta^*=0$ the flat plate can still be slightly tilted with respect to the normal on the incident beam, as indicated in Figure V.5.

V.5 Transducer characterization

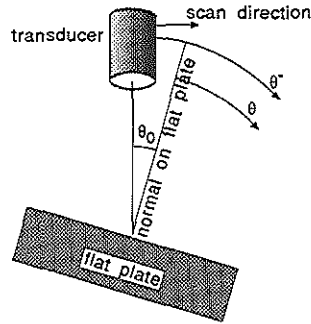


Figure V.5 Angle dependent reflection measurements on a flat plate in the focus of the transducer.

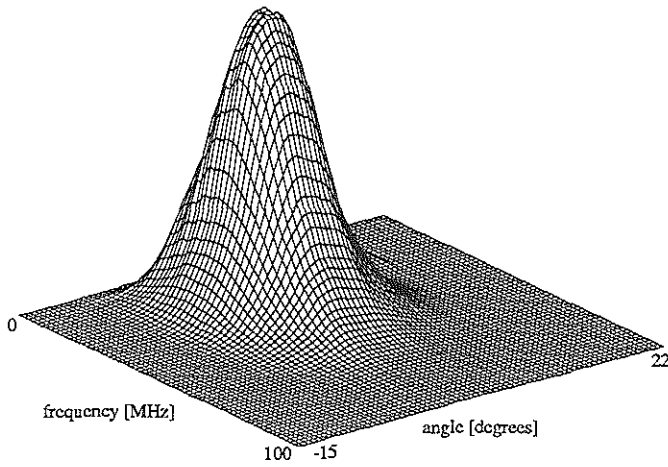


Figure V.6 Measured amplitude spectra (linear scale) at varying angle of incidence of a flat plate in focus.

Of the reflected signals the amplitude spectra are calculated by means of a Fourier transformation. The resulting amplitude spectra at varying angles θ^* are shown in Figure V.6.

V.5.3 Curve fitting

Method

The experimental results of the angle dependent measurements on the flat plate are used to calculate the transducer properties, which are the f-number, f_N , and the spectral behaviour, $V^n(k)$ and $T(k)$, of the transducer. An additional unknown parameter, which is not accounted for in equation (V.25), is the offset θ_0 in the angle of the transducer holder. The angle θ_0 is defined as the angle of the revolving transducer holder at which the main axis of the incident ultrasonic beam is perpendicular to the surface of the flat plate (Figure V.5). As such the relation between θ , θ^* and θ_0 is given by:

$$\theta = \theta^* - \theta_0 \quad (\text{V.26})$$

Then the mathematical expression for the measured pressure amplitude $P_{l,m}$ at angle θ_l^* and at frequency ω_m , is:

$$|P_{l,m}^{bsc}| = P_{0,m} e^{-2jk_m z_l} \sqrt{1 + \tan^2(\theta_l^* - \theta_0)} e^{(-16f_N^2 \tan^2(\theta_l^* - \theta_0))} \quad (\text{V.27})$$

$$\text{for } l = 1..L \quad \wedge \quad m = 1..M$$

in which L is the number of angles (θ_l^*) at which the measurement is performed and M the number of frequency components (ω_m) at which the pressure amplitude is calculated. The pressure $P_{0,m}$ is the measured pressure amplitude at perpendicular incidence ($\theta^* = \theta_0$). Theoretically $P_{0,m}$ equals:

$$P_{0,m} = \frac{1}{2} \rho_0 c_0 V_m^n T_m R \quad \text{for } m = 1..M \quad (\text{V.28})$$

A least square fit of the experimental data to equation (V.27) can more easily be applied, if this equation is approximated by:

$$P_{l,m}^{bsc} = P_{0,m} e^{-2jk_m z_f} e^{\left(\frac{1}{2} - 16f_N^2\right) (\theta_l^{exp} - \theta_0)^2} \quad (V.29)$$

The deviation of this approximation from the exact solution of equation (V.27) is smaller than 4% for angles $(\theta_l^* - \theta_0)$ between -45 and 45 degrees.

Taking the natural logarithm of equation (V.29) results in a polynomial of the second degree with its parameters depending on the f-number, the angle offset θ_0 and the spectrum $P_{0,m}$. The least squares estimates of the parameters can easily be calculated (Appendix G).

Results

The estimated f-number of the applied transducer equals 1.84, and its standard error of the mean is 0.01. The measured and fitted amplitude spectrum at perpendicular incidence are given in Figure V.7. To illustrate the change of the reflected pressure with the angle of incidence, the measured and fitted pressure versus angle curves at 29 MHz are shown in Figure V.8.

From the good agreement between the fitted curves and the experimental data it follows that the theoretical model gives a quite good description of the measurements.

V.6 Results of simulations

In the mathematical model a large number of parameters describing the scattering medium and the transducer, are free to chose. To get better insight in the effect of the individual parameters on the backscatter pressure, the backscatter properties of a few relatively simple objects and scatter media were calculated, before calculations on tissue-like scattering media were performed.

In the presentation of the results of these calculations, the distance and length parameters were normalised with the wavenumber k , which enables to present modelling results on objects without being fixed to only one frequency. This is allowed because all distance and length parameters in equation (V.16) occur in combination with the wavenumber.

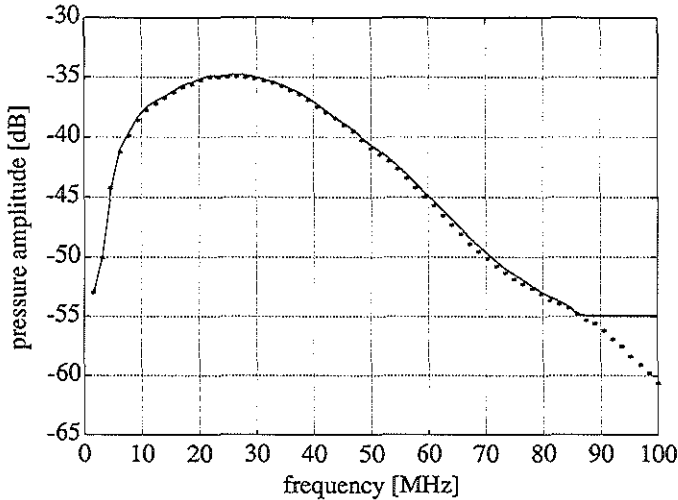


Figure V.7 Measurements and fitted amplitude spectrum of reflection from a flat plate in focus of a focussed transducer at perpendicular incidence.

V.6.1 Backscatter from one single cylinder

Varying radius at perpendicular incidence

Equation (V.13), which was deduced with the assumption that the length of the cylinder is infinite ($l_s \gg w_0$) and the radius is much smaller than the applied wavelength ($ka_s \ll 2\pi$), was used to calculate the backscatter pressure of a cylinder of infinite length for increasing ka_s . The cylinder was positioned in the focus of a focussed transducer ($f_N = 2.0$) and parallel to the xy -plane (Figure V.1). A monochromatic incident pressure wave was assumed. The same problem was solved using the solution method of paragraph V.4.3, where the cylinder surface was covered by a number of circularly arranged knife edges.

The calculated backscatter power for increasing ka_s are shown in Figure V.9. The discrepancy between both solutions indicates that the 'small radius' solution (equation (V.13)) deviates less than 5 % from the 'knife edge' solution for cylinders with ka_s smaller

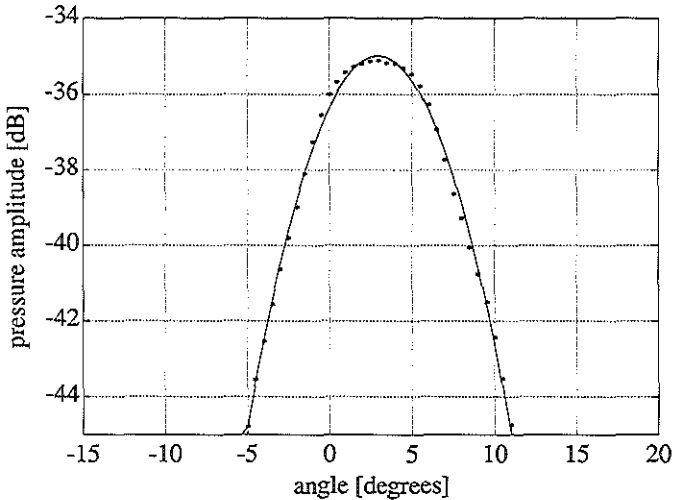


Figure V.8 Measured and fitted angle dependent reflection from a flat plate.

than 0.6. For example, at 30 MHz, the 'small radius' solution can only be used to calculate the response of cylinders with a radius smaller than 4.8 μm .

In the 'knife edge' solution, a regular pattern of minima and maxima is shown in Figure V.9. This is the result of the alternating negative and positive interference of the backscatter waves emanating from the backside and the frontside of the cylinder. This result is the same as the result obtained by Stanton [9], who calculated the (differential) backscattering cross-section¹¹⁾ of a cylinder of infinite length in a plane incident pressure wavefield.

¹¹⁾ The differential scattering cross section is defined as the squared angle directivity $f(\phi, \vartheta)$ of the scattered pressure: $P^{\text{sc}} = P_0 (c^{\text{sc}}/r) f(\phi, \vartheta)$, where ϕ is the angle between the plane through the incident beam and the cylinder axis and the plane through the detection direction and the cylinder axis, and where ϑ is the angle between the incident beam and the cylinder axis. To obtain the backscatter cross section the angle ϕ is equated to π .

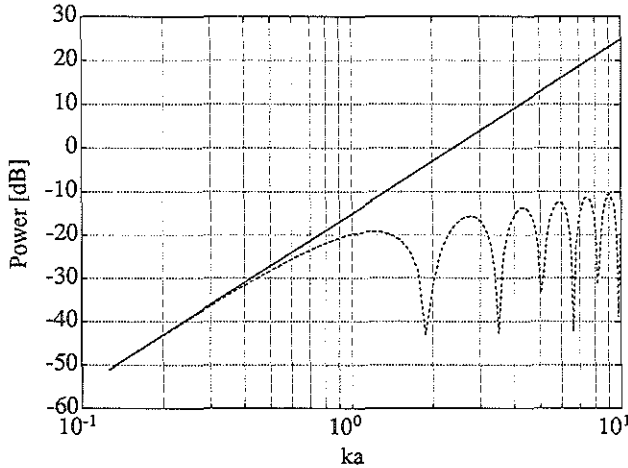


Figure V.9 Backscatter amplitude of one cylinder of infinite length in focus ($f_N=2.0$) for increasing ka ; solid line: 'small radius' solution; dashed line: 'knife edge' solution.

Varying length at perpendicular incidence

The results presented in Figure V.9 were obtained for a cylinder of infinite length. Thus, the backscatter pressure from the knife edges was calculated analytically using equation (V.17). However, if the length of the knife edges becomes smaller than the beamwidth of the applied transducer, the integral in equation (V.16) has to be solved numerically.

Again the backscatter power from a cylinder was calculated, regarding the cylinder as a number of circularly arranged knife edges, only this time the radius of the cylinder was fixed ($ka_r = 0.5$), while the length (kl) of the cylinder was varied. In Figure V.10 the 'infinite length' solution and the numerically obtained solution of the backscatter power are shown.

These results show that the 'infinite length' solution is valid within 5% for $kl > 22$. This result agrees with the applied condition for the 'infinite length' solution, i.e. $l > w_0$.¹²⁾

¹²⁾ Using footnote 9 on page 80 it follows that $l > w_0$ is equivalent with $kl > 2\sqrt{2} f_N$.

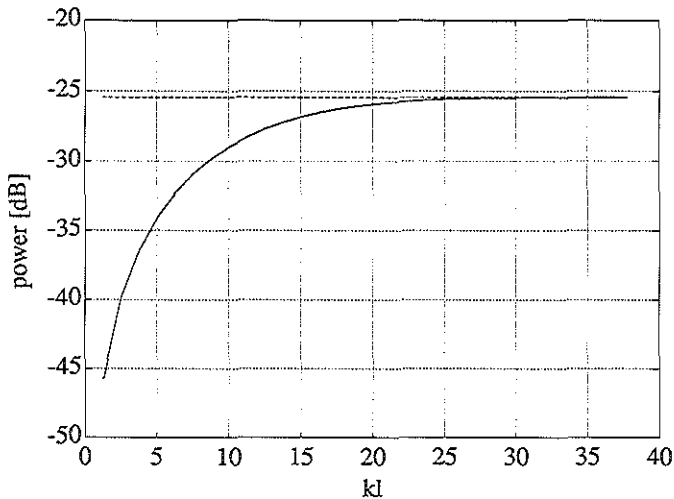


Figure V.10 Backscatter amplitude of one cylinder in focus at perpendicular incidence for increasing kl ; solid line: numerical solution (equation (V.16)), dashed line: 'infinite length' solution (equation (V.17)).

Varying angle of incidence

The angle dependent backscatter from one single cylinder was calculated for varying cylinder length. The cylinder was positioned parallel to the x -axis, while the transducer rotated in the xz -plane with the y -axis being the rotation axis. The f -number of the transducer used in the experiments of Chapter II, was applied ($f_N=1.84$)

Then, gaussian curves were fitted to the calculated angle dependent pressure curves, in the same way as was done for the experimentally obtained pressure-angle curves (Chapter II and Appendix G). This resulted in the directivity parameter and maximum power as a function of the cylinder length (Figure V.11).

Figure V.11A illustrates the effect of cylinder length on the directivity parameter. Compared to the feasible accuracy of the applied measurement system, i.e. $2.5 \cdot 10^{-4}$ dB/degree² (Chapter II), the directivity parameter appears to be quite sensitive to changes in kl in the

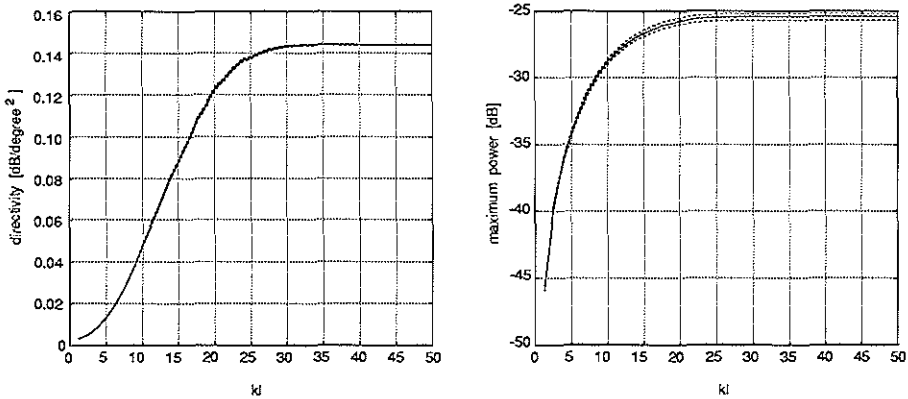


Figure V.11 Backscatter from one cylinder ($ka_s=0.5$) in focus ($f_N=1.84$) with increasing cylinder length; solid line: mean, dotted line: mean \pm standard deviation; A) directivity parameter; B) maximum power.

range of $3 < kl < 25$. At a frequency of 30 MHz this corresponds to a range in cylinder length of $20 \mu\text{m} < l < 200 \mu\text{m}$.

At high kl values ($kl > 30$) the directivity curves approach asymptotically to a maximum value. This maximum directivity only depends on the f -number of the transducer and equals the directivity measured on a flat plate, i.e. $0.142 \text{ dB/degree}^2$ for the applied transducer (see paragraph V.5). For low kl values the shape of the directivity curve is independent of the f -number of the transducer. To illustrate this the dependence of the directivity parameter on kl for several different f -numbers (1.5, 2 and 2.5 respectively) is shown in Figure V.12.

The maximum power versus kl curves (Figure V.12B) suggests that, considering the experimental accuracy of 0.023 dB (Chapter II), also the maximum power may give an indication of the cylinder length. However, a complicating factor is that the maximum power is influenced by various other scatter properties, e.g. cylinder radius and reflection coefficient. These scatter properties do not have an effect on the measured directivity.

A directivity versus size curve, as shown in Figure V.11A and in Figure V.12 can be a

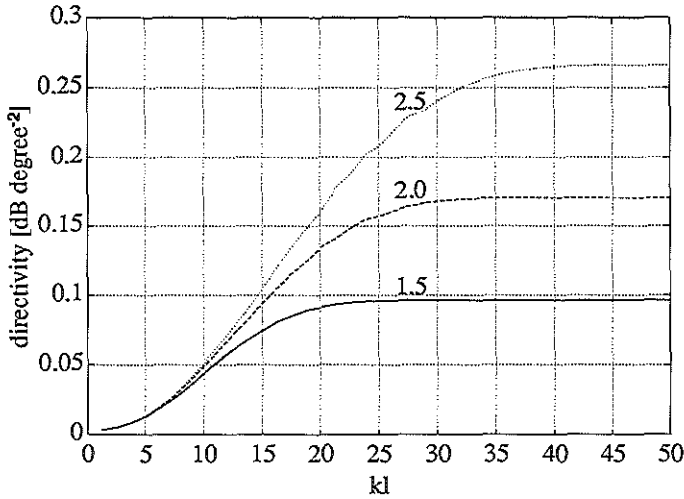


Figure V.12 Backscatter directivity of one cylinder ($ka_s=0.5$) in focus with increasing cylinder length for various f-numbers: 1.5, 2 and 2.5.

useful tool in deciding on which transducer (frequency and f-number) is to be applied for a specific application of angle measurements, if the scatter sizes are known beforehand.

V.6.2 Backscatter from a distribution of scatterers

Besides the size of the scatterers also the distribution of scatterers in space may have considerable influence on the scatter properties. To assess the influence of the grid, that defines the positions of the scatterers, the angle dependent backscatter power of various distributions of point and cylindrical scatterers was calculated. In the presentation of the results the power versus angle curves are normalised with the maximum power (i.e. power at perpendicular incidence). Table V.1 gives an overview of the scatter medium parameters applied in the simulations of which results are shown in this and the following paragraphs.

Table V.1 Medium parameters applied in simulations. Cylinders are oriented in x-direction.

figure	grid spacing (μm) ¹⁾			length (μm)	radius (μm)
	x	y	z		
Figure V.13	{80(20)140;0}	∞	∞	1	1
Figure V.14	{80(20)140;0}	∞	∞	50	4
	∞	∞	∞	50	4
Figure V.15	{80(20)140;0}	{30;0}	{30;0}	1	1
Figure V.16	{80;40}	{30;15}	{30;15}	1	1
	{80;0}	{30;0}	{30;0}	1	1

¹⁾ The following syntax is applied for stochastic uniformly distributed variables: $\{\mu;\epsilon\}$, in which μ is the average value and ϵ is the width of the uniform distribution.

To obtain a clear analogy of the defined scatter media with the morphology of tissue or RBC-suspensions, from here on the length and distance variables will no longer be expressed in terms of the wavenumber k . All results presented, were obtained at 30 MHz ($k = 1.2566 \cdot 10^5 \text{ m}^{-1}$), which is about the center frequency of the applied transducers in the experiments.

Equidistant 1D-grid

The influence of an equidistant grid is illustrated in Figure V.13 and Figure V.14.

Figure V.13 gives the backscatter power from a 1D distribution of point scatterers on the x-axis with equidistant positions. The spacing of the grid was varied from 50 μm to 140 μm . The shapes of angle dependent backscatter power curves are the result of the interference of the backscatter pressure waves of the individual scatterers.

The same grid definition was applied for calculations on a 1D distribution of cylindrical scatterers (length: 50 μm , radius: 4 μm) of which the results are shown in Figure V.14. In this figure also the angle dependent backscatter power of one single cylinder of the same size and positioned in focus is given.

These results demonstrate that with decreasing grid spacing the effect of the grid on the

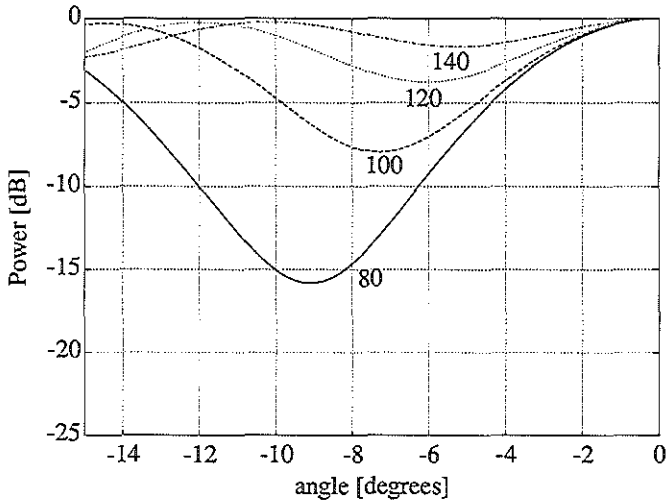


Figure V.13 Backscatter pressure versus angle of incidence for a 1D distribution of point scatterers on the x-axis for various regular spacings. (Table V.1).

directivity increases. For grid spacing smaller than 120 μm the grid directivity is stronger than the cylinder directivity.

Regular 3D-grid

For a regular 3D grid, the interference pattern will be more complicated, but the effect of a regular grid on the directivity is as prominent as in the 1D situation. This is illustrated in figure Figure V.14, which shows the backscatter pressure of point scatterers regularly distributed in space.

Irregular spacing

An irregular spacing was obtained by adding to the coordinates of the regular grid points a random deviation, which was taken out of a uniformly distributed stochastic variable. The backscatter power of point scatterers positioned at the resulting irregularly spaced grid-points was calculated. This was repeated twenty times, each time using a new set of

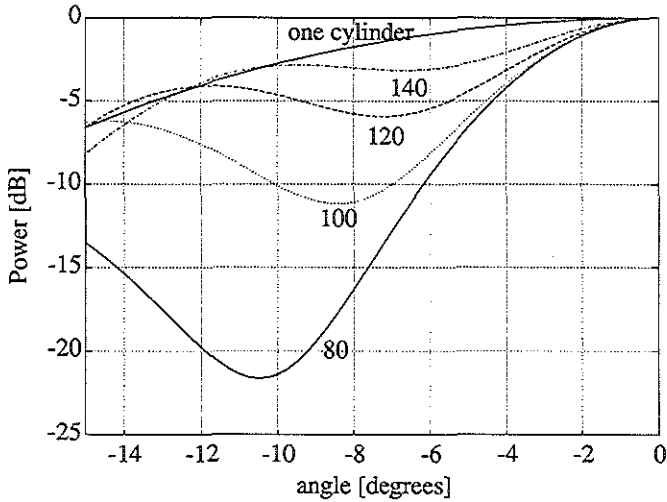


Figure V.14 Backscatter pressure versus angle of incidence for a 1D distribution of cylindrical scatterers on the x-axis for various regular spacings, and for one cylinder in focus (Table V.1).

samples taken out of the same stochastic variables and the twenty calculated backscatter power curves were averaged. The resulting averaged backscatter power curve is shown in Figure V.16, together with the backscatter power curve of point scatterers on a regular grid with the same spacing. According to this result, the influence of an irregular grid on the backscatter directivity is much smaller than the influence of a regular grid.

V.6.3 Modelling of muscular media

As described in Chapter II, the muscular media predominantly consists of circularly and concentrically arranged smooth muscle cells, which are 25-80 μm long and 1-8 μm in diameter, with some connective tissue in between.

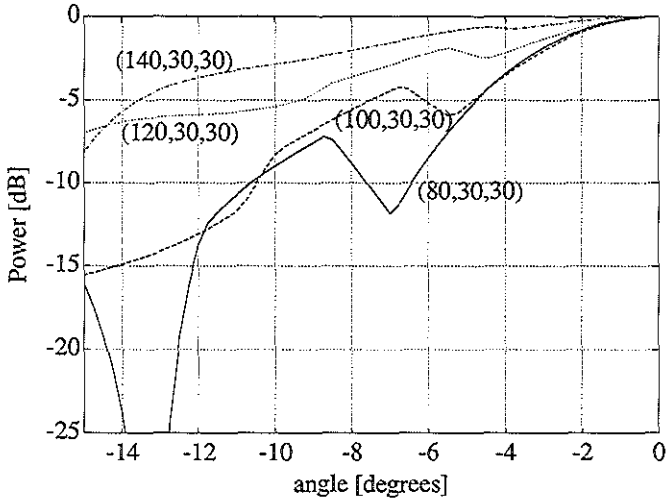


Figure V.15 Backscatter pressure versus angle of incidence for a 3D distribution of point scatterers for various regular spacings (Table V.1).

The angle dependent measurements on the muscular media were simulated by describing the muscular media as a distribution of cylindrical scatterers oriented in one direction. Since in the modelling geometry the scatter volume was always rotated in the xz-plane (paragraph V.4.4), the main orientation of the cylinders was chosen parallel to the x-axis to simulate the tangential scan and parallel to the y-axis to simulate the axial scan. The cylindrical scatterers were distributed over an irregular grid and the same procedure was followed to obtain the averaged backscatter power versus angle curve as described in paragraph V.6.2.

Scatter-medium definition

Calculations on four different scattering media, of which the parameters are given in Table V.2, were performed. In the first scattering medium the average length of the cylinders was 30 μm , which is supposed to be smaller than the average length of the smooth muscle cells. The average length of the cylinders of the second medium is 60 μm , which corresponds to the average length of the smooth muscle cells. In the third medium the same

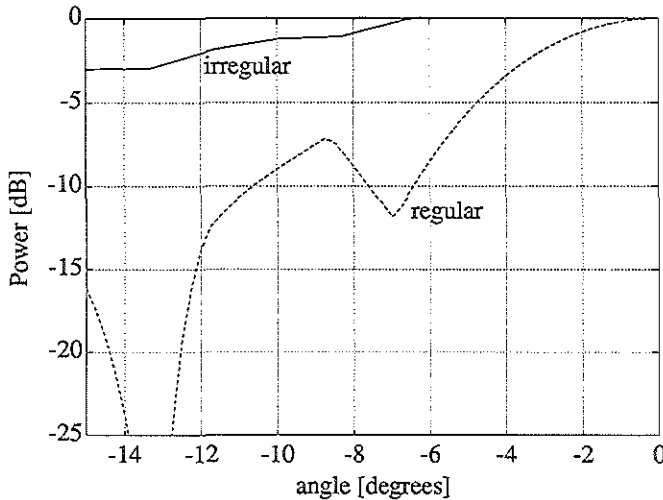


Figure V.16 Backscatter pressure versus angle of incidence for a 3D distribution of point scatterers; solid line: irregular grid, dashed line: regular grid (Table V.1).

cylinder length was defined as in the second medium, only a variation in the orientation of the cylinders was applied. This variation was a sample from a normally distributed stochastic variable with mean value equal to zero and standard deviation equal to 10 degrees. Finally the fourth medium contains cylinders with average length equal to 120 μm , which is considerably longer than the average length of the smooth muscle cells.

Results

The tangential angle dependence of backscatter power, resulting from calculations on the scatter media as defined in Table V.2, are presented in Figure V.17. The applied grid spacing was the same in all simulated scattering media. From additional calculations with varying grid spacings, it appeared that the influence of the grid spacing was small compared to the influence of the scatterer size, as long as the grid was irregular.

The grey area in Figure V.17 is the 68% confidence range (i.e. the calculated standard deviation) of the measured normalised power-angle curves of the muscular media (Chapter

V.6 Results of simulations

Table V.2 Model parameters used in computer simulations of muscular media.

marker in Figure V.17	cylinder length (μm)	cylinder radius (μm)	grid spacing (μm)			varia- tion in orien- tation ($^\circ$) ¹⁾
			x	y	z	
•	{30;15}	{4;2}	{60;30}	{30;15}	{30;15}	0
▲	{60;30}	{4;2}	{120;60}	{30;15}	{30;15}	0
◇	{60;30}	{4;2}	{120;60}	{30;15}	{30;15}	10
□	{120;60}	{4;2}	{120;60}	{30;15}	{30;15}	0

¹⁾ Main orientation of cylinders is in x direction.

²⁾ The following syntax is applied for stochastic uniformly distributed variables: $\{\mu;\varepsilon\}$, in which μ is the average value and ε is half the width of the uniform distribution.

II). Also the calculated backscatter versus angle curve of one cylinder of 60 μm length positioned in focus is shown in Figure V.17.

The same statistical analysis was applied to the curves of Figure V.17 as was applied to the experimental results (Chapter II). From this analysis it followed that the differences between the curves are significant ($P < 0.001$). The results presented in Figure V.17 suggest that the third medium, with average cylinder length of 60 μm and a 10 degrees variation in the orientation of the cylinders, gives an appropriate description of the scatterer distribution in the muscular media. However, the possibility that simulations on other scatterer distributions results in the same angle dependent behaviour of the backscatter power cannot be precluded. E.g. the response of a distribution of cylinders with an average length somewhere between 30 μm and 60 μm will probably correspond as well to the experimental results. However, the exact properties of the scatterers are not known.

Figure V.18 shows the results of simulations on the influence of the angle variation in the axial plane on the backscatter power from the second scattering medium of Table V.2. These results correspond well to the experimental results, indicated by the grey area (68% confidence range). No different effect on the axial angle dependence is to be expected from

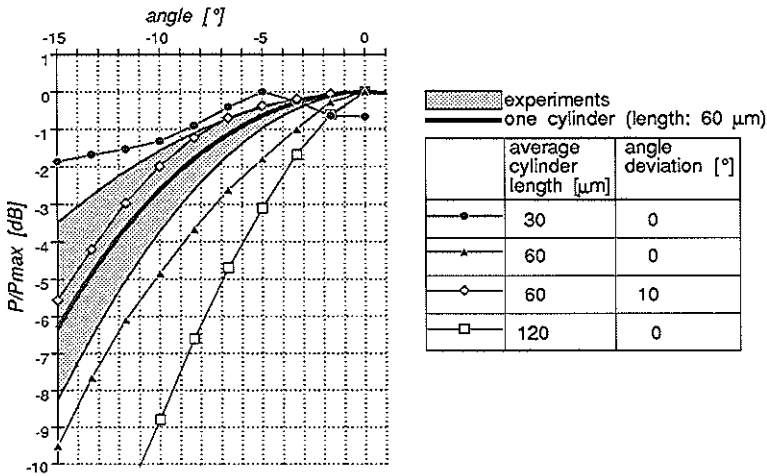


Figure V.17 Simulated backscatter pressure versus angle of incidence in the tangential plane of scattering media representing the muscular media (Table V.2) in comparison with the experimental results.

the other three scattering media of Table V.2, because these media only have different scatter properties in the plane perpendicular to the axial plane.

Also the results of the simulations on one cylinder of 60 μm length and with a radius of 4 μm correspond well to the experimental results.

V.6.4 Modelling of elastic media

The elastic media is formed of numerous and distinct concentric elastic lamellae, which are extensively fenestrated and interconnected by branches so that they form a three-dimensional meshwork. The elastic lamellae have spirally arranged smooth muscle cells with surrounding collagen sandwiched in between (Chapter I). Generally it is assumed that the elastin, present in the elastic lamellae and their branches are mainly responsible for the acoustic behaviour of the elastic media. With the current knowledge of the morphology of the elastic media, it is impossible to find a plausible analytical expression for the inhomogeneity function of this tissue type.

V.6 Results of simulations

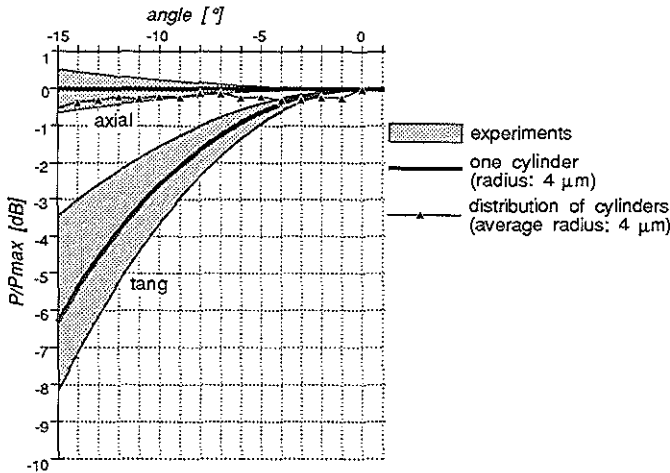


Figure V.18 Simulated backscatter pressure versus angle of incidence in the axial plane of a scattering medium representing the muscular media, in comparison with the experimental results.

At first sight the lamellae look like plane reflectors. However, the measured directivity is much lower than the reflectivity of a flat plate. Apparently the deviations of the lamellae from a plane reflector (fenestrations, branches, surface irregularities) are not small compared to the wavelength. Based on Figure V.11 and the measured directivity, i.e. 0.073 ± 0.010 (mean \pm standard deviation) in tangential direction and 0.038 ± 0.009 in axial direction, the characteristic dimensions of these irregularities are estimated to be 90 - 115 μm in tangential direction and 60 - 80 μm in axial direction. There is no histologic evidence of these dimensions to be characteristic for the elastic media.

V.6.5 Modelling of collagen lesions

Scatter-medium definition

On histologic sections both dense and loose collagen lesions exhibit threadlike structures with random orientation parallel to the surface of the arterial wall.

Simulations were performed on a irregular distribution of thin cylinders with random orientation parallel to the xy -plane at $\theta=0$ (Figure V.2). Two different average cylinder lengths were applied: infinite length and 120 μm .

Results

Results of these simulations, together with the 68% confidence region of the experimentally obtained normalised backscatter-angle curves are shown in Figure V.19.

The results of the simulations on the cylinders with the average length equal to 120 μm corresponds well to the experimental results. However, from histological sections of the collagen lesions there is no evidence that the average fiber length is approximately equal to 120 μm .

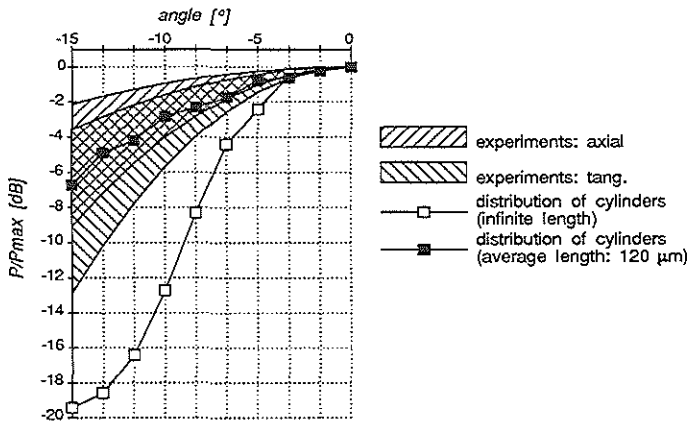


Figure V.19 Simulated backscatter pressure versus angle of incidence of scattering media representing collagen lesions, in comparison with the experimental results.

V.6.6 Modelling of blood

Scatter-medium definition

Aggregated red blood cells were represented by a irregular distribution of cylinders oriented perpendicular to the incident pressure beam. Aggregation of red blood cells was simulated by increasing the average cylinder length with a proportional decrease of the number of

cylinders. The backscatter power (at 30 MHz) at perpendicular incidence was calculated for cylinder distributions with increasing average cylinder length: 50 μm , 80 μm , 100 μm , 120 μm and 150 μm . This corresponds to an average aggregate length of approximately 20, 32, 40, 48 and 60 RBCs. The simulated Hematocrit value was 30%.

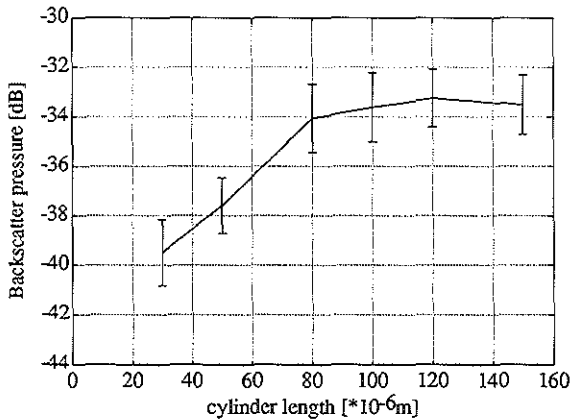


Figure V.20 Simulated backscatter power of blood with increasing aggregate size.

Results

The results of these calculations are shown in Figure V.20. To the numerical results the same statistical analysis was applied as was applied to the experimental results of backscatter measurements on static blood samples (Chapter IV.2). It followed that the effect of aggregate length on the backscatter power is significant ($P < 0.001$). Applying the method of Scheffé the pair wise differences between the simulation results were evaluated. It followed that the backscatter power from each scatter medium with cylinders shorter than 100 μm is significantly different from the backscatter power of all the other media. The results of scatter media with cylinders of 100 μm and longer cannot be distinguished from each other.

These result show that for short aggregates the backscatter power increases with the aggregate length. Obviously, the effect of increasing cylinder length on the backscatter

power is stronger than the effect of decreasing concentration for aggregates smaller than 100 μm . If the aggregates become longer than 100 μm , no significant effect of the simulated aggregation on the backscatter power was found.

V.7 Discussion

As mentioned in the introduction, the main differences between the mathematical modelling of tissue scattering applied in this Chapter and the mathematical modelling reported by others [8][10] are:

- in the present modelling there are no restrictions to the dimensions of the scatterers, while others assume Rayleigh scattering [8][10].
- the concentration of scatterers is not limited, while others assume low particle concentration [8][10].

Although these features open new possibilities in the simulation of tissues and blood, at the same time they cause that the resulting mathematical expression depends on a large number of scatter-medium parameters.

A complication of this large number of parameters is that it is very difficult to get insight into the effect of each of these parameters on the backscatter behaviour of the scatter-medium. So far the modelling results presented above showed that the effect of the spacing of the scatterers is predominant if the scatterers are positioned on a regular 3D grid. However, if a random deviation is added to each coordinate of each grid point, the effect of spacing on the backscatter behaviour is much less important. It was also shown that there exists a significant effect of the average cylinder length on the backscatter power. The influence of a random variation in orientation of a distribution of equally oriented cylinders on their backscatter behaviour was also demonstrated. The influence of many other parameters remains to be investigated.

Another problem is that the values of the medium parameters have to be deduced from other than acoustical observations, e.g. from histological studies on tissues or from optical microscopic images of blood. Often the values of some parameters remain unknown or uncertain. However, correspondence with the experimental results can be obtained with various combinations of medium parameters.

Unless these uncertainties in the modelling, the results help to get better insight in the

acoustic behaviour of arterial tissue and blood. For instance it was shown that the directivity parameter is directly related to the size of the scatterer. This fortifies the idea that the directivity parameter will have a specific value for each tissue type, because scatter sizes vary per tissue type. When the size of a representative structure in a specific tissue type is known, the directivity can be estimated using Figure V.10. Or the other way around, when the directivity of a tissue specimen is measured, the size of the responsible scatterers can be estimated.

The measured angle dependent properties of the muscular media and of collagen lesions were simulated defining scatter-media that correspond to the observed morphology of these tissue types. Because different scatter media can give the same results in the mathematical simulation, only a qualitative description of the properties of the tissue mimicking scatter media can be given as follows.

For the muscular media the scatter medium consists of irregularly spaced cylindrical scatterers, oriented in the tangential direction. The length of these cylinders might vary between 30 and 80 μm . The radius of the cylinders is much smaller than the wavelength (i.e. 50 μm). Also a small random variation in the orientation of each cylinder might be present.

For dense and loose collagen the scatter medium consists of irregularly spaced thin cylinders. The cylinders have random orientation parallel to the surface of the arterial wall. Probably, the average length of these cylinders is approximately 120 μm .

Finally the results of the simulations on scatter media that represent blood correspond well to the experimental results. Because approximately the same backscatter power was measured from whole blood as from rouleaux enhanced blood, it is deduced from Figure V.20 that the average length of aggregates in whole blood is approximately 100 μm (i.e. 40 RBCs). Then, extrapolating the simulation results to zero cylinder length, the backscatter pressure from rouleaux suppressed blood (aggregate length $\rightarrow 0$) is estimated to be 9 dB lower than the backscatter pressure of whole blood. In the experiments a 13 dB difference between whole blood and rouleaux suppressed blood was observed.

The mathematical model can be useful in the future to assess the effect of changed experimental conditions. E.g. the influence of changed transducer conditions can be predicted or the influence of accidental misalignment of the tissue can be predicted from new calculations with the mathematical model.

V.8 Conclusion

The directivity parameter, as defined in Chapter II.2, appears to be related to the size of the scatterers in the tissue. However, the measured directivity is also slightly affected by the spacing of the scatterers.

The backscatter behaviour of the muscular media and of collagen lesion was simulated, defining tissue mimicking scatter-media, that consist of a distribution of cylindrically shaped scatterers. Also the backscatter power of blood with various degrees of aggregation of RBCs was simulated with a irregular distribution of cylindrical scatterers. Good correspondence between simulation results and experimental results was found.

References

- [1] Berkhout AJ: Applied seismic wave theory. Amsterdam, Elsevier 1987
- [2] Chernov LA: Wave Propagation in a Random Medium (McGraw-Hill, New York, 1960), Chap.IV
- [3] Hanss M., Boynard M.: Ultrasound backscattering from blood: heamtocrit and erythrocyte aggregation dependence. Ultr. Tissue Char. II, M. Linzer (Ed.), National Bureau of Standards, Spec. Publ.: 525, 1979.
- [4] Kuo I.Y., Shung K.K.: High frequency ultrasonic backscatter from Erythrocyte suspension. Submitted for IEEE Trans Biomed Eng.
- [5] Lizzi FL, Greenebaum M, Feleppa EJ, Elbaum M: Theoretical Framework for Spectrum Analysis in Ultrasonic Tissue Characterization. J.Acoust.Soc.Am.73(4):1366-1373, 1983
- [6] Morse PM, Ingard KU: Theoretical Acoustics. Princeton University Press, 1968
- [7] O'Neil H: The Theory of Focusing Radiators, J.Acoust.Soc.Am.21,516-526(1949)
- [8] Romijn L: On the Quantitative Analysis of Ultrasound Signals and Application to Intracular Melanomas. Nijmegen, 1990
- [9] Stanton T.K.: Sound scattering by cylinders of finite length. I. Fluid cylinders. J Acoust Soc Am 83(1): 55-63, 1988.

References

- [10] Ueda M., Ozawa Y.: Spectral Analysis of Echoes for Backscattering Coefficient Measurement. *J.Acoust.Soc.Am.*77(1):38-47, 1985

Appendix A Shear rate between coaxial cylinders

Bird et al. [1] derived the following expression for the shear rate $\dot{\gamma}$ in a Newtonian¹³⁾ fluid between two coaxial cylinders, the outer one of which is rotating with an angular velocity Ω (Figure IV.1).

$$\dot{\gamma}(r) = 2 \Omega \frac{1}{R_o^2 - R_i^2} \left(\frac{R_i R_o}{r} \right)^2 \quad (\text{A.1})$$

In this equation R_o is the radius of the outer cylinder, R_i is the radius of the inner cylinder and r is the radial distance to the cylinder axes.

If the width of the interstice is small compared to the radius of the inner cylinder, this equation can be simplified using a Taylor series expansion around $r=(R_i+R_o)/2$. For this purpose the radial distance r is replaced by $R_x+\Delta r$, where Δr is the radial distance between any point in the interstice to the centre of the interstice and R is the radial distance from the cylinder axes to the centre of the interstice ($R=(R_i+R_o)/2$). First and higher order terms in $\Delta r/R_x$ are neglected, resulting in the following approximation.

$$\dot{\gamma} \approx 8 \Omega \frac{R_i^2 R_o^2}{(R_o + R_i)^2 - (R_o^2 - R_i^2)} \quad (\text{A.2})$$

Figure A.1 gives the relative error as a function of the radial distance r , for the Couette cylinders of the present study ($R_i=35$ mm and $R_o=38$ mm). The relative error is smaller than 8 %.

¹³⁾ Because blood is not a Newtonian fluid, the presented relations will not be exactly true for blood.

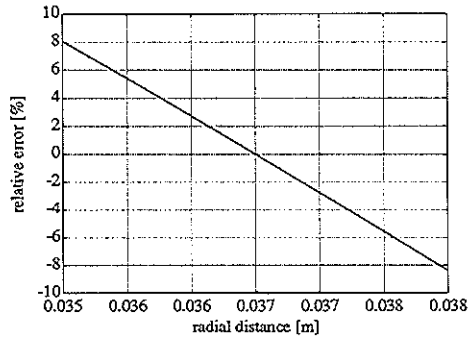


Figure A.1 Relative error in shear rate calculated according to equation (A.2) with respect to the exact solution of equation (A.2).

References

- [1] Bird R.B., Stewart W.E., Lightfoot E.N.: Transport phenomena. John Wiley & Sons, 1960.

Appendix B Mathematical expression for backscatter pressure from scattering volume

The incident pressure field is scattered by the inhomogeneities in volume V_s . The part of this scattered pressure field that travels back, is recorded by the same transducer. The configuration of this so-called backscatter measurement is shown in Figure V.1.

Generally, the backscatter pressure from a scattering volume measured by a transducer can be calculated in three steps. First the incident pressure at the scattering volume is calculated. This pressure field is generated by a transducer and has propagated from the transducer surface to the scattering volume. Secondly, the change in the pressure wave field caused by the inhomogeneities in the scattering volume is considered. And finally the propagation of the changed pressure wave field back to the transducer and the detection by the transducer is taken into account.

The mathematical operations corresponding to these three steps are dealt with in the next three paragraphs.

B.1 Incident pressure field

The acoustic pressure at any point r_s in an homogeneous medium with density ρ_0 and velocity c_0 radiated by a transducer with surface velocity equal to V^n can be evaluated by the following integral, known as the Rayleigh-I integral:

$$P_i(r_s, \omega) = 2jk \rho_0 c_0 \int_{S_t} G(r_s, r, \omega) V_n(r, \omega) d^2r \quad (\text{B.1})$$

where r is the position vector of a point on the transducer aperture. The integration is performed over the aperture surface S_t . $G(r_s, r, \omega)$ is the Greens function, which describes the propagation from a monopole impulse source in r to the point of observation r_s in a homogeneous background medium with propagation velocity equal to c_0 . Accordingly, $G(r_s, r, \omega)$ is the solution of the following wave equation:

$$k^2 G + \nabla^2 G = -\delta(\mathbf{r}_s - \mathbf{r}) \quad (\text{B.2})$$

which is:

$$G(\mathbf{r}_s, \mathbf{r}, \omega) = \frac{1}{4\pi} \frac{e^{-jk|\mathbf{r}-\mathbf{r}_s|}}{|\mathbf{r}-\mathbf{r}_s|} \quad (\text{B.3})$$

It can be shown [5] that equation (B.1) is also applicable for the pressure field of a slightly curved transducer with surface vibration normal to the transducer aperture.

If the vibration of the transducer is uniform in phase and amplitude over its surface, $V^n(\mathbf{r}, \omega) = V^n(\omega)$, equation (B.1) can be simplified into:

$$P_i(\mathbf{r}_0, \mathbf{r}_s, \omega) = 2jk \rho_0 c_0 V_n(\omega) G_t(\mathbf{r}_0, \mathbf{r}_s, \omega) \quad (\text{B.4})$$

in which $G_t(\mathbf{r}_s, \mathbf{r}_0, \omega)$ is the so-called transducer Greens function, which gives the pressure at \mathbf{r}_s generated by the transducer. The vector \mathbf{r}_0 points at the center of the transducer. As such $G_t(\mathbf{r}_s, \mathbf{r}_0, \omega)$ is defined by:

$$G_t(\mathbf{r}_s, \mathbf{r}_0, \omega) := \int_{S(\mathbf{r}_0)} G(\mathbf{r}_s, \mathbf{r}, \omega) d^2\mathbf{r} \quad (\text{B.5})$$

B.1.1 Transducer Greens function G_t

The pressure in the far field of a plane circular transducer in an homogeneous medium is described by the following relation (far field solution of equation (B.5)):

$$G_t(\mathbf{r}_0, \mathbf{r}, \omega) = A D(\phi, \omega) \frac{e^{-jkr}}{4\pi r} \quad (\text{B.6})$$

in which $D(\phi, \omega)$ is the so-called directivity of the transducer:

B.1 Incident pressure field

$$D(\phi, \omega) = \frac{2J_1(ka_t \sin\phi)}{ka_t \sin\phi} \tag{B.7}$$

In these equations r and ϕ are the spherical position coordinates of vector r defined with respect to the center of the transducer aperture. A is the aperture area and a_t is the transducer radius. $J_1(x)$ is the Bessel function of the first kind and the first order with argument x . The function $2J_1(x)/x$ in equation (B.7) is known as the Besinc function.

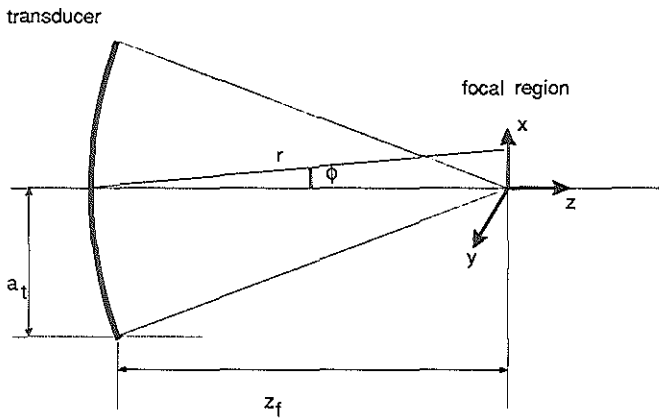


Figure B.1 Geometry for analysis of pressure field of focussed transducer.

O'Neil [5] has shown that these expressions (equation (B.6) and (B.7)) also hold for the pressure field in the focal region of a weakly focussed circular transducer (Figure B.1).

In Appendix C it is shown that the distance r to a point in the focal region, used in the amplitude and phase in equation (B.6), can be replaced by $z + z_f$, if $z_f \ll ka_t^2/15$. If in addition the axial size of the scattering volume is much smaller than the focal distance ($\nabla_{z \in V_s} z \ll z_f$) then equation (B.6) simplifies into:

$$G_i(r_\phi, r, \omega) = A D(\phi, \omega) \frac{e^{-jk(z+z_f)}}{4\pi z_f} \quad (\text{B.8})$$

According to this equation, in the focal region the phase fronts of the pressure wave are approximated by those of a local plane wave.

For small angles (ϕ), the directivity function of equation (B.7) can be approximated by a Gaussian function:

$$D(\phi, \omega) = e^{-(ka, \sin\phi)^2/8} \quad (\text{B.9})$$

or in Cartesian coordinates:

$$D(x, y, \omega) = e^{-\frac{k^2(x^2+y^2)}{32f_N^2}} \quad (\text{B.10})$$

where f_N is the so-called f-number of the transducer, which is the ratio of the focal distance and the transducer diameter: $f_N = z_f/2a_t$.

B.2 Scattering by inhomogenities

The scattered wavefield $p_s(r, t)$ is defined as the difference between the actual (total) wavefield $p(r, t)$ and the incident wavefield $p_i(r, t)$, i.e. the wavefield which would be present in a homogeneous background medium without any scatterers:

$$p_s(r, t) = p(r, t) - p_i(r, t) \quad (\text{B.11})$$

The incident pressure p_i in the homogeneous background medium with velocity c_0 has to obey the homogeneous wave equation:

B.2 Scattering by inhomogeneities

$$\frac{1}{c_0^2} \frac{\partial^2 p_i}{\partial t^2} - \nabla^2 p_i = 0 \quad (\text{B.12})$$

The total pressure p in an inhomogeneous medium without acoustic sources or sinks has to obey the wave equation for acoustic pressure [1][2]:

$$\frac{1}{c^2} \frac{\partial^2 p}{\partial t^2} - \nabla^2 p + \nabla \ln \rho \cdot \nabla p = 0 \quad (\text{B.13})$$

in which c is the propagation velocity of sound and ρ is the density.

The inhomogeneities in the tissue are characterized as spatial fluctuations in density, $\Delta\rho$, and propagation velocity, Δc , about their mean values, ρ_0 and c_0 respectively:

$$\begin{aligned} \rho(\mathbf{r}_s) &= \rho_0 + \Delta\rho(\mathbf{r}_s) \\ c(\mathbf{r}_s) &= c_0 + \Delta c(\mathbf{r}_s) \end{aligned} \quad (\text{B.14})$$

in which \mathbf{r}_s is the position vector of any point in the scattering volume. Transforming equation (B.13) to the frequency domain and applying the expressions of equation (B.14) results in:

$$k^2 P + \nabla^2 P = k^2 \left(1 - \left(\frac{c_0}{c} \right)^2 \right) P + \frac{1}{\rho} \nabla(\Delta\rho) \cdot \nabla P \quad (\text{B.15})$$

where $k=\omega/c_0$ is the wavenumber in the homogeneous background medium, ω is the radial frequency, and $P = P(\mathbf{r},\omega)$ is the temporal Fourier transform of $p(\mathbf{r},t)$. If the spatial fluctuations in density $\Delta\rho$ and velocity Δc are small compared to their mean values, ρ_0 and c_0 respectively ($\Delta\rho \ll \rho_0$ and $\Delta c \ll c_0$) equation (B.15) can be approximated by:

$$k^2 P + \nabla^2 P = k^2 \frac{2\Delta c}{c_0} P + \frac{1}{\rho_0} \nabla(\Delta\rho) \cdot \nabla P \quad (\text{B.16})$$

Also applying the Born approximation ($|p_s| \ll |p_i|$), which neglects multiple scattering, and using equation (B.11) and the homogeneous wave equation (B.12) for the incident pressure,

equation (B.16) can be simplified into [2]:

$$k^2 P_s + \nabla^2 P_s = k^2 \frac{2\Delta c}{c_0} P_i + \frac{1}{\rho_0} \nabla(\Delta \rho) \cdot \nabla P_i \quad (\text{B.17})$$

Equation (B.17) shows that under the influence of the primary wave P_i each inhomogeneity of the scattering medium becomes a source of secondary scattered waves P_s . The right hand side of equation (B.17) gives the density of the secondary sources and therefore it is usually referred to as the secondary source term Q for the scattered pressure:

$$-Q(\mathbf{r}_s, \omega) = k^2 \frac{2\Delta c(\mathbf{r}_s)}{c_0} P_i(\mathbf{r}_s, \omega) + \frac{1}{\rho_0} \nabla(\Delta \rho(\mathbf{r}_s)) \cdot \nabla P_i(\mathbf{r}_s, \omega) \quad (\text{B.18})$$

The total scattered pressure in \mathbf{r} resulting from this secondary source Q is given by the solution of the inhomogeneous wave equation (B.17), which is:

$$P_s(\mathbf{r}, \omega) = \int_{V_s} G(\mathbf{r}, \mathbf{r}_s, \omega) Q(\mathbf{r}_s, \omega) d^3 \mathbf{r}_s \quad (\text{B.19})$$

In this equation \mathbf{r} is the position vector of the point of observation. $G(\mathbf{r}, \mathbf{r}_s, \omega)$ is the Greens function (equation (B.3)), which describes the propagation from a inhomogeneity at \mathbf{r}_s in the scattering volume to the point of observation \mathbf{r} .

The source function Q depends on both the scatter properties ($\Delta \rho(\mathbf{r}_s)$ and $\Delta c(\mathbf{r}_s)$) of the inhomogeneities in the scatter volume and the pressure field $P_i(\mathbf{r}_s)$ incident on these inhomogeneities. An expression for the incident pressure field in the scatter volume was given in paragraph B.1.

B.3 Pressure measured by transducer

In backscatter measurements only the scattered pressure which impinges upon the transducer surface is recorded. If the transducer is plane or only slightly curved, the voltage output of the transducer is proportional to the scattered pressure spatially averaged over its aperture. Thus, the backscatter pressure from the inhomogeneities in the scatter volume V_s , measured by the transducer equals:

B.3 Pressure measured by transducer

$$P^{bsc}(\mathbf{r}_0, \omega) = \int_{S_t(\mathbf{r}_0)} T(\mathbf{r}, \omega) P_s(\mathbf{r}, \omega) d^2r \quad (\text{B.20})$$

In this equation integration is performed over the aperture surface S_t . The function $T(\mathbf{r}, \omega)$ represents the local sensitivity of the transducer over its aperture. Assuming that $T(\mathbf{r}, \omega)$ is uniform over the transducer aperture: $T(\mathbf{r}, \omega) = T(\omega)$, and applying equation (B.19) it follows that:

$$P^{bsc}(\mathbf{r}_0, \omega) = T(\omega) \int_{S_t(\mathbf{r}_0)} \left[\int_{V_s} G(\mathbf{r}, \mathbf{r}_s, \omega) Q(\mathbf{r}_s, \omega) d^3r_s \right] d^2r \quad (\text{B.21})$$

Changing the order of integration and applying the definition of the transducer Greens function G_t (equation (B.5)), results in:

$$P^{bsc}(\mathbf{r}_0, \omega) = T(\omega) \int_{V_s} G_t(\mathbf{r}_0, \mathbf{r}_s, \omega) Q(\mathbf{r}_s, \omega) d^3r_s \quad (\text{B.22})$$

B.4 Backscatter pressure

Combining the expression for the incoming pressure (equation (B.4)), the expression for the secondary source term due to scattering Q (equation (B.18)), and the expression for the backward propagation and detection (equation (B.22)) results in:

$$P^{bsc}(\mathbf{r}_0, \omega) = 2jk \rho_0 c_0 T(\omega) V_n(\omega) \int_{V_s} G_t(\mathbf{r}_0, \mathbf{r}_s, \omega) \left[k^2 \frac{2\Delta c(\mathbf{r}_s)}{c_0} + \frac{1}{\rho_0} \nabla_s(\Delta \rho(\mathbf{r}_s)) \cdot \nabla_s \right] [G_t(\mathbf{r}_0, \mathbf{r}_s, \omega)] d^3r_s \quad (\text{B.23})$$

To obtain this equation also the reciprocity theorem was applied, which says that $G_t(\mathbf{r}_s, \mathbf{r}_0, \omega) = G_t(\mathbf{r}_0, \mathbf{r}_s, \omega)$ [1].

References

- [1] Berkhout A.J.: Applied seismic wave theory. Amsterdam, Elsevier 1987
- [2] Chernov L.A.: Wave Propagation in a Random Medium (McGraw-Hill, New York, 1960), Chap.IV
- [3] Lizzi F.L., Greenebaum M., Felleppa E.J., Elbaum M.: Theoretical Framework for Spectrum Analysis in Ultrasonic Tissue Characterization. J Acoust Soc Am 73(4):1366-1373, 1983
- [4] Morse P.M., Ingard K.U.: Theoretical Acoustics. Princeton University Press, 1968
- [5] O'Neil H.: The Theory of Focusing Radiators, J Acoust Soc Am 21,516-526(1949)
- [6] Ueda M., Ozawa Y.: Spectral analysis of echoes for backscattering coefficient measurements. J Acoust Soc Am 77(1): 38-47, 1985.

Appendix C Fraunhofer condition in focal region

The pressure in the focus of a slightly curved circular transducer in an homogeneous medium (Figure B.1) is described by the following relation (equation (B.6)):

$$P(r, \phi, \omega) = A D(\phi, \omega) \frac{e^{-jkr}}{4\pi r} \quad (\text{C.1})$$

in which $D(\phi, \omega)$ is the so-called directivity of the transducer (equation (B.7)).

$$D(\phi, \omega) = \frac{2J_1(ka_r \sin\phi)}{ka_r \sin\phi} \quad (\text{C.2})$$

In these equations r is the distance between the apex of the transducer and the point of observation, ϕ is the angle with respect to the main axis of the transducer (Figure B.1) and k is the wavenumber ($k=\omega/c$).

In the following the condition for which r in equation (C.1) can be replaced by $z + z_f$ (z_f is the focal distance) is deduced.

The distance r between the point of observation and the apex of the transducer equals:

$$r = \sqrt{(z_f + z)^2 + x^2 + y^2} \quad (\text{C.3a})$$

or

$$r = (z + z_f) \sqrt{1 + \frac{(x^2 + y^2)}{(z + z_f)^2}} \quad (\text{C.3b})$$

Expanding of the square root in equation (C.3b) into a Taylor series and confining to quantities of the first order in $(x^2 + y^2)/(z + z_f)^2$, the above equation evaluates to:

$$r \approx (z+z_f) \left(1 + \frac{1}{2} \frac{x^2 + y^2}{(z+z_f)^2} \right) \quad (\text{C.4})$$

From this equation it follows that, the amplitude $1/4\pi r$ of the pressure field (equation (C.1)) can be approximated by $1/4\pi(z+z_f)$, if:

$$\frac{x^2 + y^2}{(z+z_f)^2} \ll 1 \quad (\text{C.5})$$

The phase $-2kr$ of the incident pressure can be approximated by $-2k(z+z_f)$, if the following condition is satisfied:

$$\frac{k(x^2 + y^2)}{(z+z_f)^2} \ll 1 \quad (\text{C.6})$$

Equation (C.6) is known as the Fraunhofer condition [1].

The beamwidth in the focal region might be that small that the above condition is satisfied in the whole focal region. As a measure of the beamwidth the distance between the first two zero crossings of the Besinc directivity function of equation (C.2) is chosen. At the first zero crossings, the argument of the Besinc function equals ± 3.83 :

$$ka_t \sin\phi = \pm 3.83 \quad (\text{C.7})$$

Then it follows that x_0 , y_0 and r_0 , which are the values of x , y and r respectively at the first zero crossing of the besinc directivity function, are related as:

$$\sqrt{\frac{x_0^2 + y_0^2}{r_0^2}} = \frac{3.83}{ka_t} \quad (\text{C.8})$$

Using the expression for r of equation (C.3), this equation evaluates to:

$$x_0^2 + y_0^2 = \frac{15(z_f + z)^2}{k^2 a_t^2 + 15} \quad (\text{C.9})$$

in which the value of the square of 3.83 is approximated by 15.

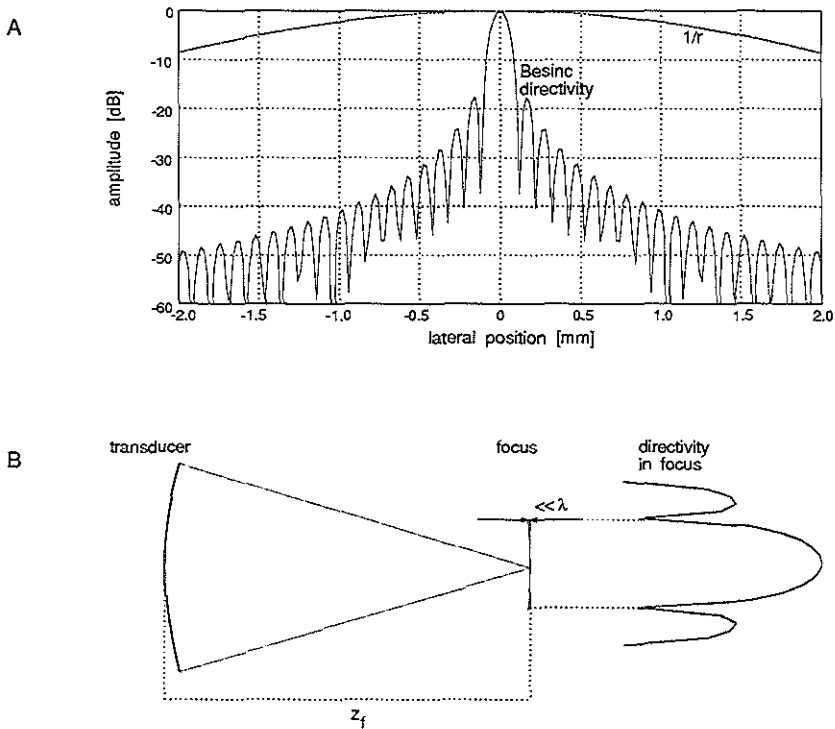


Figure C.1 Fraunhofer condition of amplitude (A) and phase (B) behaviour of the pressure field in the focal region of a curved transducer.

If $k^2 a_t^2 \gg 15$, the above equation can be approximated by:

$$x_0^2 + y_0^2 \approx \frac{15 (z_f + z)^2}{k^2 a_t^2} \quad (\text{C.10})$$

If the beamwidth $x_0^2 + y_0^2$ satisfies the Fraunhofer condition of equation (C.6), then for each point within the main lobe of the directivity function the variable r in equation (C.1) may be replaced by $z + z_f$. Combining equation (C.6) and (C.10) it follows that the beamwidth satisfies the Fraunhofer condition if:

$$z + z_f \ll k a_t^2 / 15 \quad (\text{C.11})$$

If the length l in z -direction of the scattering volume is much smaller than the focal length z_f ($l \ll z_f$), this condition can be simplified to:

$$z_f \ll k a_t^2 / 15 \quad (\text{C.12})$$

Both the approximation in amplitude and in phase are illustrated in Figure C.1. The condition of equation (C.12) need not violate the weak focussing condition ($a_t \ll z_f$) provided that $a_t \gg \lambda$.

References

- [1] Berkhout A.J.: Applied seismic wave theory. Amsterdam, Elsevier 1987

Appendix D Scattering from inhomogenities

D.1 Density inhomogenities

The backscatter pressure from a scattering inhomogeneity with spatial fluctuations in density $\Delta\rho$ and in velocity Δc with respect to the reference medium with density ρ_0 and velocity c_0 can generally be described by (equation (B.23)):

$$P^{bsc}(\mathbf{r}_0, \omega) = 2jk \rho_0 c_0 T(\omega) V_n(\omega) \int_{V_s} G_t(\mathbf{r}_0, \mathbf{r}_s, \omega) \left[k^2 \frac{2\Delta c(\mathbf{r}_s)}{c_0} + \frac{1}{\rho_0} \nabla_s(\Delta\rho(\mathbf{r}_s)) \cdot \nabla_s \right] [G_t(\mathbf{r}_0, \mathbf{r}_s, \omega)] d^3 r_s \quad (\text{D.1})$$

in which $G_t(\mathbf{r}_0, \mathbf{r}_s, \omega)$ is the so-called transducer Greens function, which gives the pressure at \mathbf{r}_s generated by the transducer. The vector \mathbf{r}_0 points at the center of the transducer.

In this paragraph a condition is deduced, which enables to apply the following approximation:

$$G_t \nabla_s(\Delta\rho) \cdot \nabla_s G_t = -jk \frac{\partial(\Delta\rho)}{\partial z} G_t^2 \quad (\text{D.2})$$

For the following analysis it is convenient to apply cylindrical coordinates defined with respect to the origin in the scattering volume (Figure B.1). In relation to the Cartesian coordinates (x, y, z) these cylindrical coordinates (R, α, z) are given by:

$$\begin{aligned} R &= \sqrt{x^2 + y^2} \\ \alpha &= \text{atan}(y/x) \\ z &= z \end{aligned} \quad (\text{D.3})$$

Then the expression for the transducer Greens function is (equation (C.4)):

$$G_t(r_0, r, \omega) = A D(R, \omega) \frac{e^{-jk(z+z_p)}}{4\pi z_f} \quad (\text{D.4})$$

in which the directivity function $D(R, \omega)$ is given by:

$$D(R, \omega) = e^{-k^2 R^2 / 32 f_N^2} \quad (\text{D.5})$$

where z_f is the focal distance and f_N is the so-called f-number of the transducer ($f_N = z_f / 2a_c$).

If $ka_t < 1$, the second term in the integrand of equation (D.1) can be rewritten as:

$$G_t \nabla_s(\Delta\rho) \cdot \nabla_s G_t = \nabla_s(\Delta\rho) A^2 \left(\frac{e^{-jk(z+z_p)}}{4\pi(z+z_p)} \right) \left(e_R D \frac{\partial D}{\partial R} - e_z j k D^2 \right) \quad (\text{D.6})$$

In this equation e_R and e_z are unit vectors in directions of increasing R (cross-range) and z (range) respectively. For most applications the inhomogenities are randomly distributed within the scattering volume. Then the cross-range term of equation (D.6) can be neglected if the summed contribution of all scatterers, at any fixed depth level z within the scattering volume and at any fixed angle α , to the cross-range component is much smaller than their contribution to the range component:

$$\int_0^\infty D(R, \omega) \frac{\partial D(R, \omega)}{\partial R} dR < k \int_0^\infty D^2(R, \omega) dR \quad (\text{D.7})$$

Using equation (D.4) and (D.5) this inequality evaluates into:

$$f_N > \frac{1}{2\sqrt{\pi}} \quad (\text{D.8})$$

This condition says that the cross-range component of the backscatter pressure from density inhomogenities may be neglected if focussing is not too sharp.

For the transducer used in the experiments of this thesis, with f-number equal to 1.84, the

D.1 Density inhomogeneity

relative error induced by neglecting the cross-range term is maximally equal to 15 %. Upon neglecting the cross-range components of $G_t \nabla_s(\Delta\rho) \nabla_s G_t$ equation (D.6) evaluates into:

$$G_t \nabla_s(\Delta\rho) \cdot \nabla_s G_t = -jk \frac{\partial(\Delta\rho)}{\partial z} G_t^2 \quad (\text{D.9})$$

Applying this approximation to equation (D.1) results in:

$$P^{bsc}(\omega) = 2k^2 \rho_0 c_0 T(\omega) V_n(\omega) \int_{V_s} \left[2jk \frac{\Delta c(r_s)}{c_0} + \frac{1}{\rho_0} \frac{\partial \Delta \rho(r_s)}{\partial z} \right] G_t^2(r_0, r_s, \omega) d^3 r_s \quad (\text{D.10})$$

D.2 Velocity inhomogeneities

Starting with equation (D.10), it will be shown in this paragraph that the effect of velocity and density inhomogeneities on the backscatter pressure can be taken together into a function of the acoustic impedance.

Applying equation (B.8) for G_t in equation (D.10) results in:

$$P^{bsc}(\omega) = 2k^2 A^2 \rho_0 c_0 T(\omega) V_n(\omega) \iiint_{V_s} \left[2jk \frac{\Delta c(x,y,z)}{c_0} + \frac{1}{\rho_0} \frac{\partial \Delta \rho(x,y,z)}{\partial z} \right] D^2(x,y,\omega) \frac{e^{-2jk(z+z_p)}}{(4\pi z_p)^2} dx dy dz \quad (\text{D.11})$$

The integrand in z of the velocity term in equation (D.11) can be replaced by:

$$\int_{z_-}^{z_+} 2jk \frac{\Delta c(x,y,z)}{c_0} e^{-2jk(z+z_p)} dz = - \int_{z_-}^{z_+} \frac{\Delta c(x,y,z)}{c_0} \frac{\partial}{\partial z} (e^{-2jk(z+z_p)}) dz \quad (D.12)$$

Partial integration gives:

$$- \int_{z_-}^{z_+} \frac{\Delta c(x,y,z)}{c_0} \frac{\partial}{\partial z} (e^{-2jk(z+z_p)}) dz = \int_{z_-}^{z_+} \frac{1}{c_0} \frac{\partial}{\partial z} (\Delta c(x,y,z)) e^{-2jk(z+z_p)} dz - \left. \frac{\Delta c}{c_0} e^{-2jk(z+z_p)} \right|_{z_-}^{z_+} \quad (D.13)$$

Generally the integration boudaries can be chosen in such a way that the velocity change Δc equals zero on the boundaries. Thus the second term in equation (D.13) can be omitted. Then the final expression for the backscatter pressure is:

$$P^{boc}(\omega) = 2k^2 \rho_0 c_0 T(\omega) V_n(\omega) \int_{V_s} \left(\frac{1}{c_0} \frac{\partial \Delta c(r_s)}{\partial z} + \frac{1}{\rho_0} \frac{\partial \Delta \rho(r_s)}{\partial z} \right) G_r^2(r_0, r_s, \omega) d^3 r_s \quad (D.14)$$

With the definition of the acoustic impedance: $Z = \rho c$, the bracketed term in the integral equals:

$$\frac{1}{c_0} \frac{\partial \Delta c}{\partial z} + \frac{1}{\rho_0} \frac{\partial \Delta \rho}{\partial z} = \frac{1}{Z} \frac{\partial Z}{\partial z} \quad (D.15)$$

Appendix E Integration of the delta function

The following 2D integral is evaluated.

$$I = \iint e^{f(x,z)} \chi(x,z) dx dz \quad (\text{E.1})$$

with $\chi(x,z) = \delta(z - g(x))$

in which the 'delta'-function δ is defined as:

$$\delta(z - g(x)) = \lim_{\varepsilon \rightarrow 0} \begin{cases} \frac{1}{\varepsilon} & \text{for } z \in \left[g(x) - \frac{\varepsilon_z}{2}, g(x) + \frac{\varepsilon_z}{2} \right] \\ 0 & \text{elsewhere} \end{cases} \quad (\text{E.2})$$

The meaning of ε and ε_z is illustrated in Figure E.1, for the linear function $g(x) = n_z x + q_z$. For a general function $g(x)$ the relation between ε and ε_z is given by:

$$\varepsilon_z(x) = \varepsilon \sqrt{1 + g_x^2(x)} \quad (\text{E.3})$$

with $g_x(x) = \frac{\partial g(x)}{\partial x}$

Substituting equation (E.2) in equation (E.1) results in:

$$I = \lim_{\varepsilon \rightarrow 0} \frac{1}{\varepsilon} \int_{x_-}^{x_+} e^{f(x,g(x))} dx \int_{g(x) - \varepsilon_z/2}^{g(x) + \varepsilon_z/2} dz = \int_{x_-}^{x_+} \sqrt{1 + g_x^2(x)} e^{f(x,g(x))} dx \quad (\text{E.4})$$

If $g(x)$ is the linear function of Figure E.1, this equation can be simplified into:

$$I = \sqrt{1 + n_z^2} \int_{x_-}^{x_+} e^{f(x, n_z x + q_z)} dx \quad (\text{E.5})$$

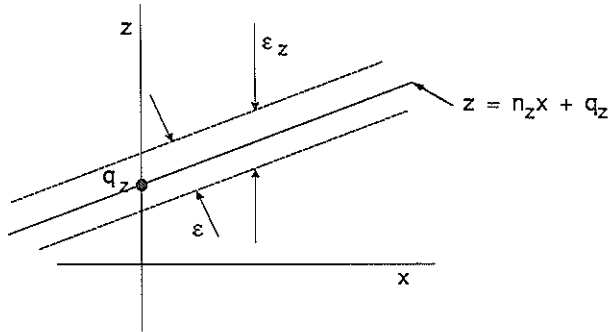


Figure E.1: Geometric presentation of ϵ and ϵ_z of a delta function around $z = g(x) = n_z x + q_z$.

Appendix F Some standard integral solutions

F.1

$$\int_{x_-}^{x_+} \exp[-(a_2 x^2 + a_1 x)] dx = \frac{1}{2} \sqrt{\frac{\pi}{a_2}} \exp\left[\frac{a_1^2}{4a_2}\right] (\operatorname{erf}(p_+) - \operatorname{erf}(p_-)) \quad (\text{F.1})$$

$$\text{with } p_{\pm} = \sqrt{a_2} x_{\pm} + \frac{a_1}{2\sqrt{a_2}}$$

in which *erf*, the so-called error-function, is defined as:

$$\operatorname{erf}(z) = \frac{2}{\sqrt{\pi}} \int_0^z \exp(-x^2) dx \quad (\text{F.2})$$

for $z \rightarrow \infty$ the error-function equals:

$$\operatorname{erf}(\infty) = \lim_{z \rightarrow \infty} \frac{2}{\sqrt{\pi}} \int_0^z e^{-x^2} dx = 1 \quad (\text{F.3})$$

F.2

$$\lim_{s_{\pm} \rightarrow \pm\infty} \int_{s_-}^{s_+} e^{-\gamma s^2} e^{-j\alpha s} ds = \sqrt{\frac{\pi}{\gamma}} e^{-\frac{\alpha^2}{4\gamma}} \quad (\text{F.4})$$

Appendix G Least squares estimates

Suppose N measurements of P_i^{bsc} are performed at N different angles of incidence. The assumed relation between the pairs (P_i^{bsc}, θ_i) is:

$$P_i^{bsc} = P_0 \exp(-a_s (\theta_i - \theta_0)^2) \quad \text{for } i=1..N \quad (\text{G.1})$$

Given the definitions:

$$\begin{aligned} y_i &:= \ln(P_i^{bsc}) \\ y_0 &:= \ln(P_0) \end{aligned} \quad (\text{G.2})$$

Equation (G.1) can be rewritten into:

$$y_i = y_0 - a_s (\theta_i - \theta_0)^2 \quad (\text{G.3})$$

The sum of least squares, Q , for equation (G.3) is:

$$Q(y_0, \theta_0, a_s) = \sum_{i=1}^{i=N} [y_i - y_0 + a_s (\theta_i - \theta_0)^2]^2 \quad (\text{G.4})$$

The principle of least squares estimate now says: calculate the values of the parameters (y_0 , θ_0 , and a_s) for which Q is minimum.

Samenvatting

Het doel van dit promotiewerk was de haalbaarheid van kwantitatieve weefseldifferentiatie van vaatwandweefsel te onderzoeken, op basis van ultrasonische puls-echo metingen met behulp van een intravasculaire ultrasonische catheter (30 MHz). Twee verschijnselen, waardoor de kwantitatieve weefseldifferentiatie wordt bemoeilijkt, zijn nader onderzocht. Deze zijn het hoekafhankelijke gedrag van het teruggestrooide drukveld ('backscatter') door de vaatwand en het strooigedrag van bloed bij 30 MHz.

Dit proefschrift bestaat uit drie gedeelten. Het eerste gedeelte (Hoofdstuk II) beschrijft een experimentele studie van het kwantitatieve effect van de hoek van inval van de geluidsgolf ten opzichte van de vaatwand op het backscatter vermogen. In het tweede gedeelte (Hoofdstuk III en IV) wordt een onderzoek van het akoestische gedrag van bloed beschreven. Tenslotte wordt in het derde gedeelte (Hoofdstuk V) een wiskundige beschrijving voor het akoestische gedrag van strooimedia, zoals vaatwandweefsel en bloed, afgeleid en worden resultaten van numerieke simulaties van vaatwandweefsel en bloed gepresenteerd. Voorafgaand aan deze drie deelstudies worden in de inleiding (Hoofdstuk I) de morfologie van de vaatwand en de samenstelling van bloed beschreven.

In Hoofdstuk II wordt aangetoond dat variaties in de hoek van inval van de geluidsbundel variaties in de B-mode afbeelding van de vaatwand veroorzaken, die niet direct gerelateerd zijn aan de morfologie van het betreffende bloedvat. Variaties in de hoek van inval zullen bij de in-vivo toepassing van de echo-catheter regelmatig optreden, bijvoorbeeld als de catheter excentrisch in het bloedvat ligt, als de doorsnede van het bloedvat niet cirkelvormig is of als het bloedvat gebogen is. Het hoekafhankelijke gedrag van het backscatter vermogen van de vaatwand bemoeilijkt de interpretatie van de B-mode afbeeldingen. Bovendien beperkt het de toepasbaarheid van de bestaande weefseldifferentiatiemethoden, zoals spectrale analyse van het backscatter signaal.

In een in-vitro studie is het effect van de hoek van inval op het backscatter vermogen nader onderzocht. Daarbij is onderscheid gemaakt tussen de hoekvariatie in het vlak loodrecht op de hoofdas van het bloedvat (tangentiële vlak) en de hoekvariatie in het vlak door de hoofdas van het bloedvat (axiale vlak). In-vitro metingen aan 13 stukjes weefsel van de arterie Iliaca toonden aan dat elk weefseltype een specifiek hoekafhankelijk gedrag vertoont. Het hoekafhankelijk gedrag van zowel de elastische als de musculaire media blijkt

anisotroop te zijn: in het tangentiële vlak is het effect van de hoek van inval op het backscatter vermogen sterker dan in het axiale vlak. Bij een verandering van de hoek van inval in het tangentiële vlak van 10 graden (ten opzichte van de normaal op de vaatwand) neemt het backscatter vermogen van de musculaire media ongeveer 2 dB af en van de elastische media ongeveer 7 dB. In het axiale vlak is er geen afname van het backscatter vermogen van de musculaire media meetbaar, terwijl het backscatter vermogen van de elastische media ongeveer 3 dB afneemt bij een hoekverdraaiing van 10 graden. Een mogelijke verklaring voor het anisotrope gedrag van de musculaire media is de aanwezigheid van de langgerekte gladde spiercellen, die, zoals waargenomen op histologische coupes, circulair georiënteerd zijn. De gemeten anisotropie van de elastische media is niet op basis van de histologie van dit weefseltype te verklaren.

Zowel de vaste als de losmazige collagene lesies in de intima vertonen geen anisotroop hoekafhankelijk backscatter gedrag. In beide vlakken (tangenteel en axiaal) wordt een afname van ongeveer 3 dB waargenomen bij een hoekverdraaiing van 10 graden.

Ook is het hoekafhankelijke gedrag van de adventitia en de lamina elastica externa gemeten. De resultaten van de metingen aan beide weefseltypen vertonen een relatief grote spreiding. Wat de adventitia betreft, kan dit worden verklaard door het feit dat de adventitia een zeer inhomogeen weefseltype is.

Uit iedere gemeten curve van het backscatter vermogen als functie van de hoek zijn twee weefselparameters geschat. Eén daarvan is de zogenaamde directiviteitsparameter, die de mate, waarin het backscatter vermogen van de hoek afhangt, aangeeft. De tweede parameter is het maximale vermogen, hetgeen overeenkomt met het vermogen bij loodrechte inval. Uit de metingen zijn twee directiviteitsparameters afgeleid, n.l. de directiviteitsparameter in het tangentiële vlak en de directiviteitsparameter in het axiale vlak. De resulterende berekende parameters per weefseltype wekken sterk de indruk dat weefseldifferentiatie mogelijk is door gebruik te maken van de drie parameters: de tangentiële en de axiale directiviteit en het maximale vermogen.

In **Hoofdstuk III** wordt getoond wat het effect is van het hoge backscatter nivo van bloed op de zichtbaarheid van de overgang tussen het lumen en de vaatwand bij het gebruik van de intravasculaire ultrasone catheter van 30 MHz. Een beknopt overzicht van de akoestische eigenschappen van bloed, bekend uit de literatuur, wordt gegeven. In de literatuur worden voornamelijk onderzoeksresultaten gegeven van metingen bij lagere frequenties, namelijk van 1 MHz tot maximaal 15 MHz. Bij deze frequenties wordt niet die hoge echogeniciteit

van bloed waargenomen, zoals die bij 30 MHz is waargenomen. Het is aangetoond dat bij deze frequenties de Hematocrit waarde van het bloed, het optreden van aggregatie van rode bloedcellen en de deformatie en orientatie van rode bloedcellen belangrijke invloed hebben op het akoestisch gedrag van bloed. Bovendien is het bekend dat bij deze frequenties het akoestische gedrag van bloed beïnvloed wordt door de schuifspanning in het bloed: het verhogen van de schuifspanning resulteert in een lager backscatter vermogen. Omdat rode bloedcellen aggregeren bij afnemende schuifspanning en deze aggregaten breken bij toenemende schuifspanning, wordt aangenomen dat het schuifspannings- afhankelijke gedrag van het backscatter vermogen een gevolg is van dit aggregatie proces.

De echogeniciteit van bloed, opgenomen met een intravasculaire ultrasonische catheter van 30 MHz, is gemeten in de Iliaca van drie patiënten gedurende de hartcyclus. Cyclische variaties in de echogeniciteit van bloed werden waargenomen synchroon aan de variaties in de bloeddruk. De resultaten suggereren dat deze variaties in echogeniciteit worden veroorzaakt door veranderingen in de aggregatietoestand van de rode bloedcellen ten gevolge van de variërende schuifspanning.

Hoofdstuk IV beschrijft een onderzoek naar de akoestische eigenschappen van bloed in het frequentiegebied van 20 tot 40 MHz onder variërende aggregatie condities. Behalve dat metingen zijn verricht aan samples van normaal (humaan) bloed, zijn ook gemanipuleerde bloedsamples, waarvan of de aggregatie versterkt is of de aggregatie tegengegaan is, onderzocht. Er zijn backscattermetingen uitgevoerd aan de verschillende bloedsamples, waarbij de schuifspanning is gevarieerd. Hiervoor is een speciale meetcel ontwikkeld, die gebaseerd is op de Couette viscosimeter. In deze meetcel is de schuifspanning binnen het akoestische meetvolume in benadering constant, hetgeen niet het geval is bij de door anderen uitgevoerde studies waarbij het akoestische gedrag van bloed stromend door een buis werd onderzocht.

De gemeten akoestische parameters zijn het geïntegreerde backscatter vermogen en de spectrale helling van het backscatter vermogen in het frequentie gebied van 20 tot 40 MHz. Een afname van ongeveer 13 dB werd waargenomen in het backscatter vermogen van normaal bloed als de schuifnelheid werd opgevoerd van 0.7 s^{-1} tot 200 s^{-1} . De spectrale helling nam toe van 1 tot 3 bij een schuifnelheidstoename van 0.3 s^{-1} tot 10 s^{-1} . Bij de aggregaat versterkte bloedsamples trad een vergelijkbare verandering van het geïntegreerde backscatter vermogen en van de spectrale helling op, echter er bleek een hogere schuifnelheid nodig te zijn om deze veranderingen te bewerkstelligen. Bij aggregaat

onderdrukt bloed traden geen veranderingen van het geïntegreerde backscatter vermogen en de spectrale helling onder invloed van de schuifspanning op. De resultaten van dit onderzoek tonen aan dat de schuifsnelheid, waarvan bekend is dat deze de aggregatie toestand van de rode bloedcellen beïnvloedt, een significant effect heeft op de backscatter eigenschappen van bloed in het frequentiegebied van 10 tot 40 MHz. De veranderingen in het geïntegreerde vermogen en in de spectrale helling onder invloed van de schuifsnelheid suggereren dat bij lage schuifsnelheden ($< 0.3 \text{ s}^{-1}$) er volledige aggregatie optreedt. Voor schuifsnelheden van 0.3 s^{-1} tot 200 s^{-1} worden deze aggregaten afgebroken, en voor hogere schuifsnelheden dan 200 s^{-1} zijn er alleen losse rode bloedcellen aanwezig. De gemeten spectrale helling geeft ook aan dat bij een verdere toename van de gebruikte frequentie de echogeniciteit van bloed nog meer zal toenemen, waarbij waarschijnlijk het onderscheid tussen het lumen en de vaatwand nog minder duidelijk zichtbaar wordt.

In **Hoofdstuk V** wordt een wiskundige voorstelling van het akoestische backscatter gedrag van vaatwandweefsel en bloed bij hoge frequentie (30 MHz) gegeven. Daarbij worden zowel het vaatwandweefsel als het bloed met geaggregeerde rode bloedcellen voorgesteld als een drie-dimensionale verdeling van cilindervormige verstrooiers. De eigenschappen van deze verdeling van verstrooiers zijn vastgelegd in verschillende parameters, zoals de gemiddelde afstand en de spreiding in de afstand tussen de verstrooiers, de gemiddelde afmetingen en de spreiding in de afmetingen van de cilindrische verstrooiers en tenslotte hun gemiddelde orientatie en de spreiding in de orientatie. Tevens zijn de eigenschappen van de transducent meegenomen in het wiskundige model. Deze eigenschappen zijn experimenteel bepaald met behulp van hoekafhankelijke reflektiemetingen aan een vlakke plaat.

Eerst is de invloed van de verschillende modelparameters op het gesimuleerde backscatter gedrag onderzocht. Uit de resultaten blijkt dat het hoekafhankelijke gedrag van het backscatter vermogen van een willekeurig onregelmatige verdeling van verstrooiers hoofdzakelijk wordt bepaald door de gemiddelde eigenschappen van de verstrooier: zijn afmetingen en orientatie. De gemiddelde onderlinge afstand tussen de verstrooiers heeft bij een willekeurig onregelmatige verdeling nauwelijks invloed op het hoekafhankelijke gedrag.

Vervolgens is het hoekafhankelijke gedrag van gesimuleerde weefsels onderzocht. De musculaire media is voorgesteld als een willekeurig onregelmatige verdeling van cilindervormige verstrooiers, die in dezelfde richting geïntendeerd zijn. De gekozen

afmetingen van de cilindervormige verstrooiers en de onderlinge afstand zijn de waargenomen afmetingen van gladde spiercellen en hun onderlinge afstand op histologische coupes. De resultaten van de simulaties aan een dergelijke verdeling van verstrooiers komen goed overeen met de experimentele resultaten van de hoekafhankelijkheid van het backscatter vermogen van de musculaire media. De collageen lesies zijn voorgesteld als een willekeurige verdeling van dunne cilindervormige verstrooiers met een willekeurige orientatie evenwijdig aan het vaatwandoppervlak. Uit de simulaties blijkt dat de lengte van de cilindervormige verstrooiers belangrijke invloed heeft op het hoekafhankelijke gedrag. Voor een gemiddelde cilindervormige verstrooierlengte van 120 μm komen de resultaten van de simulaties goed overeen met de experimentele resultaten. Tenslotte zijn de backscatter metingen aan bloed gesimuleerd. Een bloedsample met aggregaten van rode bloedcellen is voorgesteld als een willekeurige verdeling van cilindervormige verstrooiers met gelijke orientatie loodrecht op de richting van het inkomende golfveld. De toename van de aggregatie is gesimuleerd door een toename van de gemiddelde cilindervormige verstrooierlengte met een overeenkomstige afname van het aantal cilindervormige verstrooiers. Deze gesimuleerde aggregatie had een vergelijkbaar effect op het backscatter vermogen als in de experimenten.

Nawoord

Omdat ik me terdege realiseer dat zonder de hulp van vele anderen dit proefschrift niet tot stand zou zijn gekomen, wil ik al diegenen die hun steentje hebben bijgedragen hartelijk danken. Enkelen daarvan wil ik hier speciaal noemen.

In de eerste plaats zou dit onderzoek niet tot stand zijn gekomen als Professor N. Bom daartoe niet de aanzet had gegeven. Gedurende de jaren dat ik aan het onderzoek werkte, heeft hij mij altijd met zijn enthousiasme weten te stimuleren.

Een belangrijke rol in het onderzoeksproject heeft ook gespeeld Professor A.J. Berkhout. Dankzij de experimenteel fysische omgeving, die mede door zijn vakgroep geboden werd, en de theoretische basiskennis die in de vakgroep aanwezig is, is het mogelijk geweest om experimenteel en theoretisch werk te combineren. Zijn opbouwende kritiek, met name op het theoretische gedeelte van het onderzoek, was voor mij zeer leerzaam.

Mijn dank gaat ook uit naar de TPD, die de financiële randvoorwaarden heeft geschapen om het onderzoek te kunnen verrichten. Bovendien hebben meerdere van mijn TPD collega's het nodige bijgedragen aan het onderzoek.

Met Len van der Wal heb ik vaak (bijna wekelijks) nuttige discussies gehad. Bovendien heeft hij een regeling weten te treffen zodat ik behalve het onderzoek van dit proefschrift, ook andere interessante en leerzame onderzoeksprojecten kon uitvoeren.

Zeer dankbaar ben ik ook mijn collega-kamergenoot en zwager Uilke Stelwagen voor al de (vrije) tijd, die hij aan het lezen en corrigeren van mijn proefschrift besteed heeft. Zijn eerlijke belangstelling en zijn kritische instelling zijn het werk zeker ten goede gekomen.

Het contact met Wim van Hoorn (TUD), een lotgenoot op het gebied van het medisch ultrageluid, was zeer zinnig. Ook heb ik veel profijt gehad van de contacten met de medewerkers van de afdeling Experimentele Echocardiografie van het Thoraxcentrum: Elma Gussenhoven, Harm ten Hoff, Nico de Jong, Charles Lancée en Hans Rijstenborgh.

Mijn ouders hebben mij altijd zeer gestimuleerd en mij in raad en daad bijgestaan. Mijn vader (dr. J.P.M. de Kroon) heeft mij ten behoeve van het promotie onderzoek kennis doen nemen van het vakgebied van de toegepaste statistiek en mij het grote belang van het met kennis van zaken toepassen van de statistiek doen inzien.

Tenslotte wil ik niet onvermeld laten: Maurits van der Heiden, die zo'n interessant afstudeerproject heeft uitgevoerd, Kees van de Berg, bij wie ik altijd terecht kon als ik computer-problemen had, Corrie Eefting, voor mij het centrale aanspreekpunt op de EUR, Coby Peekstok, die altijd bereid was histologische coupes te maken van de door mij zo ongewoon uitgesneden stukjes weefsel en Ed Doppenberg, die de gebruikte engelse taal in het proefschrift heeft gecontroleerd.

Ondanks al deze hulpvaardige mensen, was het me nooit gelukt dit onderzoek te volbrengen en ter schrift te stellen als mijn man Arie mij niet zoveel had bijgestaan en vooral bij het verwerken van de laatste loodjes alle taken rondom huis en kind op zich had genomen om op die manier een rustige werkomgeving voor mij te creëren.

Publications by the Author

De Kroon M.G.M., Van der Wal L.F., Bom N.: *Arterial tissue characterization and fiber orientation*. Ultrasonic Imaging 11: 137, 1989 (Abstract).

De Kroon M.G.M., Van der Wal L.F., Bom N., Lancée C.: *Arterial tissue characterization and fiber orientation*. VIII European Workshop on Ultrasonic Tissue Characterization & Echographic Imaging October 15-18, Nijmegen: 26, 1989 (Abstract).

De Kroon M.G.M., Ten Hoff H., Gussenhoven W.J., Bom N.: *Intravasculaire ultrasonie afbeeldingstechniek*. Nederlands Akoestisch Genootschap, Journaal No. 105: 35-42, 1990.

Bom N., Ten Hoff H., Gussenhoven W.J., Reiber J.H.C., De Kroon M.G.M., Lancée C.T., Roelandt J.: *Quantification of arterial obstructions with intra-arterial echography: technical problems*. Echocardiography 1990 (Dagianti A, Feigenbaum H, eds) Elsevier Science Publishers: 69-76, 1990.

De Kroon M.G.M., Van der Wal L.F., Gussenhoven W.J., Bom N.: *Angle dependent backscatter from the arterial wall*. Ultrasound Med Biol 17: 121-126, 1991.

De Kroon M.G.M., Slager C.J., Gussenhoven W.J., Serruys P.W., Roelandt J.R.T.C., Bom N.: *Cyclic changes of blood echogenicity in high-frequency ultrasound*. Ultrasound Med Biol 17: 723-728, 1991.

De Kroon M.G.M., Van der Wal L.F., Gussenhoven W.J., Rijsterborgh H., Bom N.: *Backscatter directivity and integrated backscatter power of arterial tissue*. Int J Cardiac Imaging 6: 265-275, 1991.

De Kroon M.G.M., Van der Wal L.F., Bom N.: *The anisotropic nature of arterial tissue and its impact on backscatter measurements*. Ultrasonoor Bulletin 20, Abstracts of the 9th European Workshop on Ultrasonic Tissue Characterization and Echographic Imaging 10-13 May, Nijmegen: 6, 1992 (Abstract).

Bom N., Lancée C.T., Gussenhoven W.J., Roelandt J., Li W., De Kroon M.G.M.: *Intravascular scanning devices and their clinical value*. Innovations in Abdominal Ultrasound, Heyder N, Hahn EG, Goldberg BB eds. Berlin, Springer Verlag: 81-86, 1992.

De Kroon M.G.M., Van der Wal L.F., Bom N.: *Anisotropic nature of arterial tissue and its impact on backscatter measurements*. Ultrasonic Imaging 14: 191, 1992. (Abstract)

Bom N., De Kroon M.G.M.: *New developments in cardiac ultrasound technology*. Proceedings of the VI Mediterranean Conference on Medical and Biological Engineering July 5-10 Capri, Italy (M. Bracale and F.Denoth, eds), Napels: 665-667, 1992.

De Kroon M.G.M., Van der Heiden M.S., Bom N., Borst C.: *Quantitative characterization of arterial tissue and blood: complications and perspectives*. Intravascular Ultrasound 1993. Ed.: Roelandt J., Bom N., Gussenhoven W.J.

Curriculum Vitae

Machteld de Kroon, de schrijfster van dit proefschrift is geboren op 29 januari 1964 te 's-Gravenhage. Zij bezocht het Augustinianum te Eindhoven en behaalde daar in 1982 het Gymnasium-B diploma. Aan de Technische Universiteit van Eindhoven studeerde zij vervolgens Technische Natuurkunde. In 1988 voltooide zij de studie op een afstudeerwerk over de invloed van de stromingseigenschappen in het bloedvat op het deeltjestransport tussen bloed en vaatwand. Vanaf 1 januari 1988 is zij als wetenschappelijk medewerkster in dienst van de Technisch Fysische Dienst (TPD) van de organisatie voor Toegepast Natuurwetenschappelijk Onderzoek (TNO) in Delft. Het onderzoek van haar proefschrift vond plaats in samenwerking tussen de TPD, de Erasmus Universiteit van Rotterdam en de Technische Universiteit Delft. Naast haar promotieonderzoek verrichtte Machteld in opdracht van het bedrijfsleven ook onderzoekingen naar toepassingsmogelijkheden van het "meten met ultrageluid". Op 3 januari 1993 werd zij moeder van een zoon, Johan.